Flt1 determines the structural design of the arteriolar tree

Zur Erlangung des akademischen Grades eines

DOKTORS DER NATURWISSENSCHAFTEN

(Dr. rer. nat.)

von der KIT-Fakultät für Chemie und Biowissenschaften

des Karlsruher Instituts für Technologie (KIT)

genehmigte

DISSERTATION

von

Dipl.-Ing. Alina Klems

aus

Friedberg

KIT-Dekan:	Prof. Dr. Willem Klopper
Referent:	Prof. Dr. Ferdinand le Noble
Korreferent:	Prof. Dr. Christian Kupatt
Tag der mündlichen Prüfung:	10.02.2017

Acknowledgements

First of all I would like to thank Ferdinand le Noble for great support of my work during the last years. It was a pleasure working with you. I appreciate your dedication to science and your constant enthusiasm.

I would particularly like to thank Raphael Wild. Discussing with you meant a lot to me, scientifically but also personally. I wish you all the best for your future career.

I would like to thank Janna Krüger for her help at the MDC.

My gratitude goes to Katja Meier at the MDC as well as Karolin Rahm and Claudia Winter at the KIT for great technical assistance.

Last but not least I want to thank my parents Gudrun and Andreas for their encouragement during the last years.

1 Abstract 7
2 Zusammenfassung 8
3 Introduction 10
3.1 The vascular system – life is a flow 10
3.2 Vessels – building blocks of the vascular system 10
3.3 How do blood vessels emerge? 13
3.3.1 The zebrafish embryo – studying vascular development *in vivo* 14
3.3.2 Angiogenesis – a fine line between health and disease 15
3.3.3 Lumen formation 16
3.3.4 Collaterals and arteriogenesis 19
3.4 Regulation of the vasculature at the genetic level – the VEGF family 21
3.4.1 Expression of the VEGF family members 23
3.4.2 VEGF-A – KDR signalling 25
3.4.3 VEGFR-1 (Flt1) and its specific ligands PlGF and VEGF-B 26
3.4.4 The VEGF family and the tip cell concept – many open questions 28
3.5 Hemodynamics – an architect of the vascular system 29
3.6 Regulation of the vascular network by nerves – the neurovascular link 31
4 Results 33
4.1 Previous work and aim of the current study 33
4.2 *Flt1* expression and protein localization in the zebrafish embryo 35
4.2.1 *Plgf* expression in the zebrafish embryo 39
4.2.2 *Vegfb* identification and its embryonic expression in the zebrafish 43
4.3 Flt1 regulates arterial diameter 44
4.3.1 Somitic *vegfaa* GOF 46
4.3.2 Overexpression of the Flt1-exclusive ligands *plgf* and *vegfb* – release of the endogenous Vegfaa reservoir? 49
4.4 Analysis of the vascular development of *plgf*$^{-/-}$ mutants 62
4.5 Cerebral vascular development in *plgf*$^{-/-}$ mutants 65
4.6 Analysis of *flt1*$^{-/-}$;*plgf*$^{-/-}$ double mutants 67
4.7 Functional conservation of *plgf* in zebrafish 68
4.8 The early neurovascular link – are Vegf ligands angioneurins? 70

5 Discussion 78
5.1 Arterial Flt1 scavenges Vegfaa to control vessel diameter 78
5.2 The impact of blood flow and shear stress on arterial remodelling 83
5.3 Clinical implications 86
6 Material and methods 88
6.1 Material 88
6.2 Methods 90
6.2.1 Zebrafish methods 90
6.2.2 Staining methods 91
6.2.3 Molecular biological methods 92
6.2.4 Generation of mutants and transgenics 97
6.2.5 Biochemical methods 99
6.2.6 Microscopy 101
6.2.7 Computational methods 101
6.2.8 Statistical analysis 102
7 Bibliography 103
8 Abbreviations 110
9 List of figures 113
10 List of tables 114
11 List of publications 115

1 Abstract

During evolution higher vertebrates were developing a hierarchically branched vascular system allowing efficient distribution of oxygen- and nutrient-rich blood towards metabolically active tissues as well as removal of cellular waste products. Organ blood flow needs to carefully match tissue metabolism, as compromised blood flow in ischemic cardiovascular diseases, for example induced by atherosclerotic lesions and occlusion of main feed arteries, results in organ damage. Conversely, improving blood flow towards infarct regions either by promoting growth of new vessels (angiogenesis), or by stimulating native arterial collateral bypasses is considered therapeutically relevant.

Although the cytokine vascular endothelial growth factor (VEGF) constitutes in theory an ideal candidate for therapeutic approaches as it promotes arterial identity, vascular branching and remodelling, experimental and clinical trials with VEGF have thus far not yielded the expected results. As vessels react very sensitive to changes in VEGF levels, the major obstacles in efficient promotion of arteriolar outward remodelling are VEGF dosage and location. An endogenous scavenger of VEGF and thus a regulator of VEGF receptor (VEGFR)-2 (Kdrl) signalling is VEGFR-1 (Flt1). Thus, we reasoned that balancing Flt1 levels might be useful in tuning local VEGF levels in the context of promoting arteriolar growth.

Using genetic approaches in the zebrafish model we demonstrated in this study that Flt1 protein was predominantly expressed at or in close proximity of the endothelial cell membrane of arterioles. Loss of *flt1* stimulated outward remodelling of arterioles, presumably due to increased Vegfaa bioavailability. While *vegfaa* gain-of-function (GOF) approaches resulted in completely dysfunctional arterioles due to harmful Vegfaa levels, gain of the Flt1-specific ligand *placental growth factor* (*plgf*) released the Flt1-bound Vegfaa by competitive binding to Flt1, and thereby arteriolar outward remodelling by the factor two was induced in an Akt-dependent manner without any adverse side effects.

Based on these observations we propose the following model: Flt1 is selectively expressed in arterioles where it binds Vegfaa. By increasing Plgf levels Vegfaa is competed away from arteriolar Flt1, resulting in local release of a non-toxic, therapeutically beneficial dosage of Vegfaa in close proximity to arteriolar Kdrl. Arteriolar Flt1 may thus act as important regulator of arteriolar diameter in response to Vegf ligands, and manipulation of the ligand-binding profile may present a novel therapeutic target aimed at promoting outward remodelling of arterioles.

2 Zusammenfassung

Im Laufe der Evolution haben höhere Vertebraten ein hierarchisch angeordnetes Blutgefäßsystem entwickelt, das die effiziente Versorgung von metabolisch aktivem Gewebe mit sauerstoff- und nährstoffreichem Blut sowie den Abtransport von zellulären Abfallprodukten ermöglicht. Die Abstimmung des Blutfluss in den Organen auf deren Metabolismus ist wichtig, da Beeinträchtigungen im Blutfluss in ischämischen Herz-Kreislauferkrankungen, hervorgerufen z.B. durch atherosklerotische Läsionen und Arterienverstopfung, Organschädigungen hervorrufen. Umgekehrt wird eine Verbesserung des Blutflusses in Richtung einer Infarktregion entweder durch Wachstumsförderung neuer Gefäße (Angiogenese) oder durch die Stimulation nativer, arterieller Kollateral-Bypässe als therapeutisch relevant angesehen.

Obwohl das Cytokin vascular endothelial growth factor (VEGF) theoretisch einen idealen Kandidaten für therapeutische Ansätze darstellt, da es arterielle Identität sowie Gefäßverzweigung und –remodellierung fördert, haben experimentelle und klinische Studien mit VEGF bisher nicht die erhofften Ergebnisse erzielt. Da Gefäße sehr sensibel auf Änderungen von VEGF-Mengen reagieren, stellen die Dosierung und Lokalisierung von Vegf die größten Hürden bei der effizienten Stimulierung struktureller Arteriolenerweiterung dar. Ein endogener „Fänger“ von VEGF und somit ein Regulator der VEGF-Rezeptor (VEGFR)-2 (Kdrl)-Signalgebung ist VEGFR-1 (Flt1). Daraus haben wir geschlussfolgert, dass das Ausbalancieren von Flt-Mengen zur lokalen Justierung von VEGF-Pegeln im Zusammenhang mit SAE nützlich sein kann.

Im Zebrafischmodell konnten wir mittels genetischer Ansätze Flt1-Protein direkt auf oder zumindest sehr nah an Endothelzellmembranen in Arteriolen nachweisen. Der Verlust von *flt1* stimulierte struktureller Arteriolenerweiterung, wahrscheinlich durch erhöhte Bioverfügbarkeit von Vegfaa. Während zwei unterschiedliche *vegfaa* Funktionsgewinn-Studien zu völlig dysfunktionalen Arteriolen auf Grund schädlicher Vegfaa-Pegel führten, konnte eine Zunahme des Flt1-spezifischen Liganden *placental growth factor* (*plgf*) das durch Flt1 gebundene Vegfaa durch kompetitives Binden befreien. Dies führte zu Akt-abhängiger struktureller Arteriolenerweiterung um den Faktor zwei ohne schädliche Nebenwirkungen.

Basierend auf diesen Beobachtungen schlagen wir folgendes Modell vor: Flt1 wird selektiv in Arterien exprimiert, wo es Vegfaa bindet. Durch Erhöhung des Plgf-Pegels wird Vegfaa von

arteriellem Flt1 vertrieben, was zu einer lokalen, nicht-toxischen und therapeutisch vorteilhaften Freisetzung von Vegfaa nah an arteriellem Kdrl führt. Arterielles Flt1 ist somit ein wichtiger Regulator des Arteriendurchmessers in Bezug auf Flt1-Liganden, und die Manipulation des Bindungsprofils der Liganden kann einen neuartigen Therapieansatz zur strukturellen Arteriolenenerweiterung darstellen.

3 Introduction

3.1 The vascular system – life is a flow

The vascular system is connected to every metabolizing tissue in the body in order to nourish it with oxygen and nutrients and to clear cellular waste from the tissue.

The vasculature is the first functional organ in an embryo, and all subsequent organogenesis crucially relies on the supply by vessels. The fact that malformations of the vasculature often lead to embryonic lethality unequivocally emphasizes the importance of the vasculature during development. Also in the adult, malfunctions of the cardiovascular system are devastating, giving rise to some of the most pervasive lethal conditions in Western countries like stroke and heart attack. Research of the recent years revealed that even many neurodegenerative disorders like Alzheimer's disease and amyotrophic lateral sclerosis (ALS) stem from vascular dysfunctions. Comparative zoological studies indicated that vascular and neuronal growth show many similarities, and neurovascular cross-talk contributes to organ homeostasis.

Therefore, understanding the mechanisms of how the vascular system develops and which factors are needed to keep it in a fully functional condition are crucial to tackle cardiovascular pathologies as well as many neurological disorders in the clinic.

By looking in detail at the functional anatomy, cellular mechanisms and molecular players that are essential in vessel growth, developmental biology can give answers to many questions that are currently unsolved. Such findings may translate into clinical applications, because many processes and key-players of blood vessel formation in the embryo are recapitulated and activated in the adult.

3.2 Vessels – building blocks of the vascular system

Based on functional anatomical terms, the circulatory system in higher vertebrates can be divided in two different system: the blood vascular system, which is a closed tubular network that allows blood circulation, and the lymphatic system, a blind-ended tubular system, which transports lymph unidirectionally from tissues towards the heart and contributes to immune responses (Eilken & Adams 2010). While both systems are lined with

specialized endothelial cells (ECs), major differences exist in the anatomy of the vascular wall.

Arteries and veins display distinct and unique architectures, adapted to their respective functions. As blood is pumped into the arteries with a high pressure and flow rate, the walls of the main conductance arteries, i.e. aorta and carotid arteries, are very thick and elastic. On a cross-section three different layers can be discerned: the tunica intima, the medial tunica media and the tunica adventitia. The large arteries are elastic; in physiological terms they show a high compliance and distensibility. These physical characteristics of the conductance arteries are important to temporarily store blood via the Windkessel function, to dampen pressure waves and to facilitate a more constant flow (Westerhof et al. 2009). The conductance arteries with their high compliance and low resistance thus mainly serve to normalize pressure waves during cardiac systole. The next section of arteries, the so-called resistance arteries, is responsible for the distribution of blood flow towards organs. To fulfil this function, these arteries are equipped with a medial layer containing smooth muscle cells that are highly responsive to vasoactive substances; they are therefore often called contractile smooth muscles as opposed to the synthetic smooth muscles found in the conductance arteries. Smooth muscle cells in resistance arteries express various receptors including alpha-adrenergic receptors, angiotensin-II receptors and endothelin receptors, enabling contractile responses to circulating levels of the corresponding ligands (Rensen et al. 2007). Endothelial cells of resistance arteries can furthermore produce substantial amounts of vasodilator substances including nitric oxide and prostaglandins. By regulating the vascular tone via the amount of vasoconstrictors and -dilators, the resistance to flow and organ perfusion can be precisely fine-tuned. In addition, resistance arteries are often innervated by sympathetic nerves allowing central control of organ perfusion (Charkoudian & Rabbitts 2009). More distal and within the organs blood flow is distributed by small arterioles, which typically display a media consisting of two layers of smooth muscle cells. Besides expressing receptors for vasoactive molecules, arterioles are highly sensitive to local changes in metabolism such as tissue-specific partial pressure of oxygen (pO_2) and local hemodynamics including pressure and flow (Pittman et al. 2005). Typically, a local rise in arteriolar pressure evokes a myogenic constriction, whereas increases in flow or low pO_2 provoke vasodilation (Sandoo et al. 2010). Ultimately, these local responses are aimed at maintaining organ perfusion within safe boundaries.

Subsequently, the blood passes through the capillaries, where exchanges of nutrients, oxygen as well as carbon dioxide take place. Pending organ, capillary ECs may display special functional characteristics including fenestrations (Satchell & Braet 2009).

After passing the capillaries, blood is returned to the heart via the venous system. The blood pressure in the veins is low, and thus their wall is comparably thinner with venous flow directionality being ensured via venous valves preventing a reflux. Yet, veins are very compliant and they serve to store considerable amounts of blood in resting conditions. Thus, the blood vessels have a hierarchical structure with arteries and veins as main vessels carrying large blood volumes. These are connected to arterioles and venules with a smaller diameter and thinner vessel walls, which eventually branch into to the highly ramified network of thin collaterals to distribute the blood (Figure 1) (Carmeliet 2000).

Vessels can adapt their structure, lumen diameter and media thickness in response to hemodynamic changes. In general, increases in flow associate with vessel dilation and structural outward remodelling, yielding a vessel with a structurally larger lumen. Increases in pressure, at the level of arterioles, associate with a myogenic constriction occurring acutely upon pressure rise, whereas long term increases in pressure associate with a thicker media and remodelling of the media around smaller lumen, collectively reducing vessel diameter and increasing resistance to flow. Vessels also adapt to changes in the metabolic demand of the tissue they are supplying. It is well known that physical exercise, via increases in muscle metabolism, promotes angiogenesis of new capillaries around muscle fibers, whereas long-term inactivity associates with vessel regression (Hoier & Hellsten 2014). However, the quality and quantity of these adaptive mechanisms vary among organs, yet they appear optimized for organ function. For example, post-capillary venules must allow circulating leukocytes to enter the lymph node, but the cerebral vasculature is tightly sealed to prevent leakage of serum proteins and cells at the blood brain barrier (Tam & Watts 2010). One of the major outstanding questions in the field is how tissues controls the distinct vascular properties including vascular diameter, vascular reactivity, branching patterning, and transport capacity (Corada et al. 2014). Little is known about how this is genetically hardwired, but evidence is emerging suggesting an intimate cross-talk between the vasculature and the surrounding tissue, for example between intersegmental vessels (ISVs) and the spinal cord in zebrafish (Wild et al. 2017).

3.3 How do blood vessels emerge?

There are different processes by which vessels can be formed (Carmeliet 2000).

In the developing embryo, the *de novo* assembly of blood vessels in primitive networks is called vasculogenesis. In a next step, new blood vessels sprout from pre-existing vessels, a process called angiogenesis, resulting in the formation of an extensively branched network. Next, vessels are assigned an arterial or venous identity, a process tightly regulated by Notch signalling and hemodynamics. To become mature and stable, blood vessels subsequently need to adapt their morphology to the blood flow they are carrying. During this vascular remodelling process their diameter enlarges, and later smooth muscle cells (SMCs) and pericytes are recruited to the vessel wall (Carmeliet 2000; Carmeliet & Collen 2000).

The vascular system is depending on genetic factors with VEGF-A being the key player, on hemodynamics, and on the neuronal system known as the neurovascular link.

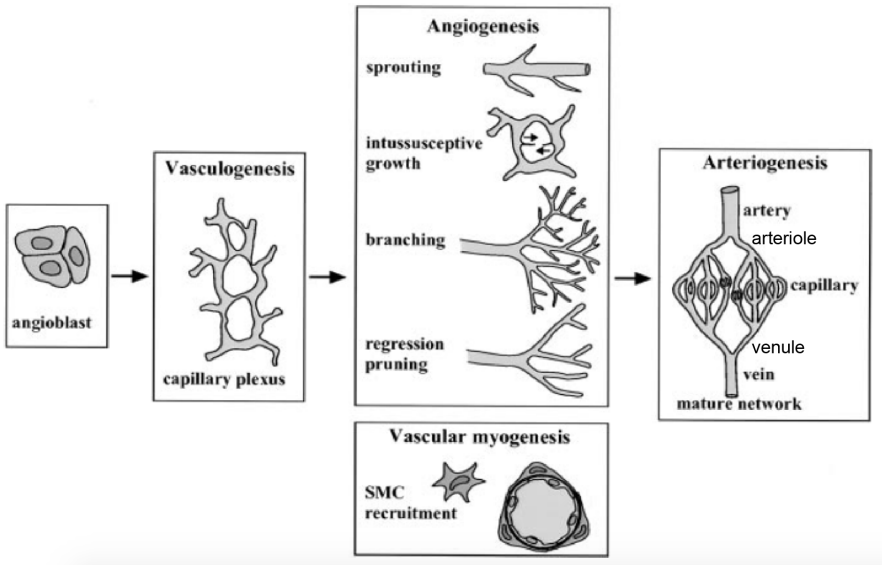

Figure 1| Schematic illustration of blood vessel development.

Angioblasts, the endothelial precursor cells, develop from mesodermal cells. Primitive vessels are formed during vasculogenesis. Subsequent enlargement of the vessel network is achieved by angiogenesis. The most important angiogenic process is sprouting angiogenesis. Subsequently, the vessels have to undergo maturation via smooth muscle cell (SMC) and pericyte coverage. The mature network consists of a hierarchical structure of arteries, arterioles, capillaries, venules and veins. Modified from Carmeliet & Collen (2000).

3.3.1 The zebrafish embryo – studying vascular development *in vivo*

Due to its transparency and the many different transgenic reporter lines available, a great part of our current knowledge on vascular development, especially sprouting angiogenesis, has been derived from studies in zebrafish.

The dorsal aorta (DA) and the posterior cardinal vein (PCV), both formed by vasculogenesis ventrally to the notochord (NC) (Figure 2), are lumenized at approximately 23 hours post fertilization (hpf) with circulation starting shortly thereafter. The trunk vasculature furthermore consists of arterial and venous intersegmental vessels (aISVs and vISVs, respectively). The aISVs start emerging via sprouting angiogenesis bilaterally from the DA at around 20hpf in a process termed primary sprouting (Figure 2i) (Isogai et al. 2003), growing dorsally within the somatic boundaries along the NC and the neural tube (NT) (Figure 2i). Once the ISVs have reached the dorsal roof plate of the NT, one branch grows perpendicularly in the rostral, the other one in the caudal direction (Figure 2ii). The perpendicular vessel branches of adjacent ISVs bilaterally form anastomoses, giving rise to the dorsal longitudinal anastomotic vessel (DLAV) at appr. 1.5dpf (Figure 2iii) (Isogai et al. 2003). This process was suggested to be supported by tissue macrophages interacting as "cellular chaperones" with EC filopodia to help the vessel fusion, but detailed studies are missing (Fantin et al. 2010). As a vascular loop is needed for the blood to circulate, in the next step of vascularization veins are formed in a process called secondary sprouting. Vessels emerge bilaterally from the PCV, grow again within the somitic boundaries and elongate towards the primary aISVs (Figure 2iv-v). About half of the secondary sprouts connect with the primary ISV, the remaining arterial connections detach and dissolve, and thereby the aISVs become veins. The other half of the secondary sprouts elongates towards the horizontal myoseptum (HM), where the sprouts branch rostrally and caudally to form the parachordal vessel (PAV). Also the vISVs can contribute to the PAV formation (Figure 2vi).

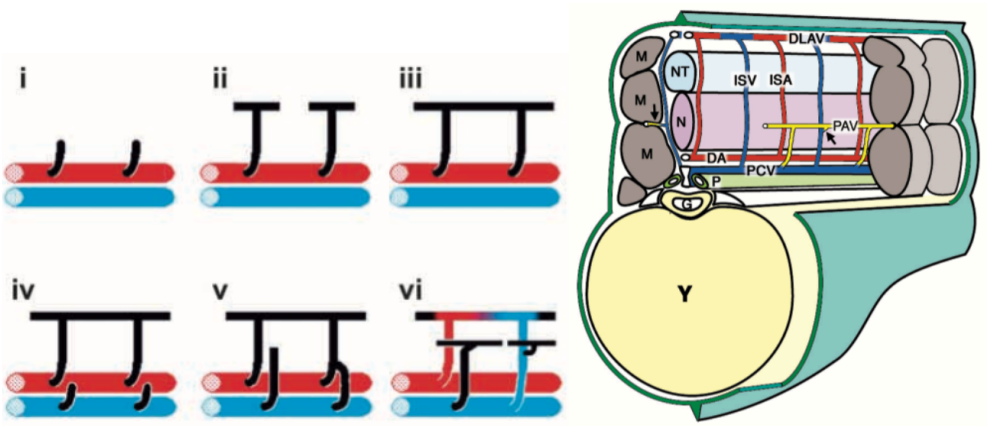

Figure 2| Blood vessel development in the zebrafish.

Left: (i) Primary aISVs (black) emerge from the dorsal aorta (red), (ii) grow dorsally and (iii) form the DLAV by anastomosis. (iv) During AV remodelling, secondary venous sprouts emerge from the PCV, (v) grow dorsally and (vi) finally 50% fuse to a primary aISV, resulting in a vISV. The other 50% form a lymphatic vessel. Right: Compartments of the zebrafish trunk. DA, dorsal aorta; DLAV, dorsal longitudinal anstomotic vessel; ISV, intersegmental vessel; M, myotomes; N, notochord; PCV, posterior cardinal vein; Y, yok sac. Modified from Isogai et al. (2003).

3.3.2 Angiogenesis – a fine line between health and disease

Historically, angiogenesis came into focus of clinical research in the 1970's in the context of tumourigenesis, when Judah Folkman discovered the dependence of tumour growth on blood vessel supply, and the secretion of pro-angiogenic factors by tumours (Folkman et al. 1971). Folkman was among the first to recognize that many pathologies including tumour growth are related to uncontrolled angiogenesis. As diseases associated with excessive angiogenesis can principally affect any vascularised organ, the disease pictures are very heterogeneous, including for example arthritis, psoriasis, primary pulmonary hypertension, and inflammatory bowel disease (Carmeliet 2003). The reverse is also true: Devastating diseases including hypertension and diabetes associate with vessel pruning and regression (Korn & Augustin 2015). While in the context of tumour growth it is beneficial to inhibit vascular growth, several other medical conditions may improve when vascular growth is stimulated. For example in the case of many ischemic cardiovascular diseases like heart infarct and stroke revascularization strategies are considered to improve the clinical outcome. Unfortunately, many clinical trials aiming at stimulating functional

revascularization in the ischemic setting have failed and more research is needed to understand the fundamental principles of building stable and perfused networks.

Formation of blood vessels in the embryo shows many molecular and functional similarities with vessel growth in pathological conditions in the adult. Therefore, deciphering the molecular mechanisms contributing to vascular growth during embryogenesis may help to identify therapeutic targets. Recent research addressing growth in zebrafish embryos and foetal/ neonatal mice identified several novel aspects to angiogenesis crucial for making functional networks. These include the formation of additional branches or vessel segments via intussusceptive or via sprouting angiogenesis (SA), the most comprehensively studied type of angiogenesis in development as well as in pathologies.

In a first step of SA, the extracellular matrix (ECM) of a mature vessel has to be degraded at the site at which the new sprout is supposed to emerge. Next, an EC has to be activated to migrate out of the existing vessel to initiate the sprout. Subsequently, this sprout has to elongate in a unidirectional manner. Thus, two different cell types participate in SA, namely tip and stalk cells. Tip cells are migratory, polarized cells at the leading front of a growing sprout, which guide the sprout and form anastomoses with other vessels. Although they extend numerous long filopodia, the function of these filopodia as guidance cue sensors has been recently challenged (Phng et al. 2013). Stalk cells are proliferating and form the sprout via adherent and tight junctions (Blanco & Gerhardt 2013). Another difference between tip and stalk cells has been reported to be their differential expression profiles.

To explain how ECs can develop these differences in function and gene expression, the tip-stalk cell concept (Gerhardt et al. 2003) involving VEGF-A – KDR signalling and lateral inhibition by Dll4 – Notch signalling was introduced, which will be explained in more detail in section 3.4.3.

3.3.3 Lumen formation

While patients with microvascular defects affecting arterioles, venules and capillaries may benefit from stimulating angiogenesis, strategies focussing on revascularization in ischemic conditions have not been successful so far in the clinic.

Importantly, in case of an arterial occlusion the highest resistance to blood flow is found in the collaterals through which the blood flow is rerouted around the occluded site (Helisch &

Schaper 2003). For a positive clinical outcome in these conditions it is therefore not critical to stimulate distal angiogenesis, but to ensure appropriate redirection of blood flow at the proximal site by promoting first the collateral bypass growth and second the remodelling of small-diameter to large-diameter collateral arteries, a process called arteriogenesis (Cristofaro et al. 2013).
Therefore, our research is not only focussing on how to extend the vascular network via branching angiogenesis, but also on how a vascular lumen is formed in this network.

To reconstruct the processes involved in clinically relevant arteriogenesis, it is important to comprehend first the initial lumen formation in a newly formed capillary, i.e. the transformation from a cord-like EC chain to a tubular vessel. Similar to sprouting angiogenesis, the embryonic zebrafish ISVs constitute a valuable model to study this process *in vivo*. To date, three different theories on the process of capillary lumenization have been put forward in the zebrafish ISVs, which constitute an ideal model to study this initial capillary lumen formation.
One of these theories describes luminal space formation via endothelial vacuoles (Kamei et al. 2006). It was suggested that vesicles emerge via fluid endocytosis, also known as pinocytosis, and fuse to larger vacuoles until these vacuoles are large enough to span the complete length of an EC (Figure 3a). To form a multicellular tube, neighbouring ECs merge their intracellular luminal compartments to give rise to unicellular tubes in which the lumen is enclosed by a single EC (Kamei et al. 2006). Two years later, Blum et al. (2008) challenged this view on intracellular vessel lumina, when they found that ISVs are multicellular tubes with cell junctions ranging over the whole ISV length (Figure 3b). They proposed that the ISV lumen is extracellular between adjacent ECs, possibly formed by exocytosis of the vesicles, which were described before by Kamei et al., into an intercellular space. Recently, Gebala et al. (2016) introduced inverse blebbing as hemodynamics-coupled mechanism of lumen expansion in the tip of angiogenic sprouts. They suggest that the prevalence of a higher pressure at the luminal compared to the cytoplasmic site causes a local actomyosin cortex weakening and a subsequent inverse membrane blebbing (Figure 3d). The bleb is consequentially resolved by actomyosin contraction of the apical membrane, and thereby the lumen is expanded. However, this concept is based on the assumption that the ISV is already perfused, but how the initial perfusion takes place was not addressed in that study.

Taken together, the mechanism of lumen formation taking place in sprouting angiogenesis in capillaries such as the zebrafish ISVs is not completely understood so far, and most likely different vascular beds and developmental stages exploit distinct lumen formation mechanisms (Betz et al. 2016).

A recent *in vitro* study reported the involvement of lateral filopodia in lumen formation (Abraham et al. 2015). The authors propose a model in which VEGF-A – KDR signalling induces a DOCK4/DOCK9/Cdc42 complex that initiates filopodia protrusions, which form EC – EC contacts prior to lumen formation (Figure 3c). However, a detailed mechanism of this process and supporting *in vivo* data are missing so far.

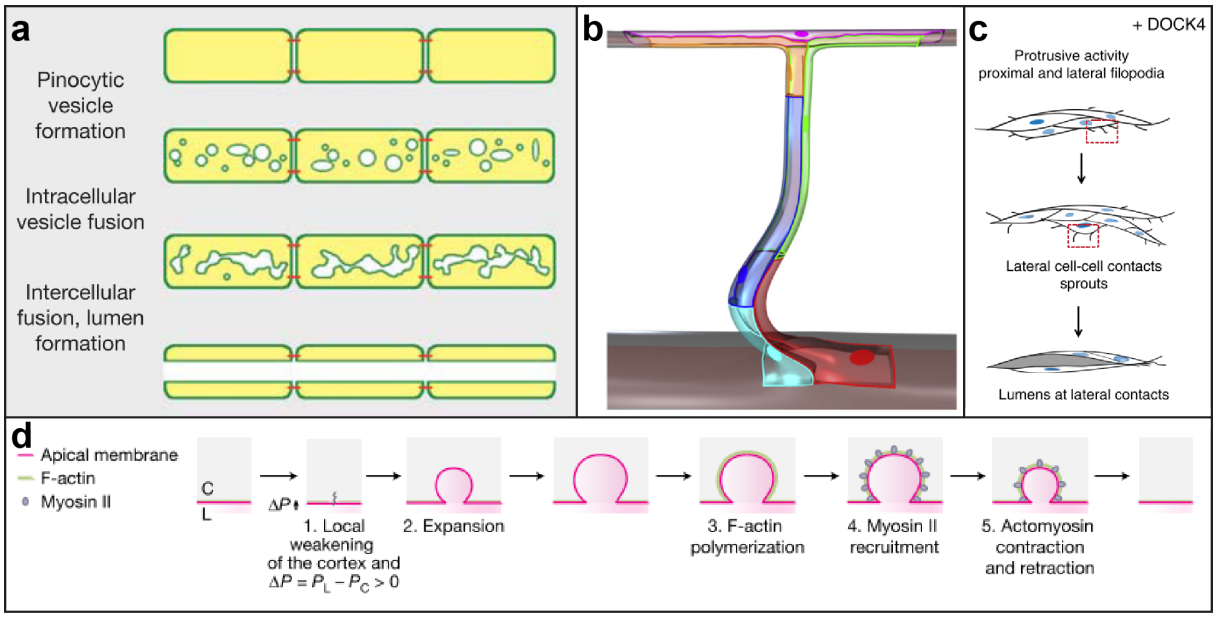

Figure 3| Proposed mechanisms of lumen formation.

(**a**) Intracellular lumen formation via vacuolar fusion. Vesicles are formed via uptake fluid endocytosis and they fuse into larger vacuoles. Unicellular tube formation is finished when vacuoles of adjacent ECs have merged. (**b**) Depiction of a multicellular ISV with in extracellular lumen between adjacent ISVs. (**c**) Concept of lateral filopodia formation, leading to EC-EC contacts. Subsequently, an interendothelial lumen is formed. (**d**) Inverse blebbing as model of lumen expansion. The pressure difference between cytoplasm and lumen causes an inverse bleb, which is resolved by EC contraction. Adapted from: a, Kamei et al. (2006); b, Blum et al. (2008); c, Abraham et al. (2015); d, Gebala et al. (2016).

3.3.4 Collaterals and arteriogenesis

Most mammalians possess a native collateral network, which is a bypass vasculature between arterial trees serving as a sort of “backup system” to preserve blood flow in case of arterial occlusion in one of the trees. Microvascular collaterals are arteriole-to-arteriole anastomoses in arterial tree crowns with the capacity to enlarge up to 10-fold upon arterial occlusion; collateral arteries are connections between feed arteries (Faber et al. 2011).

The outcome, that means the severity of the tissue damage, of acute or chronic arterial obstructions varies widely among individuals, which can be explained by differences in their endogenous backup system, i.e. in their collateral extent. Parameters determining the collateral extent are collateral number and diameter (Faber et al. 2014). Measuring collateral flow in humans revealed variations by the factor 40, and those patients with a low collateral flow had an increased risk of mortality when suffering from coronary artery disease. The native collateral network is mainly determined by genetic factors, and recently a genetic locus important for collateral extent was discovered in mice (Sealock et al. 2014). With age, the collateral extent is decreasing (Faber et al. 2011). However, not only the collateral extent, but also the functionality of the collaterals is critical for ischemic disease outcome (Cristofaro et al. 2013).

In healthy conditions, there is no or only little pressure difference over the collateral length, thus collateral blood flow is very weak. However, upon occlusion of one of the arterial trees, the pressure drops downstream of the occlusion, leading to a saltatory increase in pressure difference in the collaterals; as a consequence there is increased collateral blood flow, an event known as collateral recruitment (Faber et al. 2014).

The resulting shear stress increase induces a vascular remodelling process known as arteriogenesis including diameter enlargement and vessel wall thickness increase. Confusingly, in the literature the original definition of arteriogenesis has been frequently overlooked and the term has been adapted for a variety of other processes, for example to describe the developmental process of vessel maturation, which occurs after vessels have been formed by angiogenesis and lumenization has occurred. During this maturation process, smooth muscle cells (SMCs) and pericytes are recruited to muscularize the vessel, and proliferation takes place to increase the arterial diameter (Carmeliet 2000; Simons & Eichmann 2015).

There are four phases of collateral remodelling into mature conductance arteries after arterial occlusion (Schaper 2009). In the first phase, the silent phase, ECs sense the saltatory shear stress increase, which has to be communicated to the SMCs. Thus, cell-cell contacts are highly important for outward remodelling. ECs and SMCs undergo a change in their phenotype; the endothelium becomes more permeable, the contractile SMCs become synthetic. Shear stress induces the expression of endothelial nitric oxide synthase (eNOS) and the production of NO, which induces the secretion of VEGF-A. VEGF-A, in turn, induces Dll1 – Notch signalling, and thereby ephrin-B2 – Eph-B4 signalling is upregulated (Limbourg et al. 2007). The expression of monocyte chemoattractant protein (MCP)-1 is induced in ECs and SMCs. Blocking any of these molecules abrogates arteriogenesis, highlighting that arteriogenesis is dependent on the concerted effort of different factors. In the second phase, macrophages are attracted, infiltrate the vessel wall and secrete proteases to digest the extracellular scaffold in order to clear space for the collateral enlargement (Schaper 2009). ECs upregulate platelet-derived growth factor (PDGF)-B, basic fibroblast growth factor (bFGF) and transforming growth factor (TGF)-β1 to induce EC and SMC proliferation and thus vessel diameter increase (Carmeliet 2000). Vessel maturation takes place in the third phase. The large number of SMCs arrange in layers, integrins and connexins are upregulated to establish proper cell-cell contacts and the extracellular scaffold is rebuilt (Schaper 2009). In the last phase, unneeded vessels undergo pruning, and they are sealed by intimal proliferation.

The stimulation of arteriogenesis with growth factors has been attempted in a variety of studies. The involvement of FGF receptor (FGFR)-1 in arteriogenesis awakened the hope that FGF might be exploited as therapeutic target to stimulate arteriogenesis. However, the stimulation with FGF is much more difficult than anticipated as many FGF ligands exist, which probably contribute to arteriogenesis in a joint effort (Schaper 2009). With respect to VEGF-A, its pharmacological blockade inhibits arteriogenesis, but VEGF-A administration could not completely restore flow and many clinical trials did not result in the hoped-for results, mainly because drug delivery was not efficient (Schaper 2009; Grundmann et al. 2007).

Taken together, although pro-arteriogenic therapeutic strategies have been pursued for decades, these attempts have been of little success so far (van Royen et al. 2009). As cardiovascular pathologies are the leading cause of death in Western countries, new therapeutic approaches would be of major benefits for public health.

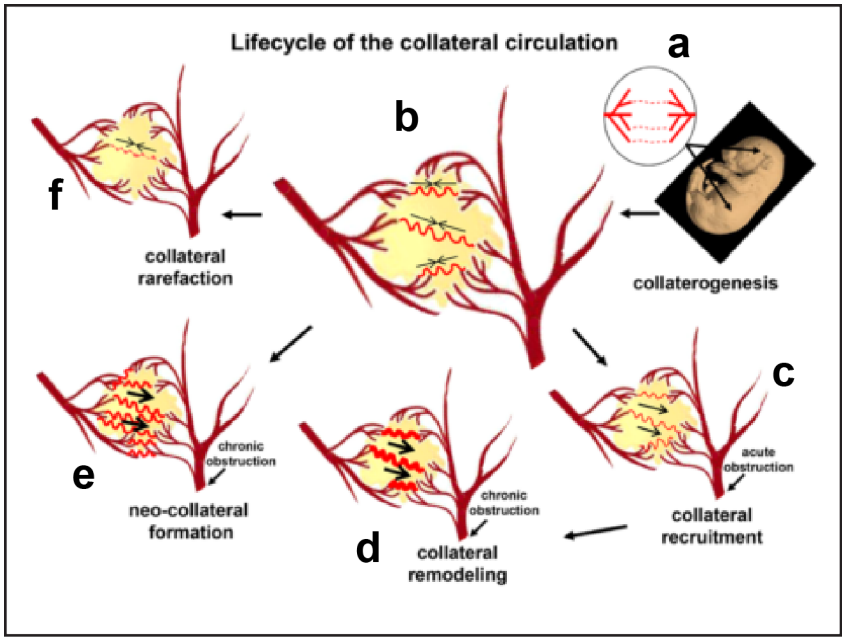

Figure 4| Collateral circulation.

(**a**) The native collateral network is already formed during embryogenesis, and the collateral extent is determined by genetic factors. (**b**) Collaterals connect two arterial trees. (**c**) Upon occlusion of one of the trees, flow increases in the collaterals to reroute the occluded site, a process termed collateral recruitment. (**d**) Increased shear stress levels in the collaterals induce the outward remodelling of the collaterals, known as arteriogenesis. (**e**) Neo-collateral formation is pursued in many different therapeutic strategies in order to protect the patient in case of arterial occlusions. (**f**) After completion of the arteriogenic process, pruning of unneeded collaterals takes place. Modified from Faber et al. (2014).

3.4 Regulation of the vasculature at the genetic level – the VEGF family

At the genetic level, one growth factor involved in all steps of vascularization in health as well as in pathologies is vascular endothelial growth factor (VEGF)-A. It belongs to the VEGF family, which consists of several ligands and receptors (Figure 5).

The VEGF receptors are composed of seven extracellular immunoglobulin (Ig)-like domains, a transmembrane domain as well as a split tyrosine kinase domain (Simons et al. 2016). They constitute one of the 20 subfamilies of the receptor tyrosine kinases (RTKs). Upon binding of

VEGF ligand dimers, the receptors dimerize and place their intracellular kinase domains next to each other to transphosphorylate the tyrosine residue of the partner receptor (Lemmon & Schlessinger 2010). Upon dimerization, the VEGF receptors are internalized, followed either by degradation or recycling to the membrane (Simons et al. 2016). The VEGF ligands can be classified according to the receptors they are binding to (Figure 5). VEGF-A, or simply VEGF, is the key player in angiogenesis and can bind to both VEGF receptor (VEGFR)-1 (or FLT1) and VEGFR-2 (or KDR, FLK1). Placental growth factor (PlGF) and VEGF-B exclusively bind to FLT1. VEGF-C and –D are the ligands of VEGFR-3 (FLT4), and processed forms of these ligands can also bind to KDR. The virus-expressed VEGF-E exclusively binds to KDR (Ferrara et al. 2003). The central pathways of angiogenesis are induced by VEGF-A – KDR signalling. VEGF-C – VEGFR-3 signalling is mainly important for lymphangiogeneis.

FLT1 primarily acts as VEGF-A scavenger in sprouting angiogenesis (Shibuya 2006).

Additional regulation of VEGFR signalling is achieved by the co-receptors neuropilin (NRP)-1 and -2, which are composed of a large extracellular ligand-binding domain, a transmembrane domain and a cytoplasmic domain with a PDZ protein-binding domain. NRP1 is mainly a co-receptor of KDR, NRP2 of VEGFR3 (Koch & Claesson-Welsh 2012). In addition, they can act as VEGF ligand sink. Whether they can signal remains a matter of debate (Snuderl et al. 2013; Simons et al. 2016).

In zebrafish, the *KDR* ortholog is *kdr-like* (*kdrl*), also known as *kdrb* (Bussmann et al. 2008; Covassin et al. 2009). Due to the genome duplication there are two paralogs of *vegfa*, with *vegfaa* as the relevant form for angiogenesis. *Vegfaa* has two isoforms, *vegfaa121* and *vegfaa165* (Rossi et al. 2016). Also the neuropilins have two paralogs, namely *nrp1a*/*b*, and *nrp2a*/*b* (Martyn & Schulte-Merker 2004). *Flt1* and *Plgf* do not have a second paralog in the zebrafish genome.

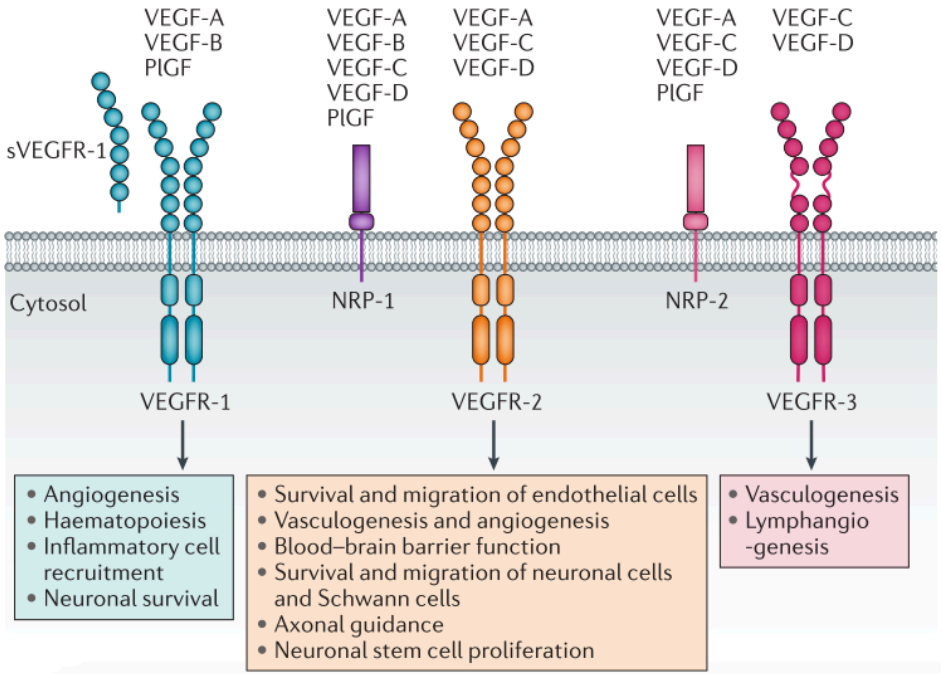

Figure 5| The VEGF family.

The VEGF family consists of the three receptors VEGFR-1, -2 and -3, which are forming dimers upon ligand binding. Their diverse functions are partly derived from their differential ligand binding profile. The co-receptors NRP-1 and -2 can in addition aid in VEGF receptor signalling. The majority of angiogenic signalling occurs via VEGFR-2 (KDR). VEGFR-3 is mainly important for lymphangiogenesis. Modified from Lange et al. (2016).

3.4.1 Expression of the VEGF family members

Kdr is mainly expressed in endothelial cells in mice. Likewise, the zebrafish homologue *kdrl* is expressed in all blood vessel ECs; therefore, transgenic lines expressing a fluorophore under the *kdrl* promoter are widely used for blood vessel analyses in zebrafish (Beis et al. 2005). Recently, neurons were identified as *Kdr* expression domain in mice as well as in zebrafish (Selvaraj et al. 2015; Wild et al. 2017). *Flt1* expression is found in arteries (Hogan et al. 2009; Krueger et al. 2011) and in neurons in the zebrafish embryo (Wild et al. 2017). Surprisingly, neuronal *flt1*, not vascular *flt1* is important for vascular development (Wild et al. 2017). This is contradictory to the current tip cell concept, which is based on the assumption that vascular *flt1* is crucial for proper vessel sprouting. According to this concept, *flt1* is upregulated by Dll4 – Notch signalling in stalk cells to form an antiangiogenic corridor, while the tip cell is void of *flt1*, resulting in a “salt and pepper” expression pattern (Chappell et al. 2009; Herbert & Stainier 2011). As we found that Flt1 is not required for sprouting

angiogenesis (Wild et al. 2017), the proposed expression pattern is questionable. Another expression domain of *Flt1* are macrophages (Clauss et al. 1996; Sawano et al. 2001), and during gestation particularly *sFlt1* is expressed in trophoblasts (Fan et al. 2014). While *Flt4* is expressed in all blood vessel ECs in early developmental stages, its expression becomes restricted to venous and lymphatic ECs in mice and zebrafish (Kaipainen et al. 1995; van Impel et al. 2014).

In zebrafish, *vegfaa* is expressed in the somites in early development (Jensen et al. 2015), and we could show that *vegfaa* is furthermore expressed in neurons (Wild, Klems et al. 2017). Given the fact that the function of vascular Flt1 in vessel development is not understood yet, it is surprising how little attention has been paid to the role of its specific ligands PlGF and VEGF-B. A fundamental first step herein would be to understand their developmental expression patterns. This lack of studies is presumably due to the fact that *Plgf* expression has been described as neglectable during development and health (Carmeliet et al. 2001), with the exception of pregnancy where *Plgf* is expressed in trophoblasts and placental villi (Dewerchin & Carmeliet 2012). In contrast, various studies report substantially increased *Plgf* expression levels in disease conditions (Dewerchin & Carmeliet 2012). *Plgf* is upregulated in the ischemic brain (Liu et al. 2006; Du et al. 2010) and in ECs during the acute phase of myocardial infarction (Iwama et al. 2006). However, it does not seem plausible why a factor with tremendous functions including vascular remodelling in disease conditions would not have a function in the greatest remodelling process, i.e. in embryonic vascular development. A detailed analysis of *Plgf* expression domains would be critical to fully understand its mechanism of action. Due to its upregulation in disease conditions, PlGF is regarded as a potential biomarker in the clinic. For example in patients having suffered from an acute myocardial infarction, increased PlGF levels are associated with an improved outcome (Takeda et al. 2009). An increased sFlt1/ free PlGF ratio has been proven to be a useful biomarker for the prediction and diagnosis of preeclampsia (Hod et al. 2015). Also *Vegfb* expression is not well analysed yet. In zebrafish, *vegfb* expression is only shown in a single *in situ* hybridization in the embryonic head, but with a rather poor quality (Jensen et al. 2015).

In summary, it will be worthwhile to analyse the expression of *flt1*, *plgf* and *vegfb* in detail in embryogenesis.

3.4.2 VEGF-A – KDR signalling

VEGF-A – KDR signaling is the major mediator of EC biology in developmental and pathological conditions, including cell differentiation, migration, proliferation and tube formation (Koch & Claesson-Welsh 2012). The significance of this pathway for angiogenic development becomes obvious in light of the fact that the *Vegfa* gene is haploinsufficient; already the reduction of VEGF-A levels by 50% in heterozygous *Vegfa*$^{-/+}$ mice is embryonically lethal due to insufficient blood vessel growth (Carmeliet et al. 1996; Ferrara et al. 1996). Equally harmful is the increase of VEGF-A levels, as also *Flt*$^{-/-}$ mutant mice, in which the VEGF-A protein bioavailability is increased, die during embryogenesis due to excessive, disorganised vessel sprouting (Fong et al. 1995). Thus, VEGF-A mRNA and protein levels have to be tightly regulated by numerous inducers as well as negative feedback loops for the development and maintenance of a functional vasculature, the cornerstone of a healthy organism.

Adaption of the vascular system in response to metabolic demands occurs by an increase of *Vegfa* mRNA levels in conditions with low oxygen tension. Under normoxic conditions the Hif1α subunit is hydroxylated, enabling the binding to the E3 ubiquitin ligase von Hippel-Lindau (VHL), which then initiates ubiquitylation and proteasomal degradation of Hif1α. In hypoxic states, Hif1α is not hydroxylated, thus cannot bind to VHL and is consequently not degraded. The stabilized Hif1α can then dimerize with Hif1β and induce the transcription of genes with hypoxia response elements in their promoter, such as VEGF-A (Pugh & Ratcliffe 2003).

VEGF-A protein bioavailability is regulated by Flt1, which acts as decoy receptor. In addition, the VEGF-A accessibility for KDR binding is mediated by the capacity of VEGF-A to diffuse. The diffusibility of the different VEGF-A isoforms depends on the presence of a basic amino acid stretch, which allows binding to NRPs and to heparan sulphate in the ECM. VEGF-A121 is considered as diffusible isoform, as it is lacking this basic stretch. VEGF-A165 possesses one basic stretch, rendering it less diffusible, and the other isoforms VEGF-A189 and VEGF-A205 even have several of these domains, thus they are regarded as rather stably anchored

in the tissue (Carmeliet & Tessier-Lavigne 2005). The zebrafish *vegfaa* has only the two splicing forms *vegfaa121* and *vegfaa165*.

Apart from the availability of the ligand, VEGF-A – KDR signalling is regulated in various other ways. Intensity and duration of KDR signalling is mainly regulated by the rate of KDR internalization, degradation and recycling (Koch & Claesson-Welsh 2012). One regulator of KDR internalization is NRP1, acting as KDR adaptor protein. When VEGF-A – NRP1 – KDR complexes are formed in *cis*, i.e. on the same cell membrane, NRP1 binds with its cytosolic PDZ-binding domain to PDZ domain-containing adaptor proteins and mediates the endosomal translocation of KDR. On the other hand, NRP1 associated in *trans* with KDR, i.e. on adjacent cells, may be antiangiogenic as it prevents KDR internalization (Simons et al. 2016). KDR activity is furthermore regulated by its phosphorylation status, which can be regulated by phosphotyrosine phosphatases (PTPs) (Mattila et al. 2008). PTPtb, for example, was shown to regulate KDR signalling important for arteriogenesis (Lanahan et al. 2014). In addition, KDR heterodimer formation, either with Flt1 or with VEGFR-3, might regulate KDR signalling, but whether such heterodimers have a function in vascular development *in vivo* is debated (DiSalvo et al. 1995; Cao et al. 1996).

Phosphorylated KDR can bind to different SH2 domain-containing proteins and thereby activate different signalling pathways. Activation of PLCg by KDR in turn activates the RAF – MEK – ERK1/2 pathway important for EC migration, proliferation and homeostasis, as well as for regulating Flt1 and VEGF-A expression levels as feedback loop. KDR-mediated activation of PI3K induces AKT phosphorylation, important for EC survival, vessel maturation and metabolism. AKT can furthermore activate eNOS to trigger NO production in the adjacent smooth muscle cells (SMCs), important for vasodilation and vessel permeability (Simons et al. 2016).

3.4.3 VEGFR-1 (Flt1) and its specific ligands PlGF and VEGF-B

3.4.3.1 VEGFR-1 (Flt1)

VEGFR-1 (Flt1) has a membrane-bound (mFlt1) and a soluble form (sFlt1), which are produced via alternative splicing. With its 10-fold higher binding affinity to VEGF-A

compared with the Vegf-A binfing affinity of KDR, and its very weak tyrosine kinase activity Flt1 is a negative regulator of VEGF-A – KDR-mediated angiogenesis. For example, neuronal Flt1 prevents venous hypersprouting at the spinal cord in zebrafish by scavenging Vegfaa (Wild et al. 2017). The Flt1-specific ligand PlGF can replace VEGF-A from Flt1 (Park et al. 1994), suggesting that PlGF mediates VEGF-A scavenging by Flt1.

3.4.3.1.1 Can mFlt1 signal?

Whether mFlt1 is not only a VEGF-A sink but possesses the capacity to signal is controversially discussed. In embryonic sprouting angiogenesis mFlt1 signalling is not important, as *Flt1*$^{TK-/-}$ mice without the tyrosine kinase domain and *mflt1*$^{-/-}$ zebrafish do not show any vascular defects (Hiratsuka et al. 1998; Rossi et al. 2016; Wild et al. 2017), suggesting that both mFlt1 and sFlt1 act as VEGF-A scavengers to control KDR signalling. On the other hand, a recent study in zebrafish reports that both *plgf* and *vegfb* can rescue the vascular phenotype of *vegfaa*$^{-/-}$ mutants, i.e. reversal of DA defects and re-establishment of ISV growth. A mutated form of Plgf incapable of binding to Flt1 is not able to restore the vasculature in *vegfaa*$^{-/-}$ mutants, indicating that the rescue was due to Plgf – Flt1 signalling (Rossi et al. 2016). However, most studies on mFlt1 signalling report a function in macrophage chemoattraction (Murakami et al. 2006; Shibuya 2006).

Regarding Flt1 downstream signalling, VEGF-A and PlGF cause the phosphorylation of different tyrosine residues, suggesting different downstream activation pathways of the two ligands (Autiero et al. 2003). PlGF-induced Flt1 phosphorylation can stimulate the Akt pathway important for EC survival (Vieira et al. 2010). Receptor transphosphorylation is an alternative theory on mFlt1 signal propagation. KDR phosphorylation levels were reduced in *Plgf*$^{-/-}$ mice although PlGF cannot bind to this receptor, suggesting that PlGF amplifies KDR homodimer phosphorylation by inducing its transphoshorylation via the Flt1 homodimer (Autiero et al. 2003). However, the data on such a transphosphorylation are very limited, questioning the occurrence of such a transphosphorylation *in vivo.* With respect to Flt1 – VEGF-B signalling a recent study on Flt1 receptor conformation upon PlGF or VEGF-B binding could show that the two ligands bind to different Flt1 immunoglobulin (Ig) domains. Only PlGF binding induced an “activated” Flt1 dimer conformation in which its tyrosine kinases are close enough for transphosphorylation, whereas VEGF-B binding did not evoke such an activated dimer conformation, suggesting that from a conformational point of view PlGF

signalling via Flt1 is possible, whereas VEGF-B – Flt1 signalling is rather unlikely (Anisimov et al. 2013). In light of these numerous controversial reports on Flt1 signalling, it is important to pursue an unbiased experimental strategy.

3.4.3.2 PlGF – a known unknown?

Placental growth factor (PlGF) was first discovered in a human placenta cDNA library in 1991 (Maglione et al. 1991). *PlGF* has four isoforms in humans derived from alternative splicing with PlGF-1 and -3 being diffusible and PlGF-2 and -4 containing a heparin binding domain enabling the binding to the receptors NRP1 and -2 and to heparan sulphate. Mice and zebrafish express a single isoform (Dewerchin & Carmeliet 2012; Rossi et al. 2016).

PlGF was described as an important factor during the angiogenic switch in disease (Dewerchin & Carmeliet 2012), therefore most studies have focussed on PlGF in pathological conditions in which either blockade or delivery of PlGF can be beneficial. Descriptions of PlGF as functionally redundant for physiologic conditions awakened the hope of PlGF being the ideal candidate to target pathological angiogenesis without affecting any healthy tissue.

However, the outcomes of many studies were controversial, and researchers had to admit that a big flaw of the last decades of PlGF research was the lack of an in-depth characterization of the rather complex different scenarios of PlGF signalling. Proper deconstruction of these scenarios during development would be a fundamental first step in a proper understanding of PlGF's functions and usefulness in the clinic.

3.4.4 The VEGF family and the tip cell concept – many open questions

As a first step of sprouting angiogenesis, an endothelial cell of an existing vessel must be activated to become a tip cell. This occurs via VEGF-A – KDR signalling. To prevent that all ECs become a tip cell, the Dll4 – Notch signalling suppresses the tip cell fate via lateral inhibition according to the tip-stalk cell model. *Dll4* is upregulated by KDR signalling and induces Notch signalling in the adjacent cell. Notch signalling then downregulates the pro-angiogenic *KDR* and upregulates the anti-angiogenic *Flt1* in order to attribute to this EC a non-sprouting stalk cell phenotype. In turn, low *Dll4* levels in the stalk cells induce only low Notch signalling in the tip cell, leading to low *Flt1* and high *KDR* (Blanco & Gerhardt 2013).

However, according to this model Flt1 has to be expressed in a “salt and pepper” fashion, but substantial *in vivo* data on Flt1 distribution is missing to date. Another concept on sprout initiation involves the formation of an sFlt1 “corridor” to allow the activation of VEGF-A – KDR only in a single endothelial cell (Chappell et al. 2009). Again, such sFlt1 corridors or gradients have never been demonstrated by means of *in vivo* protein localization analysis. In the growing sprout, Jakobsson et al. (2010) propose that ECs permanently compete for the tip cell position, suggesting that the tip-stalk phenotype is dynamic, but the function of this shuffling remains unclear. The sprout direction in the mouse retina is proposed to be dependent on VEGF-A gradients (Ruhrberg et al. 2002; Gerhardt et al. 2003). However, how such gradients could be formed in the developing embryo is unclear.

3.5 Hemodynamics – an architect of the vascular system

Hemodynamic forces are main mediators of vessel architecture adaption to variations in blood flow, which in turn reflect changes in metabolic needs. Three forces acting on a blood vessels are important mechanical stimuli: shear stress is the force parallel to the vessel surface by blood flow friction; the circumferential stress is exerted by blood pressure; axial stress derived from vessel deformation (Hoefer et al. 2013). Due to its location at the inside of the vessel, the EC layer is directly exposed to shear stress, the most important force for remodelling and this layer possesses distinct mechanotransduction mechanisms,

The quintessence of hemodynamics and vascular architecture is the adequate supply of all tissues with the smallest possible energy input. In the early 20th century, Murray postulated that the energy to produce the blood volume that is pumped through a vessel is proportional to the energy of the actual blood pumping process through that vessel (Painter et al. 2006). According to Murray’s law, the optimum of these energies is reached in a branched vasculature, if the relation between the radius of a parent vessel (r_p) upstream of a branch and the radius of the downstream daughter vessels (r_d) conforms to $r_p^3 = r_{d1}^3 + r_{d2}^3$.

Another important haemodynamic law is from Poiseuille, describing the relation between hydraulic resistance, blood vessel length, radius and blood viscosity (Figure 6a). As the latter is usually constant, the resistance of a given vessel is depending on the vessel radius, and already small changes of the radius have a large impact on the resistance ($1/r^4$); doubling of the radius or diameter decreases the resistance by the factor 16 and consequently increases

the flow by 16 (Figure 6b). With respect to resistance it is furthermore important that in a serial vessel arrangement the resistances of the single vessels are added ($R_{total}= \Sigma R_{individual}$), whereas a parallel arrangement reduces the total resistance ($1/R_{total}=1/\Sigma R_{individual}$).

Shear stress evokes fast cellular responses, including the flow-sensitive ion channel activation, changes in the intracellular pH and induction of Ca^{2+} fluxes in the cell; subsequently, the activation of different pathways induces specific gene expression profiles, which ultimately lead to cytoskeletal reshaping and vascular remodelling (Mazzag et al. 2003). Recent studies could show that also VEGFR- and -3 were involved in mechanosensory complexes (Baeyens & Schwartz 2016). According to the shear stress set point theory any shear stress above a certain range induces outward remodelling, whereas a lower shear stress results in inward remodelling (Baeyens & Schwartz 2016). However, the gene expression profile varies with the type of shear stress acting on a vessel. Atherosclerotic plaques, for example, develop in regions of oscillatory and low shear stress, whereas such wall thickening is rare in vessels of high, constant shear stress (Mazzag et al. 2003). In the ECs in atherosusceptible regions, however, a reduced expression level of the protective eNOS as well as the Krüppel-like factor (KLF)2 and KLF4 and an increase in the pro-inflammatory nuclear factor (NF) κ B pathway is observed (Davies et al. 2013).

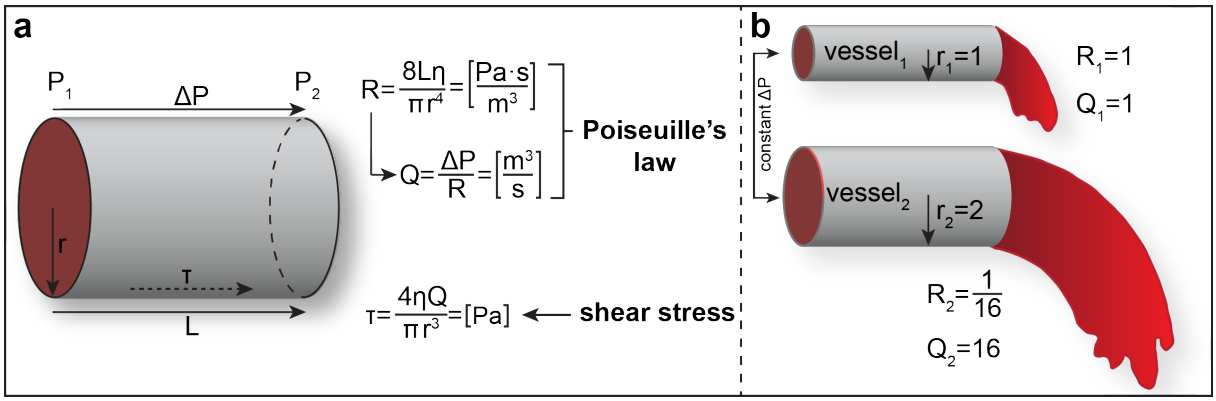

Figure 6| Poiseuille's law.

(**a**) Poiseuille's law mathematically describes flow in a cylindrical tube. Shear stress is the tangential force at the vessel wall arising from friction of the blood against the vessel. Note that shear stress is increasing with flow, and that these formulas reveal the large impact of the radius on shear stress, flow and resistance**.** (**b**) Example of the impact of radius increase on Q and R according to Poiseuille's law. In case of a constant Δ P, a doubling of the radius results in a decrease of the resistance and an increase of the flow both by the factor 16. L, length;

P, pressure; Q, flow; r, radius; R, resistance; η, viscosity; τ, shear stress. Adapted from Silverthorn et al. (2016).

3.6 Regulation of the vascular network by nerves – the neurovascular link

Another instance that regulates the vascular development is the nervous system. Nerves and vessels are running in parallel in many parts of the body (Carmeliet & Tessier-Lavigne 2005) (Figure 7). Given their parallel pathways, the questions whether nerves and vessels depend on each other by mutual guidance or whether their development occurs independently bothered scientists for decades.

At the functional level there is a mutual dependence between vessels and peripheral nerves, explaining the need for their close proximity. Nerves are highly metabolically active and thus need the close contact to the vessels, while vessels rely on nerves for various processes. In the mouse skin it was shown that peripheral sensory nerves mediate arteriogenesis, and sensory axons dictate the path of artery vessels (Mukouyama et al. 2002). Also sympathetic nerves promoted arterial differentiation (Pardanaud et al. 2016). In addition, perivascular nerves are involved in the regulation of the vascular tone by releasing vasoconstrictive substances (Burnstock & Ralevic 1994).

At the molecular level, nerves and vessels are both guided by attractive or repulsive cues (Lowery & Van Vactor 2009), and they even share some guidance factors (Eichmann et al. 2005). Such factors with a dual function in axon and vessel guidance are called angioneurins (Carmeliet & Tessier-Lavigne 2005). As all four classical axon guidance families were found to be angioneurins, the question arose whether the reverse is also true for the classical angiogenesis proteins, i.e. if the VEGF family has functions in the neuronal system (Carmeliet & Tessier-Lavigne 2005). Recently, we found that several Vegf receptors, including *flt1* and *kdrl* and Vegf ligands including *vegfaa* and *plgf* are expressed in motoneurons (Wild et al. 2017). While neuronal Flt1 has the function to limit sprouting at the neural tube, the role of the ligands in neuronal development remains unclear so far.

With respect to sensory nerve-derived VEGF-A it is known that it is involved in arterial differentiation in the mouse skin (Mukouyama et al. 2002). In addition, VEGF-A was reported to be important for motoneurons, as VEGF-A could ameliorate the symptoms of the neurodegenerative disease ALS, but studies on a detailed function are missing to date. Likewise, VEGF-B – Flt1 are proposed as neuroprotective, but any details on mechanism are lacking (Poesen et al. 2008).

However, the neuronal system is highly branched and its development is greatly dynamic; as the studies on the Vegf ligands in neuronal development are relatively poor, a detailed analysis by live *in vivo* imaging is required to better understand the function of the Vegf ligands in the neuronal system.

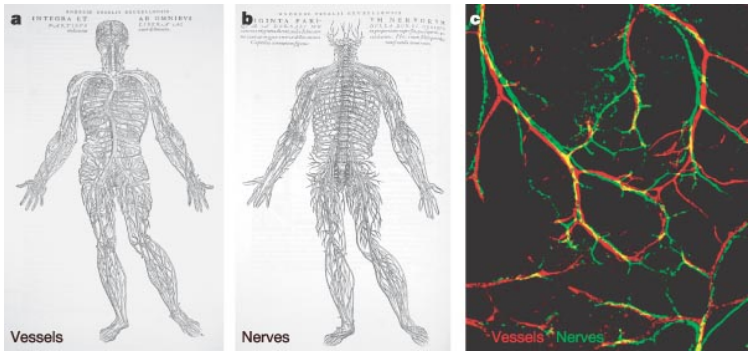

Figure 7| Neurovascular parallels.

(**a,b**) The drawing from anatomist Vesalius depicts that nerves and vessels both consist of highly branched networks. (**c**) Confocal image of aligned vessels in red and nerves in green. Modified from Carmeliet & Tessier-Lavigne (2005).

4 Results

4.1 Previous work and aim of the current study

Our research project was aimed at elucidating the role of the Vegf receptor-1 (Flt1) and its ligands in the morphogenesis of the vasculature using the zebrafish model system. Analysis of the *flt1* promoter activity as well as *mflt1* and *sflt1* expression by whole-mount *in situ* hybridization (WISH) revealed *flt1* expression in the aorta, arterial ISVs and remodelled artery-derived venous ISVs. In addition, analysis in *flt1* reporter embryos and RNAseq analysis of FAC-sorted neuronal cells derived from *Tg(HuC:EGFP)*^{as8} and *Tg(mnx1:GFP)*^{ml2} neuronal transgenic reporter embryos uncovered substantial expression of *flt1* in the neuronal system. Expression in the nervous system is interesting since Mukouyama has noticed that the peripheral sensory nerves release VEGF-A, which may promote arteriogenesis via activation of NRP1 and KDR; capillaries are “upgraded” and start to express arterial markers like *ephrinb2* and *Nrp1*.

To understand the potential contribution of vascular Flt1 and neuronal Flt1 in vascular morphogenesis, we subsequently generated tissue-specific *flt1* mutants and constitutive full- and isoform-specific mutants. We next compared the vascular and neuronal phenotypes of the tissue-specific mutants with the phenotypes observed in the constitutive *flt1* mutant embryos (Wild, Klems et al. 2017). *Flt1* full mutants developed severe vascular hyperbranching at the level of the neural tube, whereas the nervous system showed no obvious dysmorphogenesis. Neuron-specific deletion of *flt1* phenocopied the vascular hyperbranching phenotype. Interestingly, ablation of vascular *flt1* did not affect branching of the trunk vasculature in zebrafish embryos. Using a panel of mutants with *vegfaa* gain of function (GOF) scenarios, we subsequently showed that neurons are a prominent source of Vegfaa, a potent pro-angiogenic cytokine. *Pten* mutants and *vhl* mutants showed increased neuronal *vegfaa* and hyperbranching at the level of the neural tube, similar to the *flt1* mutants. Combining *flt1* mutants with *vhl* mutants resulted in even more pronounced excessive branching and complex branched networks at the spinal cord level. Based on these observations we proposed the following mechanism of action: During early embryogenesis neurons produce sFlt1, which restricts angiogenesis at the neurovascular interface in response to neuron-derived Vegfaa. Neurons are a prominent source of Vegfaa at early stages besides somatic Vegfaa, which appears relevant for promoting arterial identity in

vessels (Swift & Weinstein 2009). Loss of neuronal *sflt1* or gain of neuronal *vegfaa* promotes sprouting angiogenesis at the neurovascular interface. Loss of *sflt1* combined with increased *vegfaa* mRNA levels even promotes sprouting into the neural tube. We could furthermore show that this mechanism determines the onset and extent of vascularization during development of the nervous system in wild type (WT) embryos.

Our observations were surprising in several ways. First of all, the tissue-specific mutants indicate that neuronal Flt1 and not vascular Flt1 is relevant for guiding branching morphogenesis. In contrast, all currently proposed models to explain sprouting angiogenesis and sprout guidance propose endothelial *flt1* expression, particularly in stalk cells, as crucial for sprout differentiation. Second, we find that neurons are a rich source of Vegfaa, and we find that neuronal Vegfaa and not somitic Vegfaa determines branching after 48hpf. Vessels are very sensitive to changes in Vegfaa, as are many other cell type including cardiomyocytes (Tintu et al. 2009). The physiological relevance for neurons to produce sFlt1 may be to protect neighbouring cells from exposure to toxic Vegfaa levels and uncoordinated growth. Third, we found that in loss of *flt1* mutants or gain of *vegfaa* models angiogenic sprouting emanated from veins, a vascular domain with comparatively low *flt1* expression. Using cell tracking experiments we demonstrated that only 8% of the veins giving rise to sprouts consisted of endothelial cells expressing *flt1*. In 92% of cases venous sprouts were derived from “pure” vein-derived endothelial cells and devoid of *flt1*.

Our vessel-specific *flt1* mutants, substantiated by transplantations of *flt1*$^{-/-}$ mutant ECs into WT hosts, strongly suggest that vascular Flt1 is redundant for sprout differentiation and guidance. However, *TgBAC(flt1:YFP)*^{hu4624} and WISH using probes selective for *mflt1* or *sflt1* demonstrate vascular *flt1* expression (Krueger et al. 2011). It is thus puzzling what the physiological role of vascular Flt1 may be if it is not the regulation of branching or tip/stalk cell differentiation.

Alternatively, perhaps the current models explaining sprouting based on vascular Flt1 may show caveats. In fact, the experimental evidence conclusively showing that endothelial Flt1 in growing vessels is indeed necessary and sufficient to affect sprouting is limited to only two studies. Both studies show shortcomings in demonstrating the source, distribution, kinetics,

and half-live of (soluble) *flt1* mRNA and protein (Chappell et al. 2009; Ho et al. 2012). Thus far, to our knowledge, no studies are available showing the Flt1 protein localization in developing vascular networks. Also the potential contribution of the concentration and distribution of the Flt1 ligands has not been considered. We therefore decided to reconsider the current concepts on the role of vascular Flt1, using an unbiased approach by employing a combination of mutants, gain of function transgenics and knock-ins. We started with mapping the expression of *flt1* at the levels *flt1* promoter activity, *flt1* mRNA expression and Flt1 protein distribution. For the latter, we generated novel *flt1-HA* tagged knock-in transgenic fish (*TgTm(flt1_E3_HAHA)*^{ka601}), allowing for the first time evaluation of Flt1 protein in *in vivo* model systems. We furthermore addressed the contribution of the Flt1-specific ligand Plgf using genetic loss and gain of function approaches. Taken together, our data revealed a hitherto unknown role of arterial Flt1 in regulating the extent of structural outward remodelling of arterioles. In ischemic cardiovascular diseases, outward remodelling of collateral arteries critically determines the flow delivery to the compromised hypo-perfused regions. In this context we present a model how arterial Flt1 could act as a sink for therapeutically relevant and safe levels of Vegfa that can be released and utilized by strategically targeting of Plgf in the local environment.

4.2 *Flt1* expression and protein localization in the zebrafish embryo

Current models in angiogenesis research postulate that *flt1* is only expressed in the stalk cells but not in the tip cells of growing sprouts (Kappas et al. 2008; Chappell et al. 2009). In our unbiased approach we decided to re-examine the *flt1* expression pattern in angiogenic sprouts of developing blood vascular networks in the trunk of the zebrafish embryo. For this purpose we took advantage of the *TgBAC(flt1:YFP)*^{hu4624} transgenic fish allowing *in vivo* visualization of *flt1* promoter activity. From early developmental stages onward we found that *flt1* was predominantly expressed in the arterial system; aorta and arterial intersegmental vessels readily expressed YFP, the PCV lacked *flt1* expression. It is established that formation of the aISVs is driven by Vegfaa and depends on Notch signalling (Gore et al. 2012). In the current angiogenesis models, it is postulated that Vegfaa activates Kdrl signalling in tip cells, leading to the expression of *dll4* in the tip cells. Dll4 subsequently activates Notch receptors in stalk cells. As a consequence, *kdrl* and *flt4* are downregulated in

stalk cells, whereas *flt1* is upregulated, collectively reducing Vegfaa responsiveness in stalk cells. In the current models, active Notch is proposed to directly act on *flt1* promoter activity to stimulate expression. If this concept were indeed true, one would expect a kind of "salt and pepper" pattern for *flt1* expression/promoter activity. Careful examination of *TgBAC(flt1:YFP)*^{hu4624} in the developing arterial ISV sprouts, however, revealed *flt1* expression in tip cells, stalk cells and base cells as well as in the endothelial cell in the dorsal part of the aorta (Figure 8a-e). Similar expression patterns were previously noticed with both *sflt1* and *mflt1* mRNA *in situ* probes (Krueger et al. 2011).

However, promoter activity and mRNA expression do not reveal whether the protein is actually produced and expressed. To address this issue we considered two strategies: 1) knock-in of a reporter tag (double HA) into the endogenous *flt1* locus (Figure 8m-o), and 2) vascular specific overexpression of HA tagged soluble *flt1* constructs (Figure 8f-l). Transgenic fish and data for both strategies were generated by Raphael Wild. We considered that with this dual approach we should be able to obtain sufficient resolution to detect Flt1 protein expression by endothelial cells and the distribution of sFlt1 protein around growing vessels.

In order to analyse the endogenous Flt1 protein distribution, a CRISPR/Cas9-mediated knock-in of the HAHA tag into the zebrafish *flt1* gene was performed. By parallel injection of an sgRNA targeting Exon 3 of *flt1* (*sgRNA*^{fltE3}), *Cas9* mRNA and an oligonucleotide composed of the HAHA tag flanked by left and right *flt1* homology arms, the knock-in line *TgTm(flt1_E3_HAHA)*^{ka610} was generated. This line has a HAHA knock-in in exon 3, coding for the extracellular Ig1 domain (Figure 8m), thus both sFlt1 and mFlt1 are tagged. Surprisingly, when an anti-HA immunohistochemistry (IHC) was performed in *TgTm(flt1_E3_HAHA)*^{ka610} embryos, Flt1 protein was found on membranes and in the immediate vicinity of the aISVs at 32hpf (Figure 8n,o). In addition, Flt1 protein was found close to EC nuclei in aISVs. This staining detected both mFlt1 and sFlt1, so this experiment showed that the endogenous sFlt1 stayed contiguous to the aISVs. Flt1 in the DA was localized adjacent to the hypochord.

In a second approach, we labelled the sFlt1 with a double HA tag and expressed it under the ISV-specific *flt1*^{enh} promoter (Bussmann et al. 2010). These fish were embryonically lethal because the growth of ISVs was prevented (data not shown), suggesting that the function of sFlt1 to reduce angiogenesis by scavenging Vegfaa was not affected by the HAHA tag. In

order to generate a viable transgenic line for protein localization analysis, the HAHA-tagged *sflt1* was mutated by deleting 7 amino acids at the Vegfaa binding site (sFlt1_Δ7). Using *tol2* transgenesis the stable line *Tg(flt1^{enh}:sflt1_ Δ7-HAHA)^{ka611}* could be generated (Figure 8f).
In line with the knock-in approach, IHC with an anti-HA antibody in the double transgenic line *Tg(kdrl:hsa.HRAS-mcherry)^{s916};Tg(flt1^{enh}:sflt1_ Δ7-HAHA)^{ka611}* revealed that sFlt1 protein was localized directly on the primary aISVs at 30hpf, and no diffusion and gradient of sFlt1 could be observed (Figure 8g-i). Green dots dispersed along the complete trunk were unspecific background, as these were also found in control WT embryos (Figure 8h,k, rectangular inlets). At 48hpf sFlt1 protein was still in the immediate vicinity of the aISVs (Figure 8j-l, arrowheads in k indicate aISVs). In line with the *flt1* expression data on vISVs, which had been remodelled from aISVs, there was sFlt1 protein detectable in the dorsal part, belonging to the former aISVs (Figure 8k, asterisk indicates vISV). sFlt1 protein was furthermore found in the DA, and interestingly, it was mainly localized in its dorsal part close to the hypochord at 48hpf (Figure 8k, yellow dotted line).

Taken together, in *TgBAC(flt1:YFP)^{hu4624}* we found no “salt and pepper” *flt1* expression pattern; instead, we found *flt1* expression throughout the developing sprout in tip, stalk and base cells. In the *TgTm(flt1_E3_^{HAHA})^{ka610}* transgenic fish we found a similar pattern: Flt1 protein was expressed throughout the developing arterial sprout and in the axial arteries. Except for the remodelled artery-derived venous endothelial cells, the venous domain was devoid of Flt1 protein. In the *Tg(flt1^{enh}:sflt1_ Δ7-HAHA)^{ka611}* we found that the majority of the Flt1 protein remains at or closely around the endothelial cell membrane and, surprisingly, in the nucleus. These data suggest that all arterial endothelial cells in sprouting arterial blood vessels expressed Flt1 protein, and that sFlt1 produced by vascular endothelium, if at all, did not diffuse far.

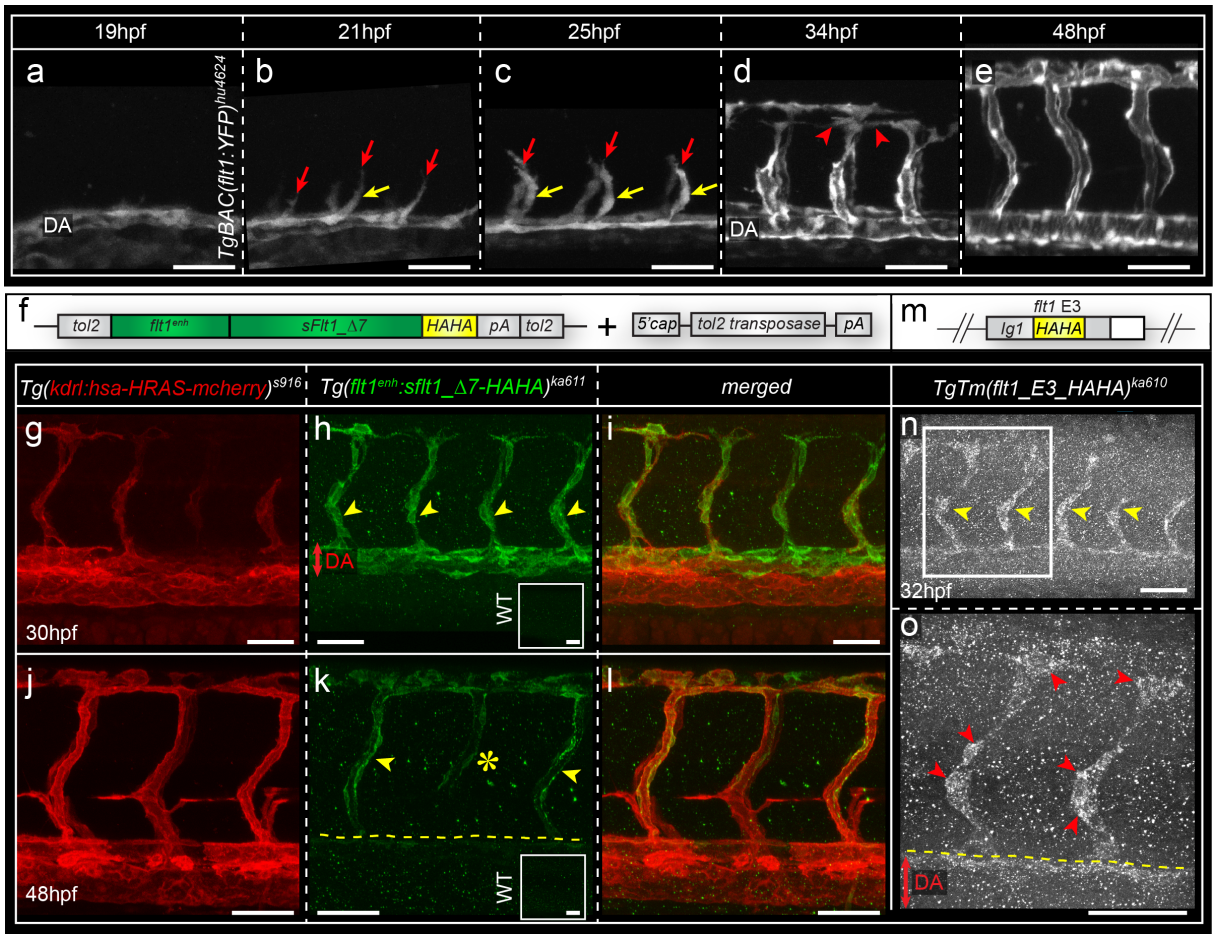

Figure 8| *Flt1* expression and protein localization.

(**a-e**) Still images of a confocal time lapse of the *flt1* reporter line *TgBAC(flt1:YFP)*^{hu4624}. (**a**) *Flt1* is expressed in the DA. (**b,c**) In the nascent arterial sprout, *flt1* is expressed in the tip (red arrows) as well as in the stalk cells (yellow arrows). (**d**) *Flt1* expression is also found in the anastomosing tip cells in DLAV formation (red arrowheads). (**e**) At 48hpf, *flt1* is expressed in the complete aISVs, the DA and in the DLAV. (**f**) Depiction of the strategy for generating the transgenic line *Tg(flt1*^{enh}*:sflt1__ Δ 7-HAHA)*^{ka611}. (**g-l**) Representative confocal images of an IHC staining with an anti-HA antibody in the double transgenic line *Tg(kdrl:hsa.HRAS-mcherry)*^{s916}*;Tg(flt1*^{enh}*:sflt1_ Δ 7-HAHA)* ^{ka611}. For control embryos (rectangular inlets in h,k) IHC was performed in WT embryos in parallel to the *Tg(flt1*^{enh}*:sflt1__ Δ 7-HAHA)* and they were imaged with the same microscope settings as the transgenic embryos in g-l. Note that sFlt1 is not diffusing away from the ISV. (**i,l**) Note that merged images reveal that sFlt1 is distributed along the complete ISVs, showing that sFlt1 is not diffusing far away from the ISVs. In the DA at 48hpf, sFlt1 is localized in the dorsal part. (**m**) Depiction of the HAHA knock-in in *flt1* exon 3 encoding the Ig1 domain (*TgTm(flt1_E3_HAHA)* ^{ka610}). (**n**) IHC with an anti-HA antibody in *TgTm(flt1_E3_HAHA)* ^{ka610} embryos at 32hpf. Note that both mFlt1 and sFlt1 are localized very close to the aISVs over the whole ISV length. Furthermore, they can be detected in the dorsal DA close to the hypochord. (**o**) Magnification of n as depicted by white rectangular inlet. Note that Flt1 protein is accumulating in EC nuclei. Yellow arrowheads in h,k,n, aISVs; yellow asterisk in k, vISV; yellow dotted line in k,o, position of the hypochord; red arrowheads in o, positionE3, exon3. Scale bar, 50µm. All data were generated by Raphael Wild.

4.2.1 *Plgf* expression in the zebrafish embryo

Our genetic data already challenged the concept that vascular Flt1 is relevant for sprouting angiogenesis involving stalk cell-specific production of Flt1 (Wild, Klems et al. 2017). Our protein distribution data confirmed our idea that current concepts on Flt1 may be incorrect. Instead, our observations suggest that Flt1 protein can be produced throughout the sprout and Flt1 protein does not diffuse far; both these aspects conflict with the proposed models. This leaves us with the fundamental question: What is then physiological the function of vascular Flt1 in growing networks? Evidence is accumulating suggesting that Flt1-specific ligands like Plgf compete with Vegfa for binding at Flt1 and thereby change Vegf bio-availability. In ischemic diseases, Plgf may be beneficial in promoting blood flow recovery. Outward remodelling – a structural increase in the diameter – of collateral arterial networks is a key-factor determining ischemic outcome. In our setting, Flt1 mRNA as well as protein is specifically expressed in arteries. Hence, this leaves open the possibility that the Plgf-Vegf-Flt1 axis may contribute to the regulation of arterial calibre. We postulate that Plgf may compete with arterial Flt1-bound Vegfa resulting in the local release of (low dose) Vegfa in direct vicinity of Kdrl receptors, thereby promoting arterial growth. To test this scenario we first cloned and mapped the expression of the Flt1 ligands *plgf* and *vegfb*.

Recently, we found that not only *sflt1* but also *vegfaa* and *plgf* were expressed in FAC-sorted cells from a pan- and a motoneuronal zebrafish reporter line (Wild, Klems et al. 2017) and we were the first to clone zebrafish *plgf* from cDNA (A. Klems, diploma thesis). By generating an RNA *in situ* probe and performing WISH, we found expression predominantly in circular areas in the centre of each somite in a bilateral fashion (Figure 9a-c), resembling the primary motoneurons (PMNs). These expression domains were specific as no signal was detectable using a sense RNA probe (Figure 9d).

To further proof that these areas were PMNs, in the present study we took advantage of two fluorescent motoneuronal reporter lines, *Tg(nrp1a:GFP)*^{js12} and *Tg(mnx1:GFP)*^{ml2} (Figure 9p,q). In these lines, *plgf* WISH was performed at 24hpf when its signal peaked (Figure 9f,i,l), followed by an anti-GFP staining (Figure 9e,h,k) to overcome possible detection limitations by photo bleaching of the GFP during the WISH procedure. Indeed, *plgf* colocalized with

mnx^{+} as well as *nrp1*$^{+}$ motoneuronal cells (Figure 9g,j,m). This was the first time that colocalization of *plgf* with its receptor *nrp1a* was shown in the embryo.

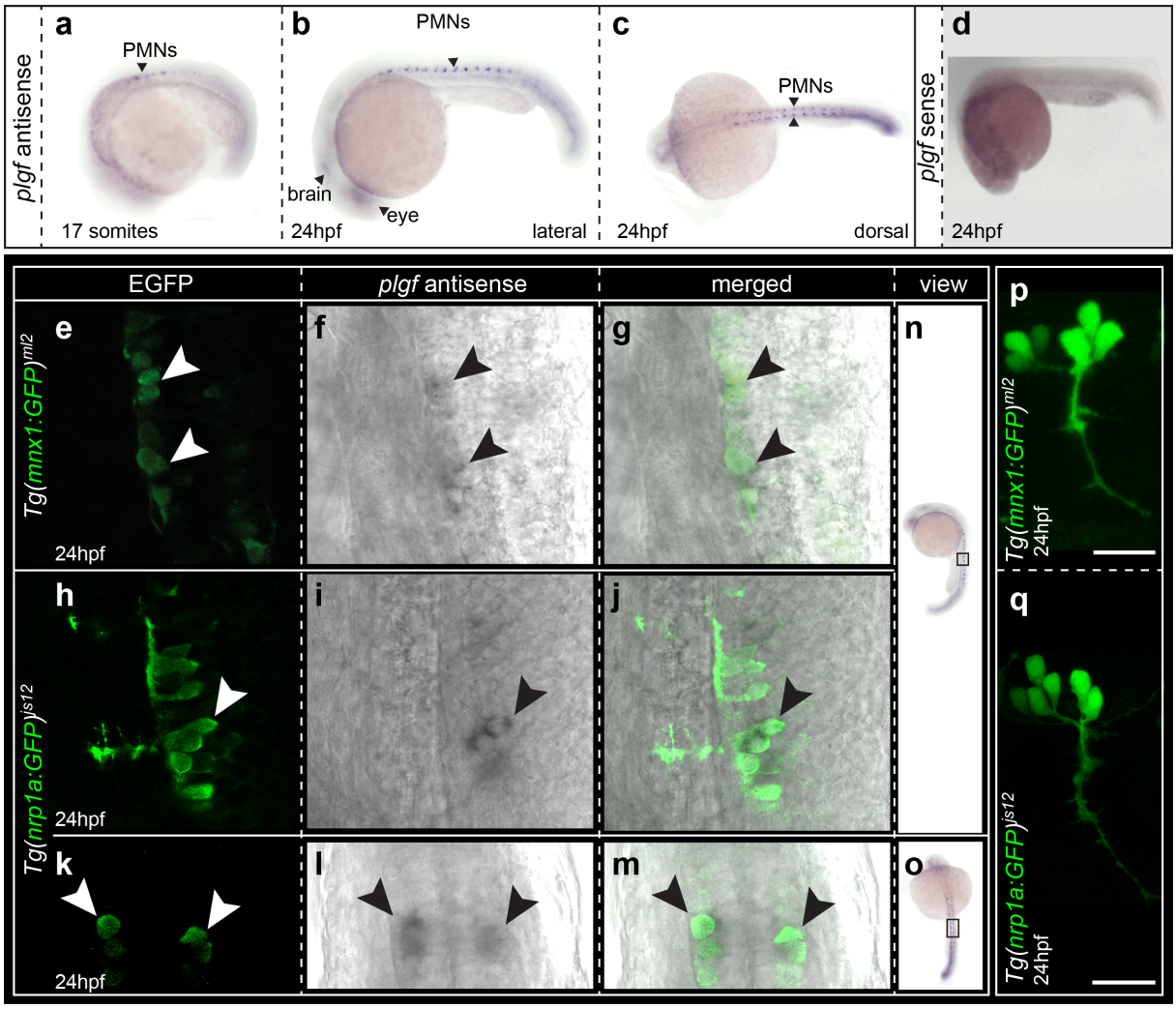

Figure 9| WISH of *plgf* in the zebrafish embryo.

(**a-c**) WISH of *plgf* using an antisense RNA probe. (**a**) *Plgf* expression in the PMNs starts at the 17 somite stage. (**b,c**) At 24hpf *plgf* is expressed bilaterally in the PMNs as well as in the eye and brain. b, lateral view; c, dorsal view. (**d**) WISH of *plgf* sense RNA probe does not show any staining, indicating that stainings in a-c are specific. (**e-m**) WISH of *plgf* antisense RNA probe in motoneuronal reporter lines at 24hpf; with e-j from a lateral and k-m from a dorsal view as outlined in o and p, respectively. (**e,h,k**) Confocal images of anti-GFP staining of *Tg(nrp1a:GFP)*^{js12} and *Tg(mnx1:GFP)*^{ml2}. The staining was performed after the WISH. (**f,i,l**) Transmitted light images of *plgf* WISH, with *plgf* expression in dark grey as indicated by black arrows. (**g,j,m**) Merged images of motoneuron transgenic lines and *plgf* expression. Note that *plgf*-expressing cells colocalize with *mnx1*$^{+}$ and *nrp1a*$^{+}$ cells as marked by arrowheads. (**p,q**) Confocal images of *Tg(nrp1a:GFP)*^{js12} and *Tg(mnx1:GFP)*^{ml2} at 24hpf. Note that both are expressed in PMNs. PMNs, primary motoneurons; WISH, whole-mount *in situ* hybridization. Scale bar, 25µm in p,q. a-d, from diploma thesis, A. Klems.

A common limitation of expression detection via WISH is that this technique is restricted to relatively young embryos. Likewise, *plgf* WISH signals were fading after 24hpf until almost no signal could be detected anymore at 32hpf. In order to analyse whether this signal decrease reflected an endogenous decline of *plgf* expression, we took advantage of another technique to visualize endogenous gene expression, namely bacterial artificial chromosome (BAC) transgenesis (Bussmann & Schulte-Merker 2011). Therefore, we chose two different BACs, which both contained the complete *plgf* gene as well as large 5' and 3' genomic regions (Figure 10r). These large upstream and downstream regions were needed to maximise the likelihood that the BACs contained all elements regulating *plgf* gene expression. Via several recombineering steps the fluorescent marker mCitrine was pasted directly behind the ATG start codon of *plgf*, and *tol2* sites were inserted into the BAC backbone. Upon injection of the BACs together with *tol2 transposase* mRNA into embryos at the one cell-stage, the endogenous *plgf* expression could be imaged in the developing embryos.

At 32hpf *plgf* expression was observed in the somata and axons of primary motoneurons with both recombined BACs (Figure 10a,p). This was in line with the WISH experiment (Figure 9) and Taqman data of motoneuronal cells (Wild, Klems et al. 2017), indicating that the detected fluorescence was specific. During development *plgf* expression was expanding in the neuronal system (Figure 10g-o). Interestingly, another expression domain of *plgf* was the hypochord (Figure 10d-q), a row of single cells directly attached to the dorsal part of the dorsal aorta, where Flt1 protein is localized (Figure 8g,j). In addition, *plgf* was expressed in the somites where also *vegfaa* expression is reported (Jensen et al. 2015), more precisely in the skeletal muscles (Figure 10g,j,m,q).

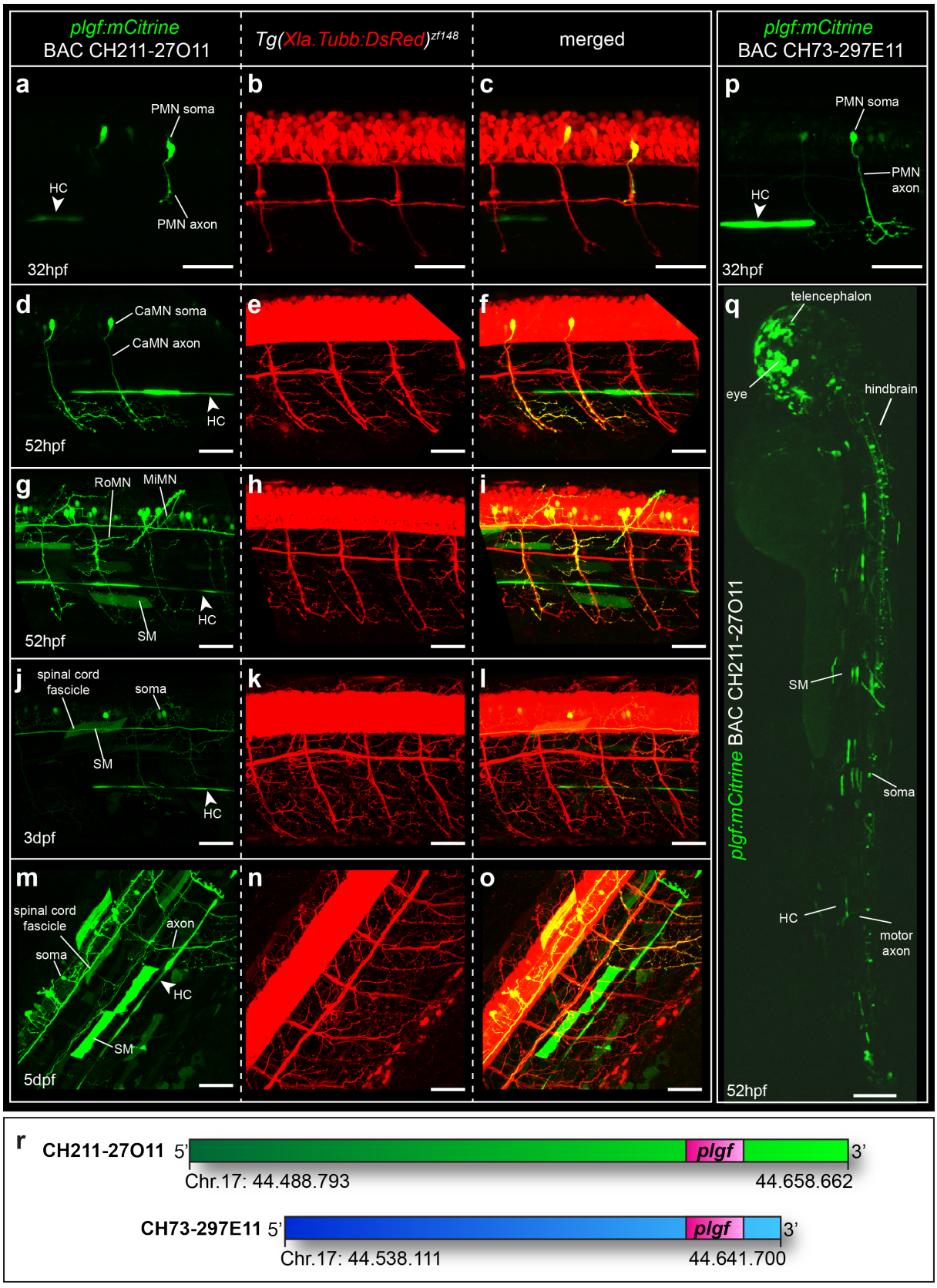

Figure 10| Analysis of *plgf* expression via BAC transgenesis.

(**a-q**) Representative confocal images of mosaically expressed *plgf:mCitrine* using BAC transgenesis; a-o in the pan-neuronal reporter line *Tg(Xla.Tubb:DsRed)*^{zf148}. (**a-c,p**) *Plgf* is expressed in PMNs and in the HC at 32hpf. Note that two different recombined BACs reveal the same *plgf* expression domains. (**c,f,i,l,o**) Colocalization of

plgf:mCitrine and *Tg(Xla.Tubb:DsRed)*^{zf148} (yellow areas) confirms *plgf* expression in neuronal somata and axons of all three motoneuron types, i.e. CaMNs, RoMNs and MiMNs, and in some interneurons. Note that *plgf* expression is expanding with age. Other expression domains of *plgf* are the HC and SMs. (**q**) Confocal tile scan of mosaic *plgf:mCitrine* expression at 52hpf. (**r**) Schematic illustration of the BACs used for recombineering and subsequent transgenesis. Note that both contain the complete *plgf* gene as well as a large 5' and a smaller 3' genomic region. CaMN, caudal secondary motoneuron; HC, hypochord; MiMN, middle secondary motoneuron; RoMN, rostral secondary motoneuron; PMN, primary motoneuron; SM, skeletal muscle. Scale bar, 50µm in a-f; 200µm in g.

4.2.2 *Vegfb* identification and its embryonic expression in the zebrafish

When we started to analyse the second Flt1-specific ligand *vegfb*, no studies on *vegfb* in zebrafish were available and the genomic annotations were rather poor. As two *vegfb* variants on different chromosomes are annotated in the genome browsers NCBI and ENSEMBL, *vegfba* (NCBI Gene ID: 101885552) and *vegfbb* (NCBI Gene ID: 100535766), in a first step we had to ascertain which of these variants was likely to be the homologue of human *Vegfb*. *Vegfba* has two annotated transcripts (Figure 11c) with isoform 2 encoding a protein with a length of 246aa (XP_005157219.1) and isoform 1 encoding a protein of 130aa (XP_009306029.1). Conserved domains search (NCBI) revealed that both isoforms contain a cysteine knot motif, which is a hallmark of all Vegf ligands, a receptor binding as well as a dimerization interface. As also the protein translated from *vegfbb* contains these three domains, we had to use another method to assess which of these forms is the homologue of the human *Vegfb*. Therefore, we took advantage of the shared gene synteny analysis, in which the genomic surroundings of *Vegfb* in zebrafish and humans were scanned for common genes. Such a shared synteny analysis revealed that both the human *Vegfb* and the zebrafish *vegfba* share a gene in their upstream region. No shared gene synteny was found between zebrafish *vegfbb* and human *Vegfb*. Given these computational analyses, we decided to focus on *vegfba* for further analysis, hereafter called *vegfb* for simplicity.

In a next step, we analysed the expression patterns of *vegfb* during embryogenesis. To discriminate between the two isoforms, we designed different RNA antisense probes (Figure 11c). Probes 1 and 3 could bind to both isoforms, with probe 3 having a longer isoform 1-specific 3' end. Probe 2 was designed to specifically bind to isoform 1. At 30hpf WISH with

probe 3 revealed that *vegfb* was expressed predominantly in the hindbrain rhombomeres, in the eye and faintly in the fore- and midbrain (Figure 11a). At 3dpf strong *vegfb* expression was found in the complete brain. The expression in the eye persisted, and further domains were the intestines and the pharyngeal arches. However, *vegfb* was not expressed in the trunk vasculature or spinal cord. WISH revealed the same expression patterns with all three probes (data not shown), indicating that probably only isoform 1 is really transcribed *in vivo*, and we used this form of *vegfb* for our further analysis.

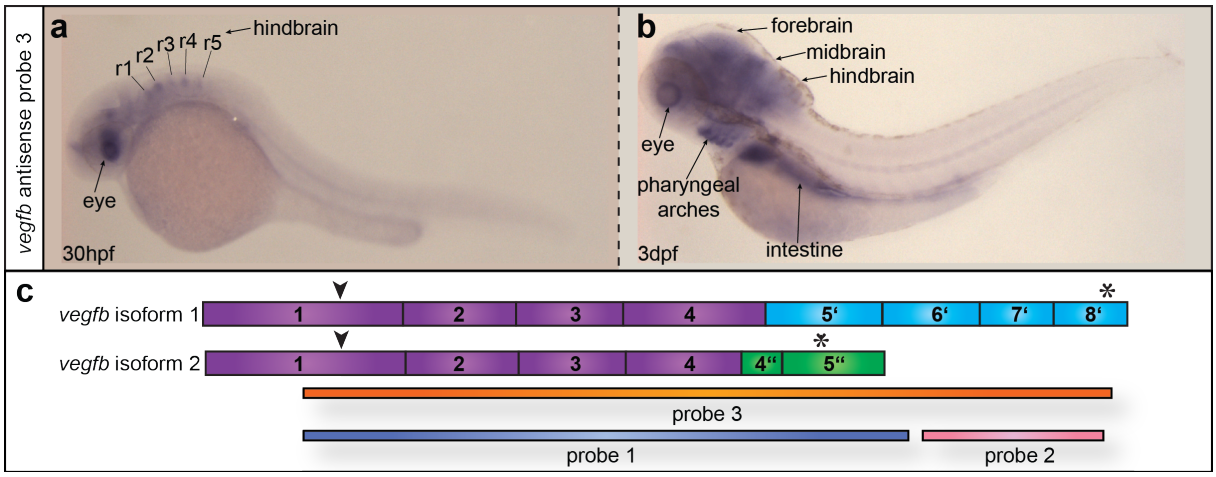

Figure 11| WISH of *vegfb* in the zebrafish embryo.

(**a**,**b**) WISH of *vegfb* using an antisense RNA probe that detects both *vegfb* isoforms (probe 3, localization is depicted in c). (**a**) At 30hpf *vegfb* expression is detected in the eye as well as in the hindbrain rhombomeres. The signal in the mid- and forebrain is relatively diffuse and weak. (**b**) At 3dpf *vegfb* is highly expressed in the complete brain as well as in the eye. Other expression areas are the intestines and the pharyngeal arches. Note that in trunk *vegfb* is neither expressed in the neuronal nor in the vascular system. (**c**) Depiction of the two *vegfb* isoforms and RNA probe localization. The first 3 exons and a large part of exon 4 are identical in the two isoforms. Due to alternative splicing isoform 1 is composed of 8 and isoform 2 only of 5 exons. RNA probes 1 and 3 detect both isoforms, whereas probe 2 should be specific for isoform 1. Arrowheads, start codon; asterisks; stop codons. Purple, common exons; blue; isoform 1-specific exons; green; isoform 2-specific exons. *Vegfb* isoform 1, XM_005157162.3; *Vegfb* isoform 2, XM_009307754.2. r1-5, rhombomeres 1-5.

4.3 Flt1 regulates arterial diameter

After having found that sFlt1 formed an arteriolar-associated pool together with mFlt1 and that *plgf* but not *vegfb* was expressed in the zebrafish trunk, we aimed at deciphering the functions of arterial Flt1 and the respective contributions of its ligands in the early arteriolar

tree in the trunk. Therefore, we performed a dynamic analysis of the ISV development during the first days of development. Time lapse confocal images of *flt1*$^{-/-}$ full mutants (*flt1*^{ka601}) lacking both *mflt1* as well as *sflt1* were carried out in the vascular reporter line *Tg(kdrl:hsa.HRAS-mcherry)*^{s916} from 25 to 73hpf (Figure 12). At 25hpf, during primary sprouting and before forming anastomoses with their neighbours, the diameter of the ventral part of the growing sprout was clearly enlarged in *flt1*$^{-/-}$ mutant compared with WT ISVs (Figure 12a,b). After the completion of anastomosis formation and the onset of blood flow at 38hpf the ISV diameter over the whole ISV length was increased in the mutants (Figure 12c,d). At 73hpf no difference in ISV diameter between WT and *flt1*$^{-/-}$ mutants could be observed anymore. To assess the diameter of a single ISV, the diameter was measured at seven points along the ISV (Figure 12c) and the average was calculated (Figure 12c). Such quantification of ISVs in time lapse series corroborated the observations of a diameter increase upon loss of *flt1* and that at 3dpf the ISV diameter was equal in WT and in *flt1*$^{-/-}$ mutants (Figure 12i).

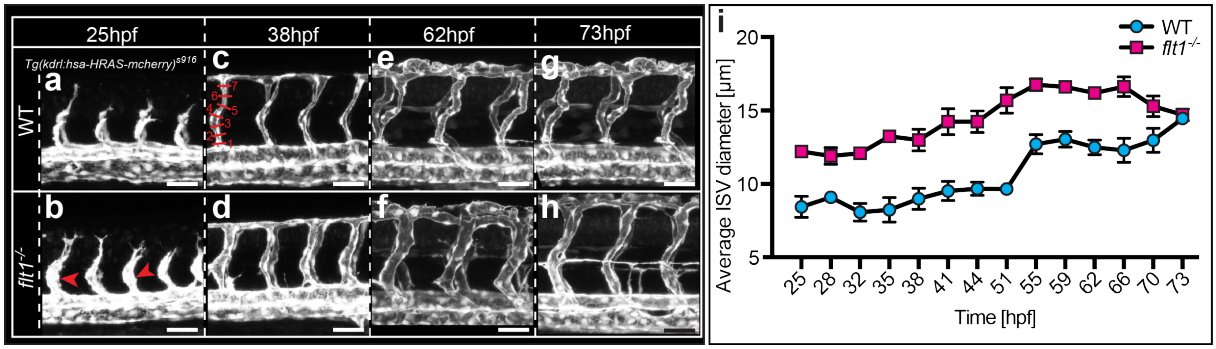

Figure 12| Dynamic analysis of ISV diameter in *flt1*$^{-/-}$ embryos.

(**a-h**) Still images of a confocal time lapse of the transgenic line *Tg(kdrl:hsa.HRAS-mcherry)*^{s916} with indicated time points. (**a,b**) The diameter of *flt1*$^{-/-}$ (*flt1*^{ka601}) ISVs is enlarged compared with WT during primary sprouting, especially in the ventral part of the emerging vessel as indicated by red arrowheads. (**c-f**) After the onset of blood circulation the vessel diameters of *flt1*$^{-/-}$ ISVs are still enlarged compared with WT. (**g,h**) At 3dpf there is no difference visible anymore between WT and *flt1*$^{-/-}$ ISV diameter. (**i**) Quantification of ISV diameter of WT and *flt1*$^{-/-}$ ISVs based on time lapse images. For each average ISV diameter, the diameter was measured at 7 points along the ISV as indicated in c and the average was calculated. Quantification in (i), mean ± s.e.m; n≥12 ISVs from ≥3 embryos per genotype and time point. Scale bar, 50µm.

4.3.1 Somitic *vegfaa* GOF

We found that the hypersprouting phenotype in *flt1*$^{-/-}$ was due to a gain of Vegfaa bioavailability at the level of the neural tube (Wild, Klems et al. 2017). To determine whether this was also the case for the diameter increase observed in *flt1*$^{-/-}$ mutants, we analysed whether overexpressing *vegfaa* could phenocopy their diameter increase. This overexpression was supposed to be done in a tissue where *vegfaa* is endogenously expressed, as increased Vegfaa levels in *flt1*$^{-/-}$ could only stem from a tissue where Vegfaa is in place anyway. As the neuronal gain of Vegfaa due to loss of neuronal *flt1* was responsible for another phenotype, namely venous hypersprouting at the neural tube at later developmental time point (Wild et al. 2017), we precluded the spinal cord as source of *vegfaa* for the observed diameter phenotype in *flt1*$^{-/-}$. As mentioned before, the other source of *vegfaa* in the early developing zebrafish embryo are the somites (Jensen et al. 2015), thus we overexpressed *vegfaa* under the skeletal muscle-specific promoter *503unc* (Berger & Currie 2013). As *Vegfa165* is the important isoform in mice (Maes et al. 2002) and because *vegfaa121* as well as *-165* both possess a similar angiogenic potential (Wild et al. 2017), we focussed on *vegfaa165* for GOF experiments. In order to track the expression of *vegfaa* with a fluorescent tag without affecting the protein functionality, the sequence of the self-cleaving peptide p2A was cloned between the GFP and the *vegfaa165* sequence (Wild et al. 2017).

In constitutive muscle cell-specific GOF of *503unc:GFP-p2A-vegfaa165* (*vegfaa165*^{cMC}, Figure 13a) the expression started before 20hpf, i.e. before the initiation of primary sprouting. At 30hpf the blood vessels were very disorganized, non-functional and resembled a tumour vasculature or hemangioma with uncontrolled EC proliferation (Figure 13c,d). This phenotype did not resemble the diameter increase observed in the *flt1*$^{-/-}$ mutants (Figure 12).

Notably, there were still ISV-like structures recognizable in *vegfaa165*^{cMC} embryos and their spacing was similar to WT (Figure 13c, white asterisks). Therefore, somatic *vegfaa* overexpression could not induce additional sprouts from the axial vessel.

We speculated that the timing of the onset of *vegfaa165* expression in the somites was crucial for the diameter increase and we decided to start the overexpression at a time point when the primary ISVs and the DLAV were already formed. A strategy for time-controlled

overexpression is the UAS/ Gal4-ERT2 system (Wild et al. 2017). Expression of *Gal4*, a yeast transcription activator protein, under a tissue-specific promoter of choice can activate the expression of upstream activator sequence (UAS)-linked genes. By fusing Gal4 to a variant of the human estrogen receptor ERT2, *Gal4* is only expressed in the presence of 4-hydrotamoxifen or endoxifen (Gerety et al. 2013; Wild et al. 2017).

For inducible *vegfaa165* GOF in the muscle cells (*vegfaa165*^{iMC}) we injected the two plasmids *503unc:gal4-ERT2* and *UAS:GFP-p2A-vegfaa165* into the one cell-stage of zebrafish embryos, added endoxifen at 28hpf, when the ISVs and DLAV were already developed, and started time lapse imaging at 32hpf (Figure 13a). At 32hpf the expression in the muscles had already commenced (Figure 13g) and the ISV diameter was increased in *vegfaa165*^{iMC} embryos compared to WT (Figure 13e,f). Over time the *vegfaa165* expression levels were rising and concomitantly the diameter continued to further augment (Figure 13h-s). Other than in *flt1*$^{-/-}$ mutants the ISVs enlargement was accompanied by a progressive disruption of the vessel integrity (Figure 13l,o,r, white arrowheads). Eventually, 20 hours after the expression induction the levels were that high that the ISVs in *vegfaa165*^{iMC} adopted a similar disorganized morphology (Figure 13u,v, red arrowheads) as in *vegfaa165*^{iMC} (Figure 13c,d). Quantification of the ISV diameter in *vegfaa165*^{iMC} embryos corroborated the observation that the diameter increased compared to WT until the ISV disintegration occurred at 48hpf (Figure 13w).

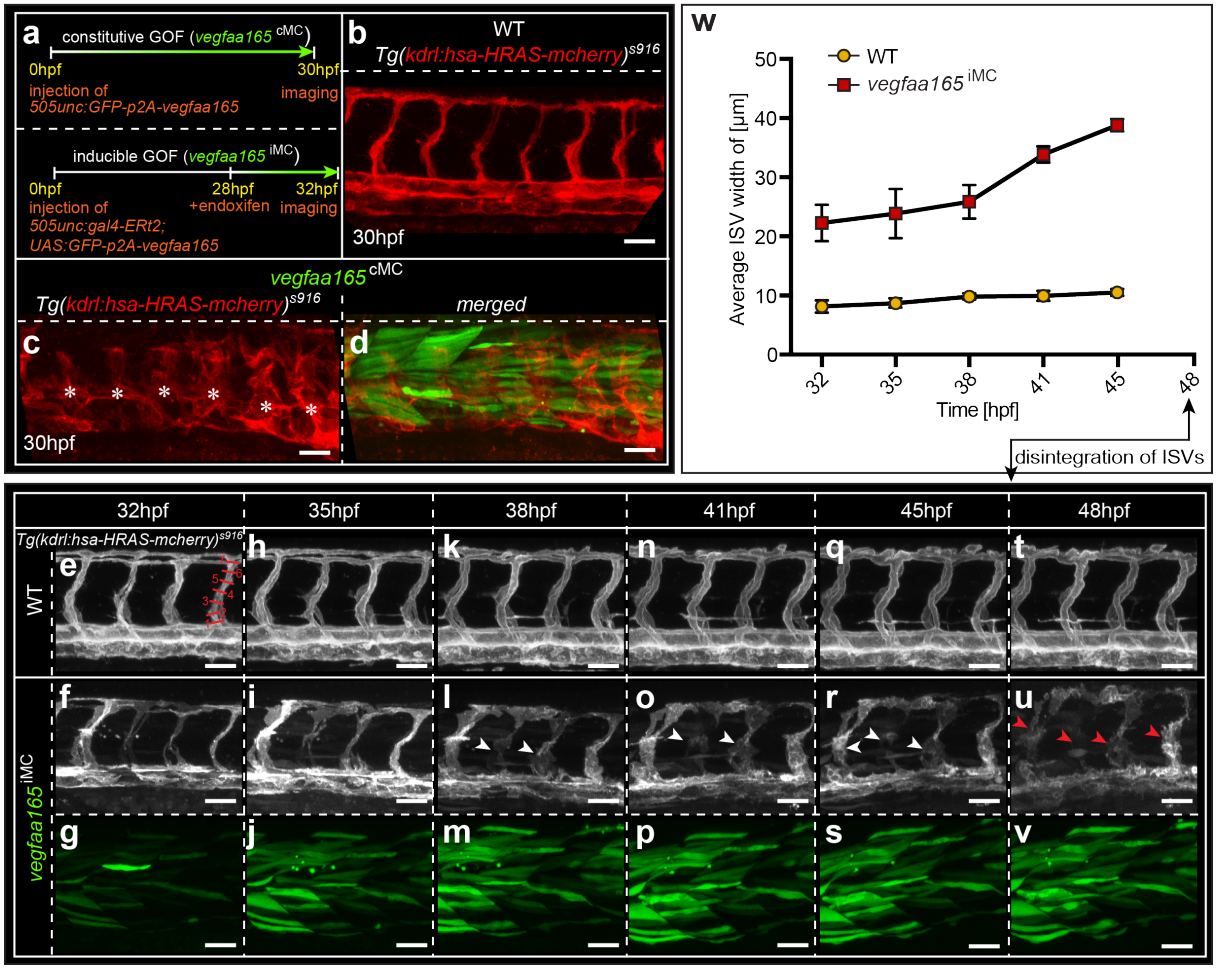

Figure 13| Analysis of the vascular phenotype of muscle-specific *vegfaa* GOF.

(**a**) Depiction of the different experimental procedures for muscle-specific *vegfaa165* GOF. For constitutive overexpression of *GFP-p2A-vegfaa165* in the somites under the muscle promoter *503unc* (*vegfaa*^{cMC}), the *vegfaa165* expression starts with the promoter activity of *503unc*, i.e. before 20hpf, and embryos are imaged at 30hpf. For inducible muscle cell-specific *GFP-p2A-vegfaa165* GOF (*vegfaa*^{iMC}) two plasmids encoding *503unc:gal4-ERT2* and *UAS:GFP-p2A-vegfaa165*, respectively, are injected at the one cell-stage and expression is induced at 28hpf via endoxifen administration; confocal imaging is started 4 hours later. (**b**) ISVs in the WT control. (**c,d**) Growth of ECs is highly uncoordinated in *vegfaa*^{cMC} embryos, resembling the non-functional vasculature of a tumour. Note that the discernible spacing between two ISV-like vessels, marked by white asterisks, resembles the normal distance between ISVs, thus no additional sprouts from the axial vessels were induced by *vegfaa*^{cMC}. (**e-v**) Still images of a time lapse of WT and *vegfaa*^{iMC} from 32hpf, i.e. 4h after the endoxifen induction, until 48hpf. (**e-g**) Note that *GFP-p2A-vegfaa165* has already commenced at the time lapse starting point and that the ISV diameter is increased compared to WT. (**h-v**) With increasing *GFP-p2A-vegfaa165* expression levels the ISV diameter is further growing. Note that ISV diameter augmentation is accompanied by progressive disruption of the vessel integrity, marked by white arrowheads in l,o,r, until they are completely disintegrated at 48hpf, indicated by red arrowheads in u,v. (**w**) Quantification of the ISV diameters in WT and *vegfaa*^{iMC} based on confocal time lapse images as shown in e-v. For determining the average diameter of one ISV, the diameter was measured at seven points as depicted in e and the average was

calculated. Note that there is a diameter increase in *vegfaa*^{iMC} until the vessels completely disintegrate. cMC, constitutive muscle cell-GOF; GOF, gain-of-function; iMC, inducible muscle cell-GOF. Quantification in (w), mean ± s.e.m; n=12 ISVs from 3 embryos per genotype and time point. Scale bar, in b-d 100µm, in e-v 50µm.

4.3.2 Overexpression of the Flt1-exclusive ligands *plgf* and *vegfb* – release of the endogenous Vegfaa reservoir?

The *vegfaa* GOF approaches showed that Vegfaa could augment the ISV diameter, but that the timing as well as the dosage was highly critical for vessel integrity. As demonstrated, the timing could be controlled via the UAS/ Gal4-ERT2 system. Controlling the *vegfaa* dosage in a gene delivery GOF scenario is way more difficult, as the exact amount cannot be fine-tuned. We assumed that a dexterous way to overcome this limitation on dosage control was to take advantage of the endogenous Vegfaa "reservoir", which is the Vegfaa sequestered by Flt1. A way to release Vegfaa from Flt1 is the competitive binding of the Flt1-exclusive ligands Plgf or Vegfb to Flt1. Such release from Flt1 by competitive binding can occur if the levels of Plgf and Vegfb are much higher than the Vegfaa levels, a scenario that may be accomplished by overexpressing *plgf* and *vegfb*. As a spatially controlled Vegfaa release at the vicinity of the ISVs was desired, a suitable promoter was again the muscle-specific *503unc* promoter.

For a traceable constitutive muscle cell-specific overexpression under the *503unc* promoter (*plgf*^{cMC}), *plgf* was cloned behind GFP, connected by the self-cleaving peptide p2A to preserve Plgf protein functionality, and the plasmid was injected together with *tol2 transposase* mRNA into zebrafish at the one cell-stage (Figure 20a). Confocal time lapse imaging of the blood vessel development of *plgf*^{cMC} in the *Tg(kdrl:hsa.HRAS-mcherry)*^{s916} line revealed that already at 32hpf there was a remarkable diameter increase compared to WT embryos, especially in the ventral part of the ISVs (Figure 14a,b). At 48hpf the diameter along the complete length of the ISVs was increased in *plgf*^{cMC} embryos (Figure 14c,d), similar to *flt1*$^{-/-}$ embryos. Remarkably, quantitative comparison of the diameters of aISVs and vISVs at 48hpf revealed that particularly the arterial diameter was increased in *plgf*^{cMC} (Figure 14k). Calculation of the remodelling index (RI) demonstrated that the arterial

diameter was almost doubled upon gain of *plgf*, while the vISVs had a much smaller RI of 1.2 (Figure 14n).

Later in development, at 62hpf, the diameter difference between *plgf*^{cMC} and WT was still observable but diminished compared to earlier time points (Figure 14e,f). However, despite having decreased, the arterial diameter was still significantly larger in *plgf*^{cMC} embryos compared to WT, whereas the venous diameter was not (Figure 14l). Again 12 hours later the ISV diameter in *plgf*^{cMC} resembled the WT ISVs (Figure 14g,h), congruent with the *flt1*$^{-/-}$ phenotype. Quantification confirmed that the aISV diameter in *plgf*^{cMC} was decreased to WT levels. However, while in WT the veins were larger than the arteries, such a difference could not be found in *plgf*^{cMC} (Figure 14m).

The complete time course of the diameter development in *plgf*^{cMC} versus WT is shown in Figure 14j in intervals of 3-4 hours, summarizing that a diameter increase proceeded until 2dpf, and subsequently the diameter was steadily normalizing until having reached WT status at 3dpf, similar to *flt1*$^{-/-}$. However, the primary artery diameter increase in *plgf* GOF embryos (Figure 14j) was larger than that in *flt1*$^{-/-}$ (Figure 12).

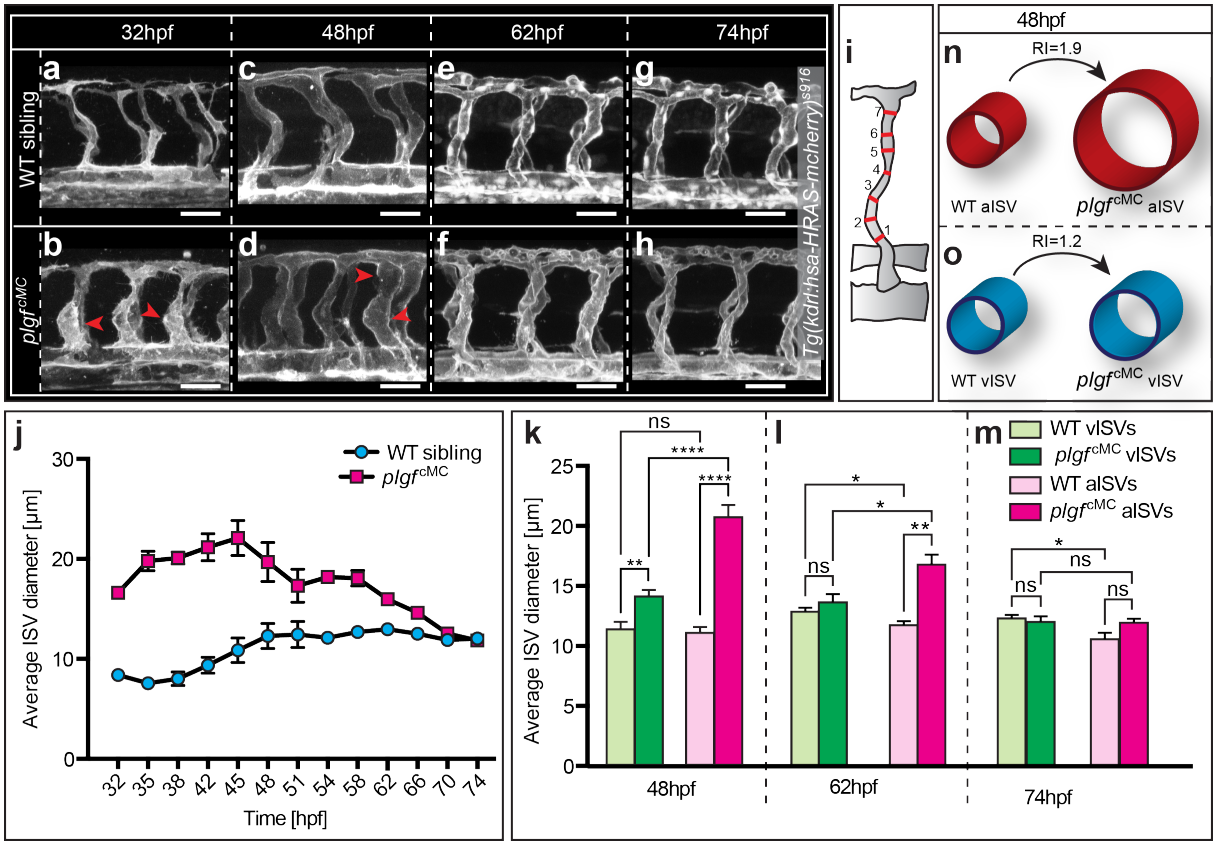

Figure 14| Analysis of the ISV diameter in *plgf*^{cMC}.

(**a-h**) Still images of confocal time lapse movies of the transgenic line *Tg(kdrl:hsa.HRAS-mcherry)*^{s916} from 32 to 74hpf. (**a,b**) At 32hpf, when the primary sprouting is completed, ISVs in *plgf*^{cMC} possess a massively increased diameter when compared to WT, especially in the ventral part as indicated by red arrowheads. (**c,d**) At 48hpf the ISV diameter of the ventral as well as the dorsal part of the ISVs in *plgf*^{cMC} is remarkably increased, indicated by red arrowheads. (**i**) Depiction of measurement points for determining the average diameter of one ISV. (**j**) Quantification of total average ISV diameters, i.e. without compartmentalization in aISVs and vISVs, in *plgf*^{cMC} and WT based on time lapse images from 32hpf until 74hpf every 3h. Note that there is a highly increased diameter in *plgf*^{cMC} compared to WT until 45hpf, the approximate time point at which artery-vein remodelling has finished. Subsequently, the vessel diameter is decreasing until there is no diameter difference anymore between *plgf*^{cMC} and WT at 73hpf. (**k-m**) Specification of total average ISV diameter as shown in j into arterial vs. venous diameter (aISV and vISV, respectively) at the indicated time points. (**k**) At 48hpf both the arterial and venous diameter are increased in *plgf*^{cMC} compared to WT. Remarkably, upon *plgf* GOF the enlargement of aISV diameter is significantly higher than that of vISVs. (**l**) At 62hpf the diameter difference of aISVs between *plgf*^{cMC} and WT has decreased but is still significant. However, the vISV diameter difference is not significant anymore. (**m**) At 74hpf also aISVs of *plgf*^{cMC} embryos are not significantly larger anymore than WT aISVs. However, while arteries are thinner than veins in WT, in *plgf*^{cMC} there is not such a difference between the two vessel types. (**n,o**) Depiction of the RIs at 48hpf of aISVs and vISVs in *plgf*^{cMC} normalized to WT. RI, remodeling index. Quantification in (j-m), mean ± s.e.m; in (k-m), t-test; (j) n≥12 ISVs from ≥3 embryos per genotype and time point; (k-m) n≥5 ISVs from ≥3 embryos per ISV type, genotype and time point. Scale bar, 50µm.

In order to examine whether the diameter increase observed in *plgf*^{cMC}, which phenocopied the effect observed in *flt1*$^{-/-}$ mutants, was due to an increase of Vegfaa – Kdrl signalling, we pursued a pharmacological blockade strategy. Therefore, the VEGFR2, or simply R2 inhibitor ki8751 was applied to *plgf*^{cMC} embryos at 32hpf, they were incubated for 1.5 days and subsequently imaged (Figure 15a). Blockade of R2 signalling reduced the aISV diameter in WT (Figure 15b,d,n) as well as in *plgf*^{cMC} embryos (Figure 15c,e,n). However, the RI of R2 inhibitor-treated *plgf*^{cMC} aISVs normalized to WT aISVs was still 1.25 (Figure 15o), thus Kdrl inhibition could not fully rescue the *plgf*^{cMC} phenotype. Interestingly, the outward remodelling of vISVs was not Kdrl signalling-dependent (Figure 15f-i,p,q).

As a second line of evidence that the diameter increase in *plgf* GOF embryos was caused by increased Kdrl signalling, we blocked PI3K, a signalling molecule downstream of Kdrl involved in the Akt pathway, with the PI3K inhibitor wortmannin using the same experimental setup as for R2 blockade (Figure 15a). However, as PI3K inhibition promotes arterial and blocks venous fate in zebrafish (Hong et al. 2006), the treatment with PI3K inhibitor resulted in

embryos having only aISVs at 2dpf, therefore the effect on vISVs could not be examined. In addition, blood flow was impaired in the ISVs. In line with the results from the R2 blockade, aISV diameter was reduced in WT upon PI3K inhibition (Figure 15j,i,r,s). In *plgf*^{cMC} embryos, pharmacological PI3K blockade could completely rescue the outward remodelling phenotype, even to lower levels than in WT aISVs (Figure 15k,m,r,s).

Taken together, these inhibitor experiments suggest that the diameter increase in *plgf*^{cMC} embryos was for the most part due to increased Kdrl signalling.

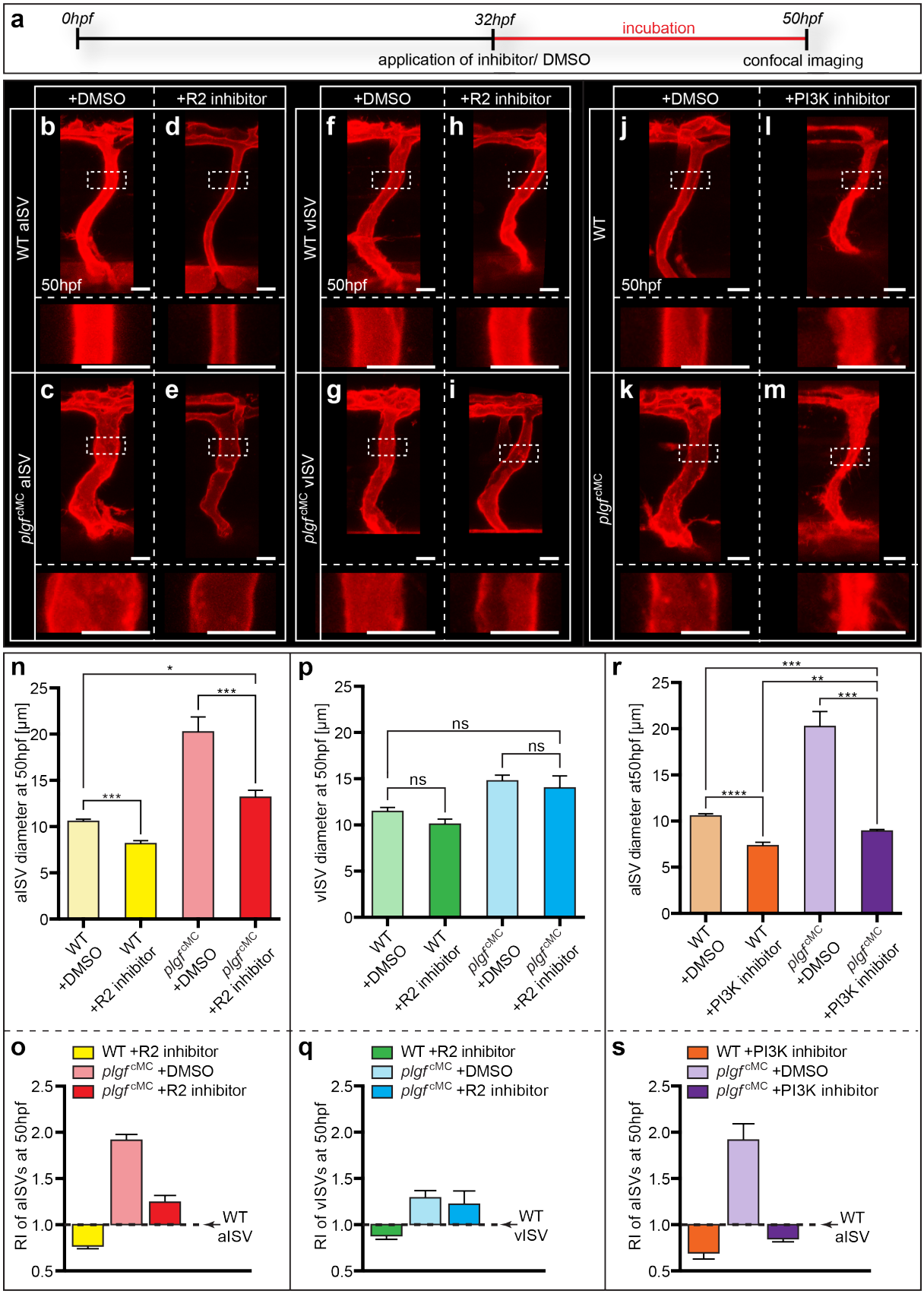

Figure 15| Analysis of downstream signalling involved in the outward remodelling.

(**a**) Time line of the experimental procedure. (**b-m**) Representative confocal images of the blood vessels of the transgenic line *Tg(kdrl:hsa.HRAS-mcherry)*^{s916} of WT and *plgf*^{cMC} with magnifications below each ISV as outlined

by white dotted rectangles. (**b,c,f,g,j,k**) DMSO-treated controls. (**d,e**) aISVs of embryos treated with R2 inhibitor. Note that aISV diameter in both WT and *plgf*^{cMC} is decreased after R2 blockade compared to DMSO controls. (**h,i**) vISVs of embryos treated with R2 inhibitor. Note that no difference in vISV diameter can be observed compared to DMSO controls in f,g. (**l,m**) aISVs of PI3K inhibitor-treated. Note that aISV diameter is decreased in both genotypes compared to DMSO controls in j,k. As AV remodelling was impaired, no vISVs were present in these embryos. (**n,p,r**) Quantification of the vessel diameter as depicted in Figure 14i. (**o,q,s**) Depiction of the RIs based on the measurements in n,p,q and normalized to the diameter of DMSO-treated WT aISVs or vISVs as indicated. (**n,o**) R2 inhibition results in a decreased aISV diameter in both *plgf*^{cMC} and WT. Note that R2 blockade cannot completely rescue *plgf*^{cMC} aISV diameter to WT level. (**p,q**) R2 blockade does not significantly affect the vein diameter. (**p**) Inhibition of PI3K completely rescues the diameter in *plgf*^{cMC}. R2, VEGFR2/Kdr; RI, remodeling index. R2 inhibitor, 0.125µM ki8751; PI3K inhibitor, 1.25 µM wortmannin. Quantification in (n,p,r), mean ± s.e.m; t-test; (n,p) n>7 aISVs, n>7 vISVs from 4-5 embryos per genotype and condition; (r) n>10 ISVs from 4 embryos per genotype and condition. Scale bar, 20µm.

After having found that Kdrl signalling and the downstream signalling molecule PI3K were involved in the outward remodelling of *plgf*^{cMC} embryos, we next analysed the phosphorylation status of Akt by Western blots (Figure 16b). When calculating the ratio of phospho-Akt (pAkt) to Akt using the Gel analysis tool of ImageJ, we found that this ratio was increased in *plgf*^{cMC} compared to WT embryos at 48hpf (Figure 16d). This corroborated the finding that the Kdrl – Akt signalling pathway participated in the arterial diameter increase.
Another Kdrl downstream pathway is ERK1/2. However, we did not find an increased ERK1/2 phosphorylation (pERK1/2) in *plgf*^{cMC} compared to WT at 32 or 48hpf (Figure 16b,c).

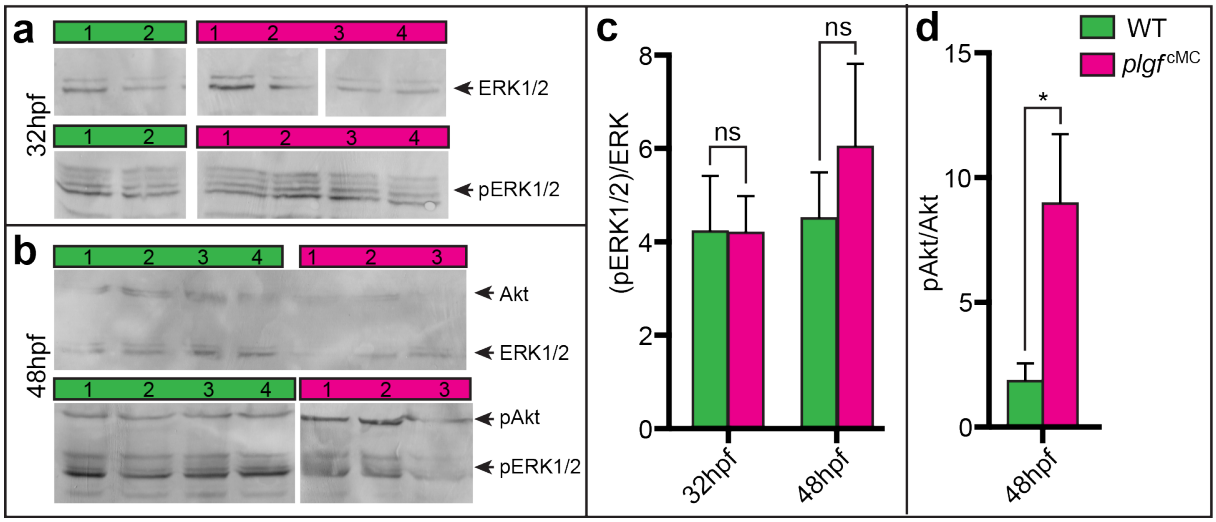

Figure 16| Western blot analysis of pAkt and pERK1/2 in *plgf*^{cMC} embryos.

(**a,b**) ERK1/2, phospho-ERK1/2 (pERK1/2), Akt, phospho-Akt (pAkt) Western blots of *plgf*^{cMC} (pink) and WT (green) at indicated time points. Numbers indicate biological replicates. (**c**) (pERK1/2)/ERK ratio is not different between the two genotypes at 32 and 48hpf. (**d**) pAkt/Akt ratio is increased in *plgf*^{cMC} embryos at 48hpf. Quantification in (c,d), mean ± s.e.m; t-test; n>80 embryos per replicate and time point.

Endothelial tip cell activation by VEGF-A – KDR signalling is associated with filopodia extensions (Gerhardt et al. 2003). Thus, we analysed whether the increased Kdrl signalling in *plgf*^{cMC} embryos also induced a change in the EC architecture with respect to filopodia. Indeed, at 32hpf the primary aISVs in *plgf*^{cMC} embryos extended significantly more filopodia with a length of more than 8µm along the complete ISVs compared with WT embryos (Figure 17a,b,i). At 52hpf especially the aISVs of *plgf*^{cMC} embryos contained more filopodia protrusions with a length of more than 4µm than WT embryos (Figure 17c,d,j). Also the ECs in the DLAV, which is formed by anastomoses of primary aISVs, displayed more filopodia protrusion longer than 4µm in *plgf*^{cMC} than in WT (Figure 17g,h,k).

Taken together, the filopodia architecture of the arterial and artery-derived ECs in *plgf*^{cMC} embryos indicated that these ECs were in an activated state due to increased Vegfaa – Kdrl signalling.

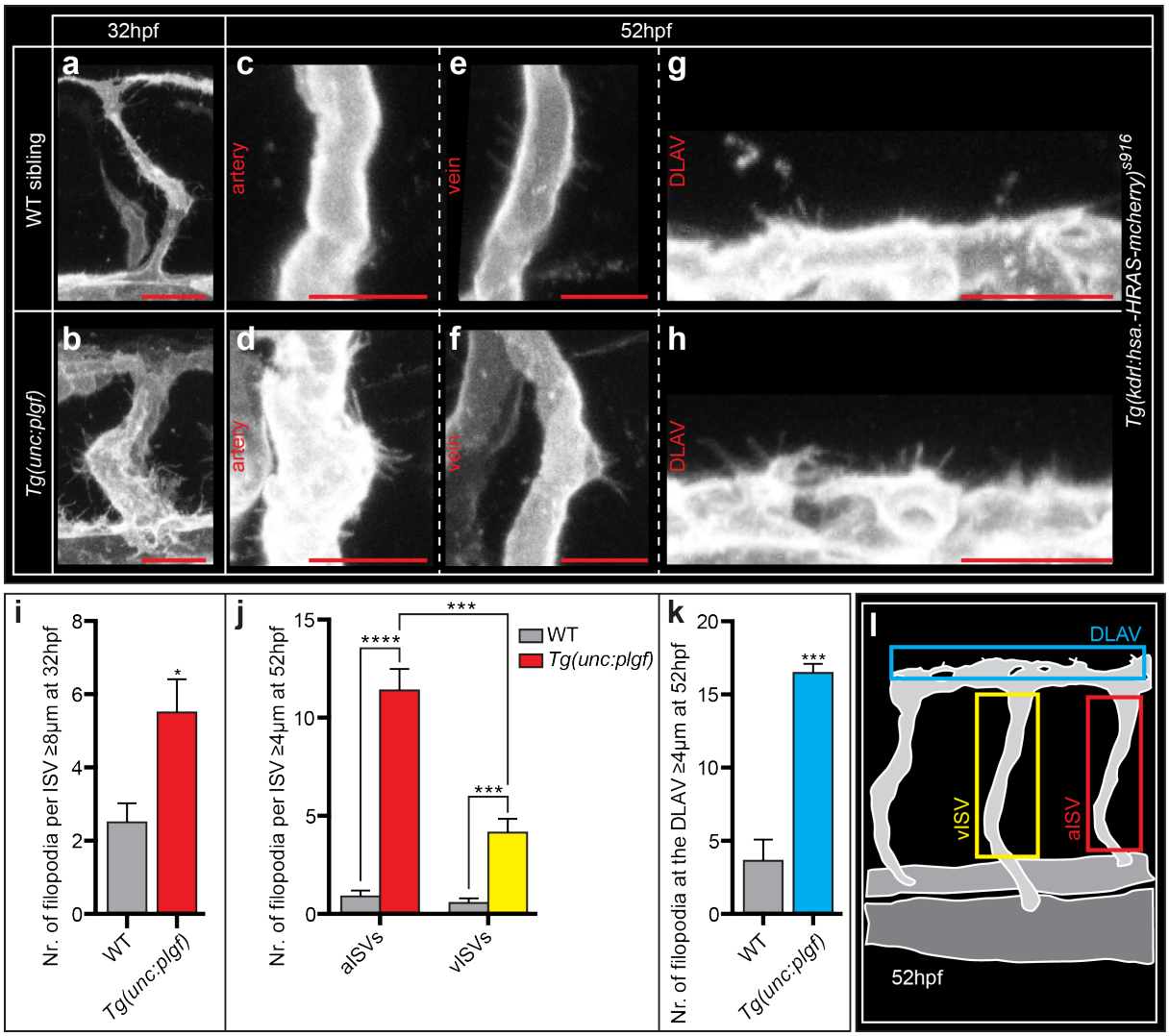

Figure 17| Analysis of filopodia in *plgf*^{cMC}.

(**a-h**) Representative confocal images of the blood vessel filopodia of WT and *plgf*^{cMC}. (**a,c,e,g**) In WT few filopodia are apparent on the ISVs at 32 and 52hpf and at the DLAV at 52hpf. (**b,d,f,h**) In contrast, the blood vessels of *plgf*^{cMC} are covered with numerous filopodia at both time points, many of them having a considerable length. (**i-k**) Quantification of filopodia as outlined in (l). (**i**) Measurement of filopodia with a length of ≥8µm at 32hpf reveals a significantly higher filopodia number on *plgf*^{cMC} than WT ISVs. (**j,k**) At 52hpf significantly more filopodia ≥4µm are present on the ISVs and the DLAV of *plgf*^{cMCv} compared to WT. Note that in *plgf*^{cMC} especially the aISVs are coated with filopodia. Quantification in (i-k), mean ± s.e.m; t-test; (i) n=10 ISVs from 4-5 embryos per genotype; (j) n=9 ISVs from 4-6 embryos per ISV type and genotype; (k) n=3 embryos per genotype. Scale bar, 25µm.

For the outward remodelling in *plgf*^{cMC} embryos the ISVs had to undergo a structural rearrangement. One conceivable possibility of this rearrangement is that the EC number in the ISVs stayed constant and that the ECs expanded in their size. The other option is that the

EC number in the ISVs increased. To test which of these scenarios is applicable to the ISVs of *plgf*^{cMC} we imaged the EC nuclei in the *Tg(fli1a:nGFP)*^{y7} reporter line. Interestingly, already in the nascent primary arterial sprout more ECs were in place (Figure 18a,b). The almost doubled ISV diameter in *plgf*^{cMC} embryos correlated with a duplication of the EC number in the ISVs at 32hpf, after aISV formation was completed (Figure 18c,d,g).

However, the increase in EC numbers and the resulting outward remodelling in *plgf*^{cMC} was not associated with an increased macrophage infiltration, as the macrophages in the reporter line *Tg(mpeg1:GAL4-VP16)*^{gl24};*Tg(UAS:Kaede)*^{s1999t} still gathered at the DA in *plgf* GOF embryos instead of dorsal migration towards the aISVs (Figure 18e,f).

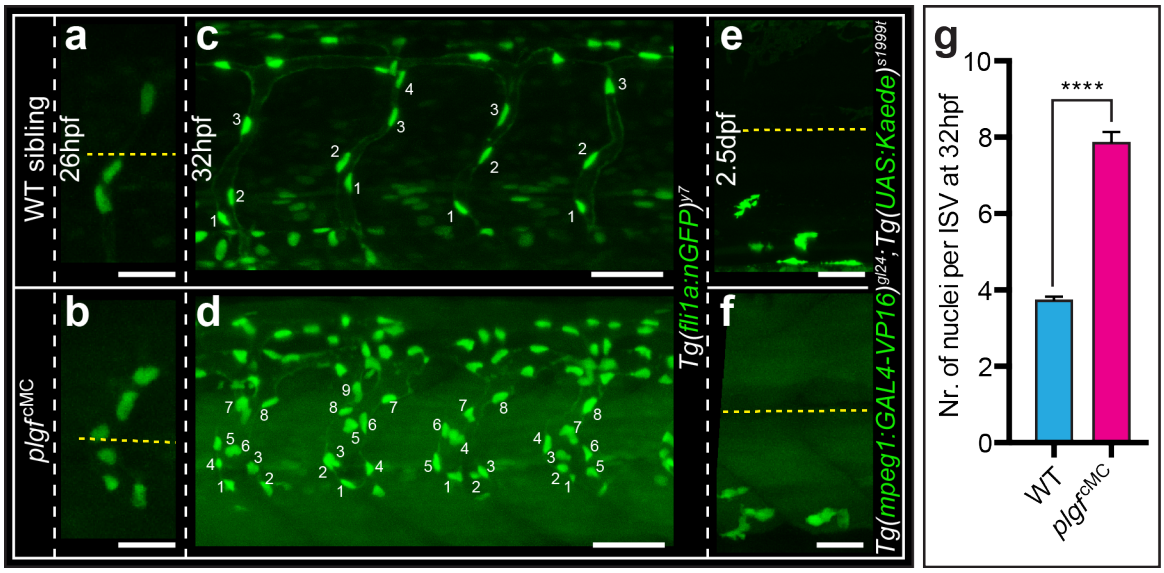

Figure 18| Analysis of EC number in *plgf*^{cMC} embryos.

(**a-d**) Representative confocal images of EC nuclei in ISVs in *Tg(fli1a:nGFP)*^{y1} in WT and *plgf*^{cMC}. (**a,b**) Primary arterial sprouting. Note that *plgf*^{cMC} sprouts contain more ECs. (**c,d**) *plgf*^{cMC} aISVs at 32hpf contain more ECs over the whole length of the ISV. (**e,f**) Representative confocal images of macrophages in the trunk in the *Tg(mpeg1:GAL4-VP16)*^{gl24};*Tg(UAS:Kaede)*^{s1999t} transgenic line. Note that the macrophage distribution in *plgf*^{cMC} embryos is not different from WT. (**g**) Quantification of EC number per ISV as shown in a,b. Quantification in (g), mean ± s.e.m; t-test; n≥54 ISVs from ≥9 embryos per genotype. Yellow dotted line in a,b,e,f, location of horizontal myoseptum. Scale bar in a,b, 25µm; in c-f, 50µm.

As the gain of Vegfaa bioavailability by loss of *flt1* induced venous hypersprouting at the neural tube (NT) around 3dpf (Wild et al. 2017), we analysed whether the replacement of Vegfaa from Flt1 by *plgf* GOF could induce a similar phenotype. Indeed, *plgf*^{cMC} ISVs started to sprout at the level of the NT shortly before 4dpf (Figure 19a,b), and similar to *flt1*$^{-/-}$ all

ectopic sprouts had venous origin (Figure 19g). These sprouts subsequently formed anastomoses with adjacent ISVs or the DLAV, and thereby the ectopic vessel network around the NT extended (Figure 19b,d-f). Constitutive neuron cell-specific overexpression of *GFP-p2A-plgf* under the pan-neuronal promoter *Xla.Tubb* (*plgf*^{cNC}) could similarly induce ectopic sprouting at the NT (Figure 19h,i).

Taken together, this experiment could show that *plgf* GOF phenocopied the *flt1*$^{-/-}$ venous NT-associated hypersprouting, further substantiating that *plgf* GOF was capable of replacing the Flt1-bound Vegfaa reservoirs.

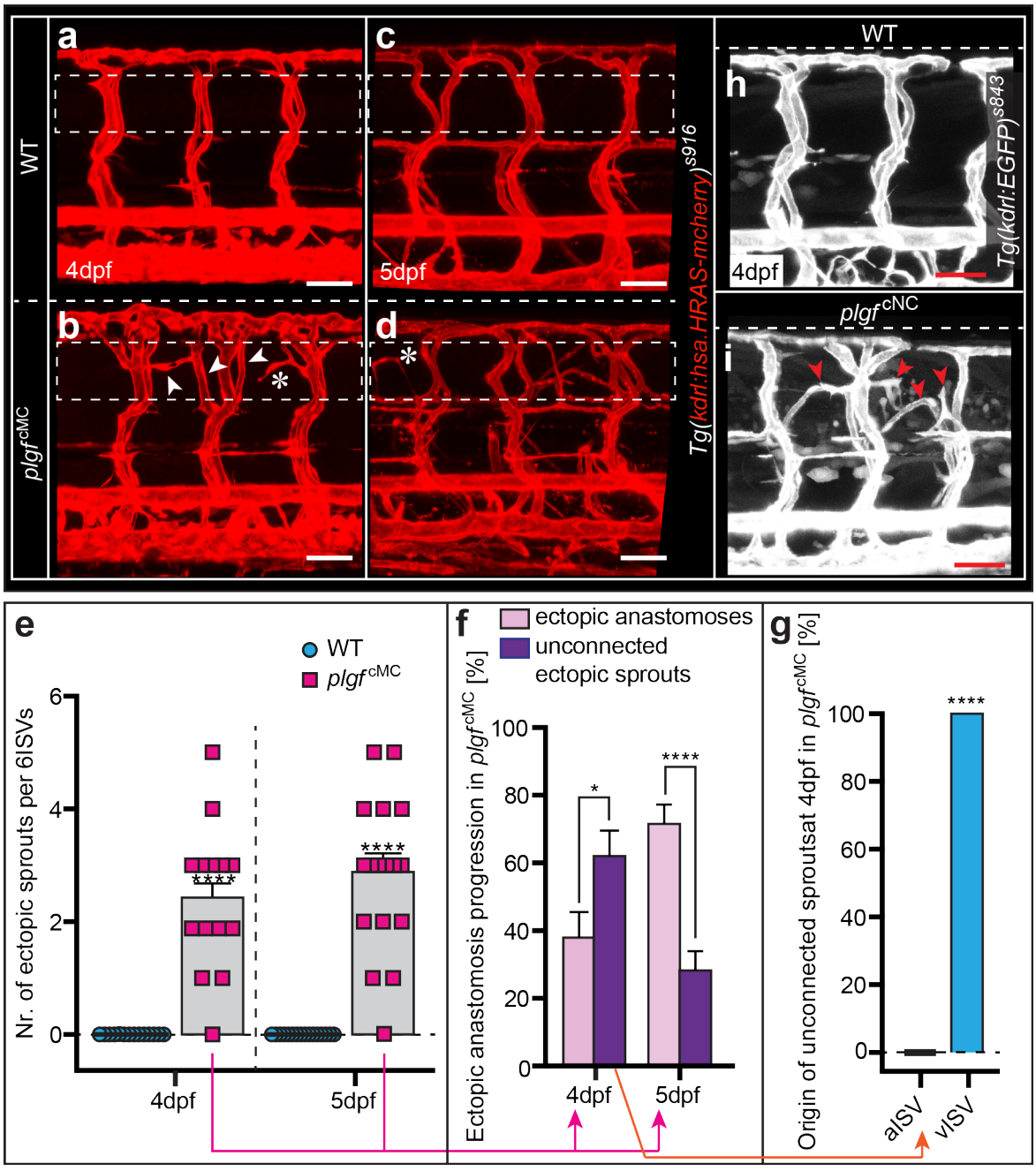

Figure 19| Analysis of ectopic sprouts in *plgf* GOF embryos at later stages.

(**a**-**d**) Representative confocal images of blood vessels in WT and *plgf*^{cMC} ; white dotted rectangles, localization of the NT. (**a**,**c**) In WT there are no sprouts at the level of the NT. (**b**) Few ectopic anastomoses exist in *plgf*^{cMC} at 4dpf, as indicated by arrowheads, and new ectopic sprout emerges from vISVs, indicated by asterisk. (**d**) At 5dpf there are numerous anastomoses at the level of the NT in *plgf*^{cMC}. (**e**) Quantification of ectopic sprouts (still growing as well as already anastomosed with another vessel) in WT and *plgf*^{cMC} at 4 and 5dpf. (**f**) Classification of the sprouts of *plgf*^{cMC} in g according to whether they have already formed anastomoses or if they are still unconnected. (**g**) Quantification of the venous vs. arterial origin of ectopic sprouts in *plgf*^{cMC}. For this analysis the unconnected sprouts at 4dpf (h, left) were analysed. (**j,k**) Similar to muscle-specific overexpression as in b,d also constitutive neuronal cell-specific overexpression of *GFP-p2A-plgf* under the *nbt* (also known as *Xla.Tubb*) promoter (*plgf*^{cNC}) activates ectopic sprouting at the NT at 4dpf, marked by red arrowheads. NT, neural tube. Quantification in (e-g), mean ± s.e.m; t-test; (e,f) n>14 embryos per genotype and time point; (g) n=9 sprouts from 7 embryos. Scale bar, 50µm.

As *plgf*^{cMC} caused a gain of Vegfaa bioavailability and Vegfaa is implicated in arterial differentiation (Dela Paz & D'Amore 2009), we next checked whether the distribution of arteries and veins was affected in *plgf*^{cMC} embryos. Therefore, blood vessels were analysed in a *Tg(flt1*^{enh}*:dTomato)*^{hu5333}*;Tg(flt4:mCitrine)*^{hu7135} double transgenic reporter line at 4dpf with aISVs completely in red and veins having a ventral part exclusively in green (Figure 20d,e). However, quantification of aISV and vISV distribution revealed that AV differentiation was regular in *plgf*^{cMC} embryos (Figure 20b,c).

Interestingly, the heart beat frequency was similar between *plgf*^{cMC} and WT embryos at 32hpf, whereas at 48hpf the heart rate was significantly increased in *plgf*^{cMC} with an average of 138 beats/min compared with 121 beats/min in WT embryos (Figure 20f).

A common side effect of *Vegfa* GOF is the formation of oedema (Dor et al. 2002). However, careful analysis of *plgf*^{cMC} embryos showed that they did not develop any form of oedema or other morphological abnormalities and that their body size was normal (Figure 20g-i).

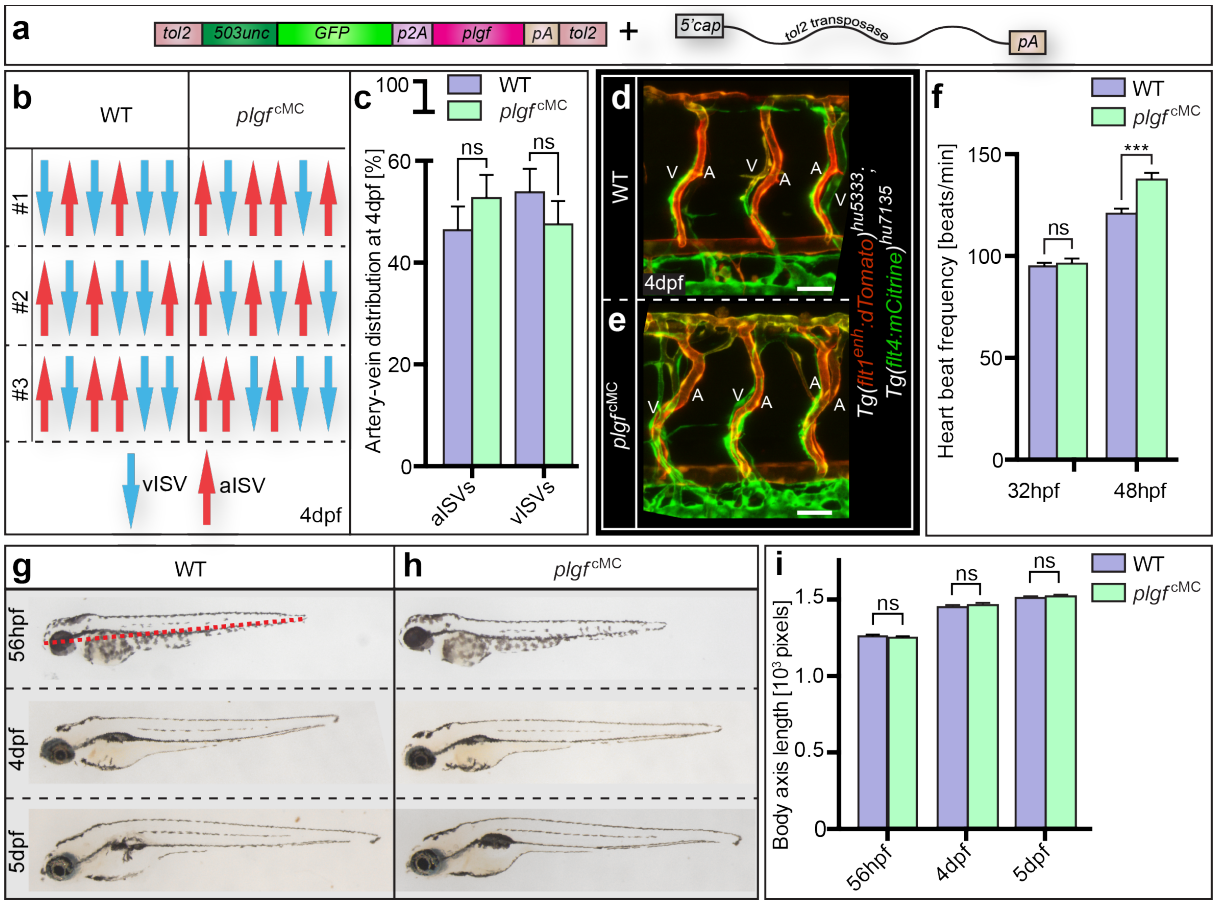

Figure 20| Analysis of the AV distribution, heart rate and morphological development of *plgf*^{cMC} embryos.

(**a**) Illustration of the approach for constitutive muscle cell-specific *plgf* GOF (*plgf*^{cMC}). The plasmid coding for *plgf*, tagged via p2A to GFP, under the *unc* promoter is injected together with *tol2* transposase mRNA. (**b-e**) Analysis of the artery-vein distribution in *plgf*^{cMC} versus WT at 4dpf. (**b**) Schematic depiction of the vessel identities of 6 ISVs above the yolk sac elongation in 3 representative embryos per group. (**c**) Quantification of aISVs and vISVs in WT and *plgf*^{cMC}. Note that there is no significant difference between the genotypes. (**d,e**) Confocal images of the blood vessels of WT and *plgf*^{cMC} at 4dpf with indicated vessel identities. (**f**) Heart rate in *plgf*^{cMC} and WT embryos at 32 and 48hpf. Note that at 32hpf no significant difference exists between the two genotypes, whereas at 48hpf the heart rate increases in *plgf*^{cMC} by the factor 1.14. (**g,h**) Transmitted light images of WT and *plgf*^{cMC}. Note that *plgf*^{cMC} emryos do not show any morphologic malformations or oedema. (**j**) Quantification of the body axis length of WT and *plgf*^{cMC}. Length measurements were performed with ImageJ as illustrated in h, red dotted line. Note that no significant size differences between the 2 genotypes were determined at all indicated time points. A, aISV; pA, poly (A) tail; V, vISV. Quantification in (c,f,i), mean ± s.e.m; t-test; (c) n≥53 ISVs from ≥9 embryos per genotype; (f) n≥10 embryos at 32hpf per genotype; n=20 embryos at 48hpf per genotype; (i) n≥18 embryos per genotype and time point. Scale bar, 50µm.

To further substantiate that the diameter increase in *flt1*$^{-/-}$ embryos was due to a gain of Vegfaa, we constitutively overexpressed also the other Flt1-specific ligand *vegfb* in skeletal muscles (*vegfb*^{cMC}) with the same approach used for *plgf*^{cMC} (Figure 20a).

Blood vessels of *vegfb*^{cMC} embryos were dynamically imaged in the *Tg(kdrl:hsa-HRAS-mCherry)*^{s916} reporter line from 31 to 74hpf. Remarkably, also in *vegfb*^{cMC} the ISV diameter was clearly enlarged compared to WT. Shortly after anastomosis formation, at 31hpf, primarily the ventral part of the ISVs were enlarged (Figure 21a,b) in line with *plgf* GOF (Figure 14b) and *flt1* LOF (Figure 12b). Later, the diameter over the whole range of the ISVs was increased in *vegfb*^{cMC} (Figure 21d,e). Consistently with *plgf*^{cMC} and *flt1* LOF, also in *vegfb*^{cMC} the ISV diameter started to normalize after 2dpf (Figure 21g), until almost no difference was observable anymore at 3dpf (Figure 21e,f).

Taken together, gain of Vegfaa bioavailability by release of the arteriolar Vegfaa reservoirs from Flt1 and increased Kdrl signalling induced arteriolar outward remodelling in a macrophage-independent manner. This release of the Vegfaa reservoir could either be achieved by loss of *flt1* or by competitive binding of the ligands Plgf or Vegfb with Vegfaa. However, Vegfaa dosage was critical and the levels upon inducible *vegfaa165* GOF were too high for functional vessels. In case of *plgf* GOF, the release of the arterial Vegfaa reservoirs put the ECs into an activated state, manifested by filopodia protrusions, and resulted in higher EC numbers in ISVs. Remarkably, *plgf*^{cMC} and *vegfb*^{cMC} both induced a higher arterial diameter increase than *flt1*$^{-/-}$, with *plgf* having the highest arteriogenic potential (Figure 21h).

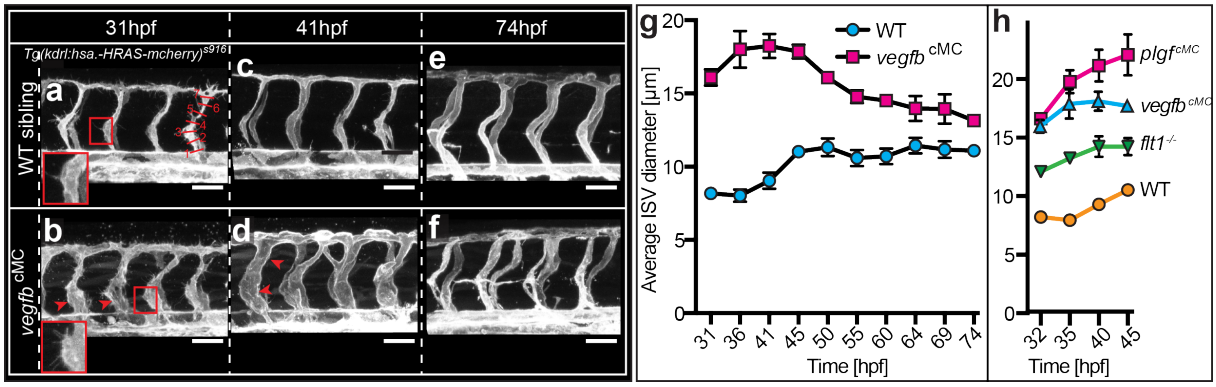

Figure 21| Analysis of ISV diameter in *vegfb*^{cMC} embryos.

(**a-f**) Representative still images of confocal time lapse movies from 31 to 74hpf of the reporter line *Tg(kdrl:hsa.HRAS-mCherry)*^{s916}. *vegfb*^{cMC}, constitutive muscle cell-specific overexpression of *GFP-p2A-vegfb*

under the *503unc* promoter. (**a,b**) ISV diameter is increased at 31hpf in *vegfb*^{cMC}, particularly in the ventral part as indicated by red arrowheads. Red outlined images are magnifications as indicated by rectangulars. Note that *vegfb*^{cMC} extend many long filopodia. (**c,d**) At 41hpf both ventral as well as dorsal parts if ISVs in *vegfb*^{cMC} exhibit an increased diameter as denoted again by red arrowheads. (**e,f**) Later in development, at 74hpf, no difference in vessel diameter between WT and *vegfb*^{cMC} is noticeable. (**g**) Quantification of total average ISV diameters, i.e. without compartmentalization in aISVs and vISVs, in *vegfb*^{cMC} and WT based on time lapse images. Individual average ISV diameters were based on 7 measurement points as indicated in a. Note that there is a highly increased diameter in *vegfb*^{cMC} compared to WT until 45hpf, the approximate time point at which artery-vein remodelling has finished. Subsequently, the vessel diameter is decreasing until there is almost no diameter difference anymore between *vegfb*^{cMC} and WT. (**h**) Comparison of the primary artery diameters of *plgf*^{cMC}, *vegfb*^{cMC}, *flt1-/-* and WT embryos. Measurements from Figure 12i, Figure 14j and Figure 21g. Note that *plgf* GOF induces the strongest ISV outward remodelling. Quantification, mean ± s.e.m; t-test; n≥12 ISVs from ≥3 embryos per genotype and time point. Scale bar, 50µm.

4.4 Analysis of the vascular development of *plgf*$^{-/-}$ mutants

After having found that gain of the Flt1-specific ligands were involved in arteriolar diameter regulation, we aimed at determining the endogenous function of *plgf* and *vegfb* in outward remodelling. As *plgf* was expressed in spinal cord neurons, skeletal muscles and the hypochord, no *vegfb* expression was found in the trunk vasculature or neurons in the vicinity of ISVs (Figure 10,Figure 11). Therefore, we reasoned that *plgf* might be a likely candidate of endogenous regulation of Flt1-bound Vegfaa and we decided to generate *plgf* mutants using the CRISPR/Cas9 technique. An sgRNA targeting the *plgf* exon 3 (*sgRNA*^{plgfE3}) was designed using CHOPCHOP in a way that no off-targets with 0,1 or 2 mismatches existed in the zebrafish genome. By screening for founder animals, a mutant with a 10nt deletion allele, which has the official designation *plgf*^{ka609}, was chosen for establishing a homozygous *plgf*$^{-/-}$ line (Figure 22c,d). The frameshift in these mutants (Figure 22ab) causes the translation of a mutant Plgf protein, in which the predicted residues important for receptor binding and dimerization are affected (Figure 22a).

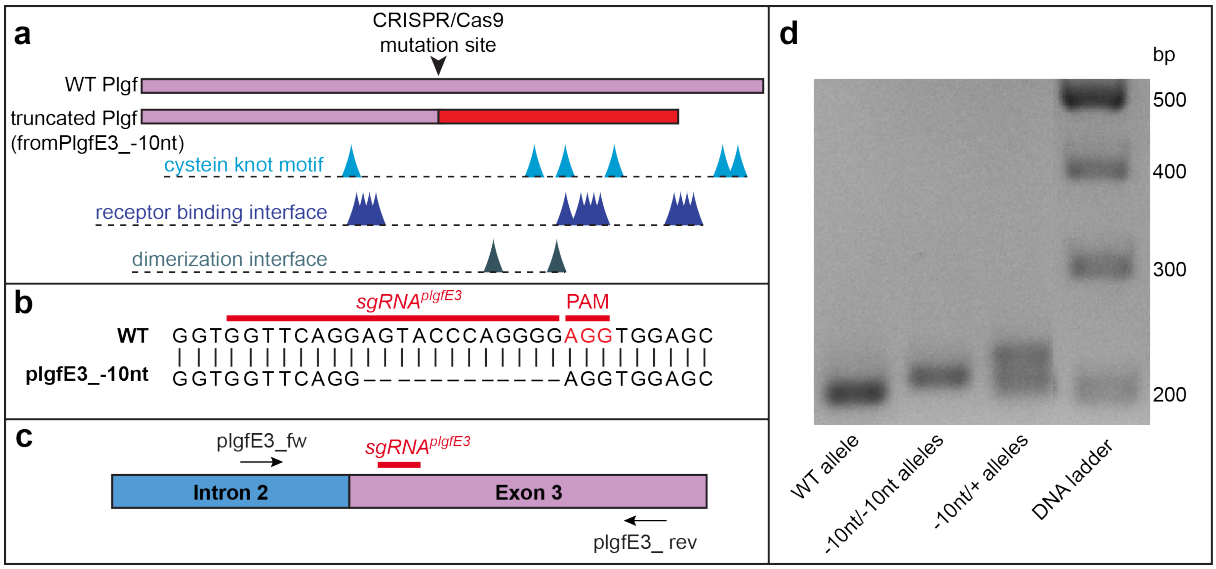

Figure 22| Generation of *plgf* mutants using CRISPR/ Cas9.

(**a**) Schematic illustration of the functional domains of the WT PlGF protein. The residue positions of the Vegf ligand-specific cysteine knot motif, the receptor binding interface and the dimerization interface are indicated by arrowheads, as predicted by the Conserved Domain Database (NCBI). The mismatched and truncated part of the Plgf protein translated from the mutated -10nt allele is depicted in red. Not that the majority of residues of the functional protein sites are affected by the mutation. (**b**) Genomic DNA sequence at the mutation site in exon 3 of the WT *plgf* and the *plgfE3-10nt* allele, including the *sgRNA*^{plgfE3} binding site and its 3' PAM site. (**c,d**) Genotyping strategy of *plgf* mutants. (c) Primer location around the mutated genomic site. (d) Representative agarose gel of the PCR products of the *plgf* genotyping as depicted in c. From left to right, WT, homozygous *plgf*$^{10/-10}$, heterozygous *plgf*$^{10/+}$. PAM, protospacer adjacent motif; sgRNA, short guide RNA.

We analysed the blood vessel development in *plgf*$^{-/-}$ mutants in the transgenic line *Tg(kdrl:EGFP)*^{s843}. Primary ISVs sprouting and anastomosis formation as well as secondary venous sprouting occurred regularly in *plgf*$^{-/-}$. However, the diameter was thinner when compared to WT at 32hpf (Figure 23a,b,g), a decrease that even persisted when blood flow set in at 48hpf (Figure 23c,d,g). Analysis of the venous and arterial diameter at 3dpf, when arterial remodelling is completed, revealed that it was the arterial, not the venous diameter that was significantly decreased with an RI of 0.71 (Figure 23e,f,h,i).

In summary, analysis of the *plgf*$^{-/-}$ mutant and *plgf* GOF embryos suggests that next to the abundance of Flt1 itself, Plgf binding to Flt1 represents another endogenous instance of Vegfaa bioavailability regulation important for arteriolar outward remodelling.

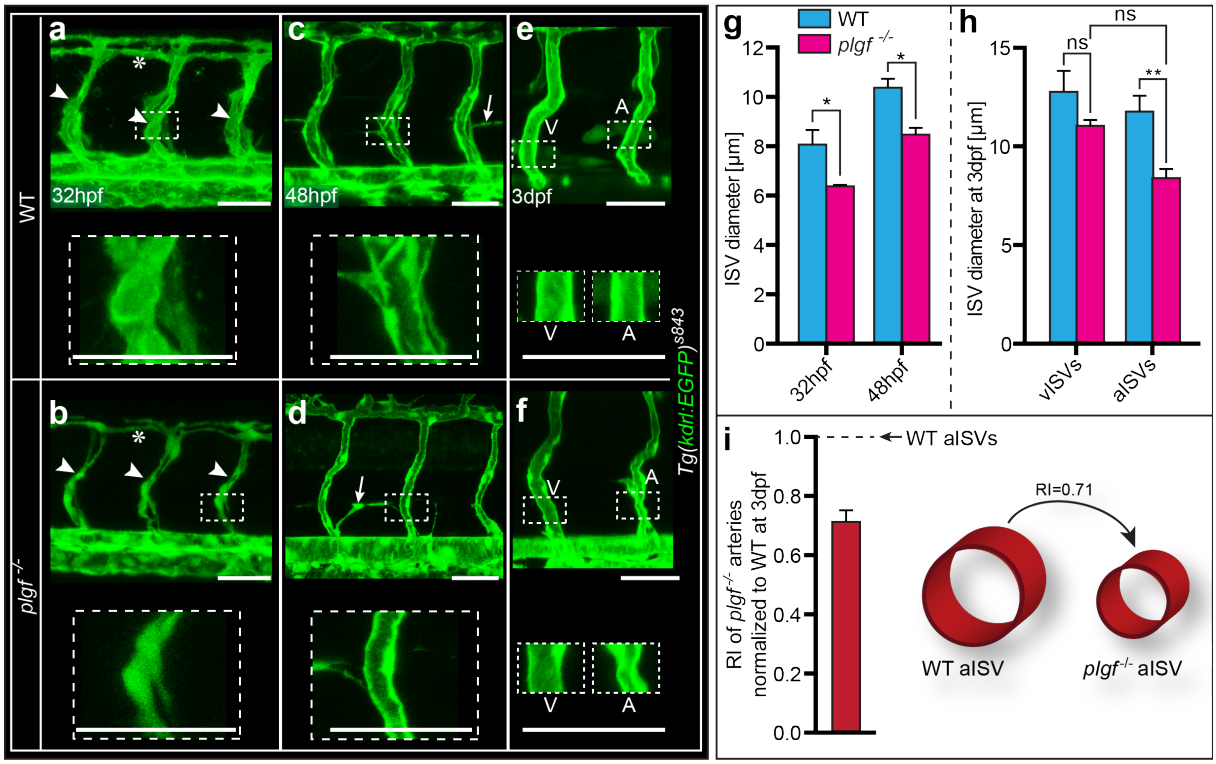

Figure 23| Analysis of early trunk vasculature in *plgf*$^{-/-}$ embryos.

(**a-f**) Representative confocal images of trunk vessels in WT and *plgf*$^{-/-}$ embryos; higher magnifications below each image as outlined by dotted rectangular boxes. (**a,b**) Primary sprouting of ISVs (white arrowheads) and anastomosis formation giving rise to the DLAV (white asterisks) is occurring regularly in *plgf*$^{-/-}$. However, ISVs are remarkably thinner in *plgf*$^{-/-}$ mutants compared to WT. (**c,d**) Secondary venous sprouting (white arrows) is also normal in *plgf*$^{-/-}$. Note that at 48hpf ISVs are still thinner in mutants compared to WT. (**e,f**) Images of arteries and veins at 3dpf, when artery-vein remodeling is fully completed. Note that venous diameter in *plgf*$^{-/-}$ resembles the WT vISV diameter, whereas arteries in *plgf*$^{-/-}$ are thinner than in WT. (**g**) Quantification of ISV diameter at 32 and 48hpf without discrimination between aISVs and vISVs. (**h**) Quantification of arterial and venous diameter in WT and *plgf*$^{-/-}$. (**i**) RI of *plgf*$^{-/-}$ aISVs at 3 dpf, normalized to WT aISV diameter. Quantification in (g,h,i), mean ± s.e.m;(g,h) t-test; (g, 32hpf) n≥16 ISVs from 3 embryos per genotype; (g, 48hpf) n≥40 ISVs from 3 embryos per genotype; (h) n≥6 ISVs from 3 embryos and genotype; (i) n=7 aISVs from 3 embryos. A, aISV; V, vISV; RI, remodelling index. Scale bar, 50µm.

As loss of *plgf* presumably affected the Vegfaa levels available for Kdrl signalling, we determined the AV distribution and morphological development of *plgf*$^{-/-}$ mutants similar to the analysis of *plgf*^{cMC} embryos. The AV distribution (Figure 24a-d) was normal, and *plgf*$^{-/-}$ mutants did not show any signs of morphological abnormalities or oedema formation (Figure 24e-g).

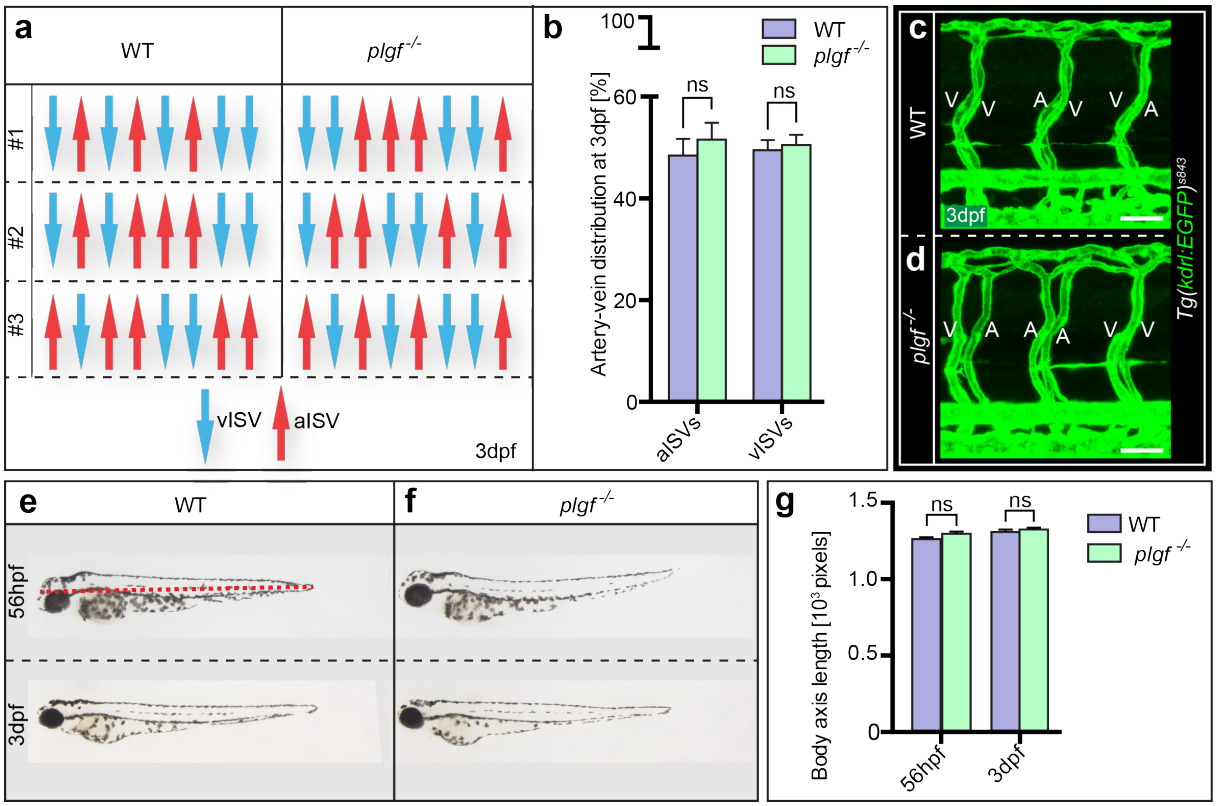

Figure 24| Artery-vein distribution and morphological development of *plgf*$^{-/-}$ mutant embryos.

(**a-d**) Analysis of artery-vein (AV) distribution in *plgf*$^{-/-}$ versus WT at 3dpf. (**a**) Schematic depiction of the vessel identities of 8 ISVs above the yolk sac elongation in 3 representative embryos per group. (**b**) Quantification of aISVs and vISVs in WT and *plgf*$^{-/-}$. Note that there is no significant difference between the genotypes. (**c,d**) Confocal images of the blood vessels of the transgenic line *Tg(kdrl:GFP)*^{s843} of WT and *plgf*$^{-/-}$ at 3dpf with indicated vessel identities. (**e-f**) Transmitted light images of WT and *plgf*$^{-/-}$. Note that *plgf*$^{-/-}$ mutants do not show any morphological malformations or oedema. (**g**) Quantification of the body axis length of WT and *plgf*$^{-/-}$. Length measurements were performed as illustrated in e, red dotted line. Note that no significant size differences between the 2 genotypes were determined at all indicated time points. Quantification in (b,g), mean ± s.e.m; (b) n=114 ISVs from 16 *plgf*$^{-/-}$ embryos, 79 ISVs from 11 WT embryos; (g) n>5 embryos per genotype pre time point; t-test. Scale bar in c,d, 50µm.

4.5 Cerebral vascular development in *plgf*$^{-/-}$ mutants

Kdrl signalling is relevant not only for angiogenesis in the trunk but also for certain aspects of cerebral artery development such as central artery (CtA) formation in the hindbrain (Ulrich et al. 2011; Bussmann et al. 2011).

As *flt1* (Bussmann et al. 2007) and *plgf* (Figure 9b) were also expressed in the brain, we questioned whether loss of *plgf* also affected a putative Flt1-bound Vegfaa reservoir in the

brain and analysed the cerebral vasculature in *plgf*$^{-/-}$ embryos. At 2dpf the hindbrain consisted of the ventrally located primordial hindbrain channel (PHBC) in WT and *plgf*$^{-/-}$ embryos (Figure 25a,b). CtAs were sprouting normally from the PHBC in *plgf*$^{-/-}$ embryos (Figure 25a,b, white arrows), and the number of ipsilateral fusion formations was not affected (Figure 25a,b, white arrowheads). Also the metencephalic artery (MtA) and mid-cerebral vein (MCeV) were developing normally in *plgf*$^{-/-}$ embryos (Figure 25a,b). As the CtAs were reported to develop in a non-stereotypic manner (Ulrich et al. 2011), the comparison of the CtA architecture between two animals is difficult; thus, a conclusive statement on possible deviations in CtA number in *plgf*$^{-/-}$ mutants is not possible. Nevertheless, all main cerebral vessels developed intact in loss of *plgf* embryos at a later developmental stage (Figure 25c,d).

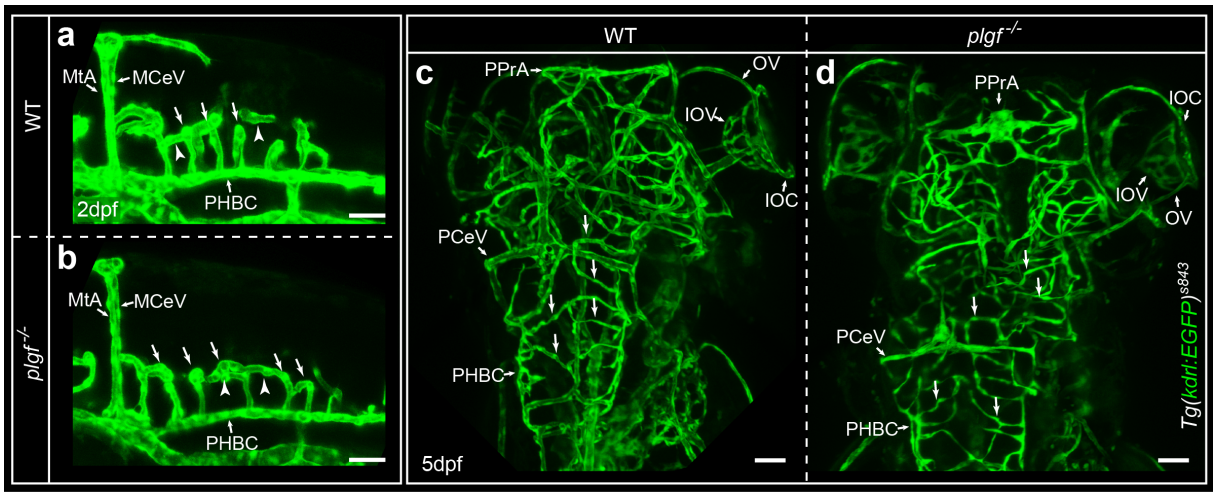

Figure 25| Cerebral vascular development in *plgf*$^{-/-}$ mutant embryos.

(**a-d**) Representative confocal images of cerebral blood vessels of *plgf*$^{-/-}$ and WT mutants. (**a,b**) Lateral view of the hindbrain vasculature at 2dpf, rostral side to the left. Arrows indicate CtAs, which grow from the PHBC in the rhombomere boundaries to invade the hindbrain and which are connected via ipsilateral CtA fusions, indicated by white arrowheads. Note that the early *plgf*$^{-/-}$ vasculature develops normally. (**c,d**) Dorsal view of the complete cerebral vasculature at 6 dpf, rostral side to the top. The main vessels in the cerebral vasculature of *plgf*$^{-/-}$ mutants are present, as indicated. White arrows indicate CtAs. Note that CtA architecture is highly variable among different embryos (Bussmann et al. 2011). CtA, central artery; IOC, inner optic circle; IOV, intraocular vasculature; MCeV, mid-cerebral vein; MtA, metencephalic artery; OV, optic vein; PHBC, primordial hindbrain channel; PPrA, primitive prosencephalic artery. Scale bar, 50µm.

4.6 Analysis of *flt1*$^{-/-}$;*plgf*$^{-/-}$ double mutants

An RNA sequencing experiment of *flt1*$^{-/-}$ mutants at 4dpf revealed a twofold upregulation of *plgf* (Wild et al. 2017). Here, we could prove a clear *plgf* upregulation via WISH at 30hpf in *flt1*$^{-/-}$ mutants in motoneurons and in the individual cells of the hypochord (Figure 26a,b). In order to examine the role of *plgf* in *flt1* full mutants, we generated *flt1*$^{-/-}$;*plgf*$^{-/-}$ double mutants (official designation *flt1*$^{ka601/ka602}$;*plgf*$^{ka609/ka609}$). However, no difference could be observed between the double mutants and the *flt1*$^{-/-}$ mutants with respect to the venous hypersprouting phenotype at the neural tube (Figure 26c-e). An additional small but consistent phenotype in *flt1*$^{-/-}$;*plgf*$^{-/-}$ double mutants at the level of the hypochord was the dual connection of aISVs with the DA, an artery-artery (AA)-shunt, a phenotype that was only very rarely observed in *flt1*$^{-/-}$ (Figure 26h,i).

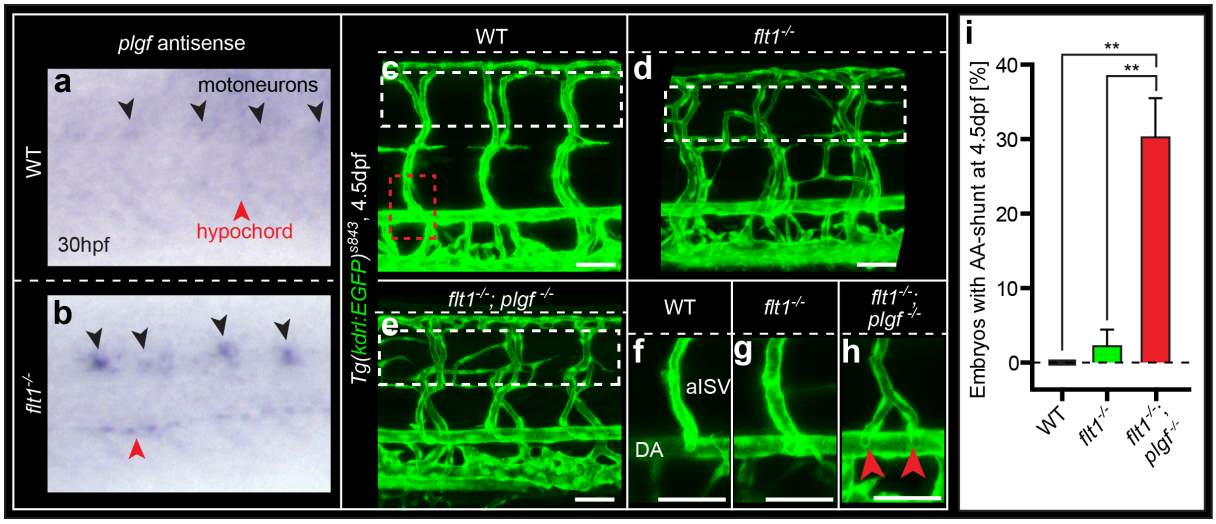

Figure 26| Expression of *plgf* in *flt1*$^{-/-}$ mutant embryos and analysis of vasculature of *plgf*$^{-/-}$;*flt1*$^{-/-}$ double mutants.

(**a,b**) Whole-mount *in situ* hybridization of *plgf* antisense RNA probe. Note that *plgf* is highly upregulated at 30hpf in motoneurons and in the hypochord in *flt1*$^{-/-}$ compared to WT. (**c-h**) Representative confocal images of blood vessels at 4.5dpf. (**c,d,e**) Position of the neural tube is outlined by white dotted rectangle. Note that there is similar ectopic hypersprouting at the level of the NT in *flt1*$^{-/-}$ and *plgf*$^{-/-}$;*flt*$^{-/-}$. (**f-h**) Representative images of aISVs as delineated with red dotted rectangle in c. Note that the aISV in *plgf*$^{-/-}$;*flt*$^{-/-}$ has 2 connections to the DA, here referred to as AA-shunt. (**i**) Quantification of embryos with AA-connection. AA, artery-artery; DA, dorsal aorta. Quantification in (i), mean ± s.e.m; t-test; n>9 embryos per genotype, with 6 ISVs analyzed per embryo. *flt1*$^{-/-}$ in b,d,g,i, *flt1*^{ka601}; double mutants in e,h,i, *flt1*$^{ka601/ka602}$;*plgf*$^{10/-10}$. Scale bar, 50µm.

4.7 Functional conservation of *plgf* in zebrafish

Some studies in mouse report that the PlGF – FLT1 axis is important for macrophage migration (Dewerchin & Carmeliet 2012). In order to substantiate the relevance of our findings on the function of Flt1 and Plgf for studies in mouse or even in the clinic, we analysed whether the function of Flt1 – Plgf with respect to macrophage migration was conserved in zebrafish. First, by expressing the zebrafish forms of *sflt1* and *plgf* tagged with a double HA and a myc tag, respectively, in HeLa cells and performing a Co-IP, we found that also in zebrafish Plgf could bind to Flt1 (Figure 27i).

Then we analysed the macrophage distribution in the trunk and tail of *flt1*$^{-/-}$ and *plgf*$^{-/-}$ by WISH for *l-plastin*, a macrophage marker (Herbomel et al. 1999). Macrophages were accumulating around the aorta and the hypochord in WT embryos, the expression areas of *flt1* and *plgf*, respectively. In loss of *flt1* and *plgf* embryos the propensity of macrophage gathering in that area was lost, and macrophages dispersed over the complete trunk and tail (Figure 27a-f). Similar results were obtained by confocal imaging of *plgf*$^{-/-}$ mutants in the macrophage reporter line *Tg(mpeg1:Gal4-VP16)*^{gl24};*Tg(UAS:Kaede)*^{s1999t} (Figure 27g,h).

Taken together, two lines of evidence (1, biochemical; 2 physiological function) suggest that Plgf is functionally conserved in zebrafish.

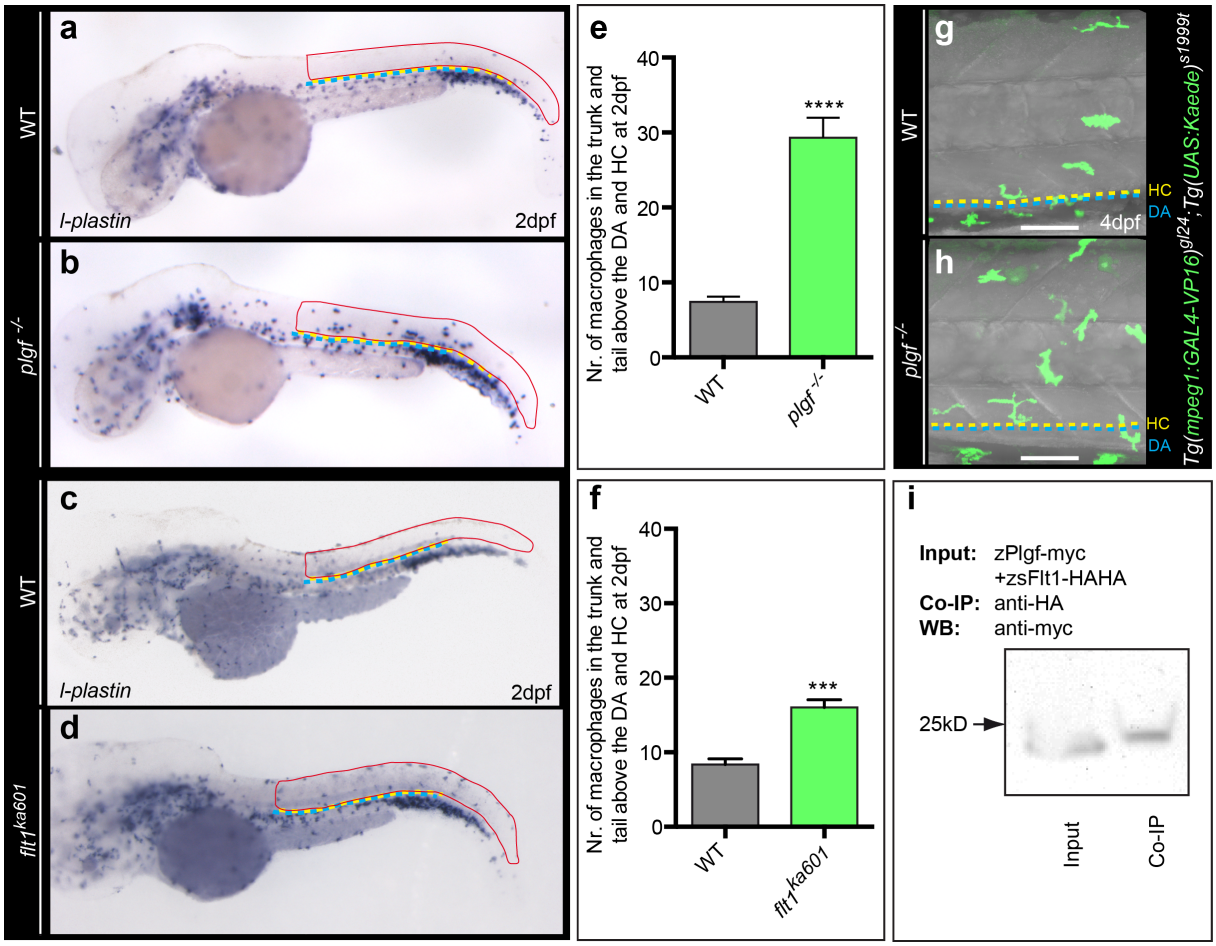

Figure 27| Functional conservation of zebrafish Plgf and Flt1.

(**a-d**) Imaging of macrophage distribution at 2dpf via WISH of *l-plastin* RNA probe, a macrophage marker (plasmid kindly provided by P. Herbomel). Note that macrophage number in the dorsal trunk and tail above the DA is increased in *plgf*$^{-/-}$ and *flt1*^{ka601} compared to WT, as outlined in red. (**e,f**) Quantification of the macrophage number in the trunk and tail dorsal to the DA, framed in red in a-d. (**g,h**) Confocal images of *Tg(mpeg1:GAL4-VP16)*^{gl24}*;Tg(UAS-E1b:Kaede)*^{s1999t}, displaying macrophages in green at 4dpf. Note that in *plgf*$^{-/-}$, also at 4dpf more macrophages are located in the dorsal part of the DA and HC when compared to WT, in line with WISH images in a,b at 2dpf. (**i**) Plgf binding to Flt1 is conserved in zebrafish. The zebrafish forms of Plgf and sFlt1 were tagged with myc and HAHA, respectively (zPlgf-myc, zsFlt1-HAHA), and transfected in HeLa cells. Note that upon anti-HA-pullldown the anti-myc detected protein corresponds to zPlgf-myc, indicating a Plgf-Flt1 interaction. Yellow dotted line in (a-d,g,h), HC; blue dotted line in (a-d,g,h), DA. Co-IP, Co-immunoprecipitation; DA, dorsal aorta; HC, hypochord; WB, Western blot. Quantification in (e,f), mean ± s.e.m, n>38 per group, t-test. Scale bar, 50µm.

4.8 The early neurovascular link – are Vegf ligands angioneurins?

In this study, we were furthermore interested in the function of the Vegf family members as angioneurins. Although there is emerging evidence suggesting that Vegf ligands like Vegfb, or Vegfa are involved in neurodegenerative pathologies (Poesen et al. 2008; Storkebaum et al. 2011), little is known about their role in early development, in particular the formation of the vascular and neuronal system. Nerves and blood vessels communicate with each other and reciprocally affect morphogenesis. It is established that neurons can release signals that direct vascular growth, for example sensory nerves can release Vegf and direct growth of blood vessels in the embryonic skin (Mukouyama et al. 2002). Certain motor neurons have been implied in directing lymph angiogenesis. Conversely, axons may use the presence of blood vessels for extending in the periphery. One outstanding question in the field is to what extent the patterning of motor/sensory neuronal axons and dendrites requires the presence of blood vessels. In other words: Do changes in vascular patterning always trigger changes in axonal projections? Here, we decided to focus on motoneurons during early development in the zebrafish embryo. For this purpose we examined embryos devoid of blood vessels (*cloche* mutants), combined with analysis in *vegf* ligand and receptor gain and loss of function embryos.

In the trunk of the zebrafish embryo, both vascular development and neuronal development can be imaged and manipulated by genetic means. We therefore decided to analyse loss and gain of function embryos and focussed on the motoneurons in conjunction with the developing vasculature.

During early development, motoneurons (MNs) can be divided in primary and secondary MNs. Primary MNs can be subdivided in caudal (CaPs), rostral (RoPs) and middle (MiPs). The patterning of the CaPs is highly stereotyped and subjected to guidance cues, similar to the intersegmental vessels. During later stages of development the primary CaP axon trajectory is followed by CaP-like secondary motoneurons, and both are called hereafter CaPs for simplicity.

As a first step of analysis of the early neurovascular interface, we performed confocal time lapse images of the double transgenic line *Tg(kdrl:GFP)*^{s843};*Tg(Xla.Tubb:DsRed)*^{zf148} in order to understand the chronology and spatial arrangement of the emerging ISVs and CaPs

(Figure 28a-o). The promoter *Xla.tubb*, also known as *NBT*, marks all mature neurons and their axonal extensions, thus allowing *in vivo* imaging of patterning events.
In line with current concepts on directed migration, both CaP axons and ISVs extended via the mechanism of directed guidance, involving the axonal growth cone and the endothelial tip cell at the leading edge, respectively, with various filopodia protrusions (Figure 28p). At around 26hpf the ISVs encountered the NT (Figure 28d-f) and around 32hpf the CaP axons ventrally reached the DA (Figure 28g-i). The ISV anastomoses were formed in direct contact with the dorsal NT (Figure 28j-o).

As a next step in analysing the function of Vegf ligands as angioneurins, we aimed at determining whether the development of CaP axons occurred independently of ISVs in the zebrafish trunk. Thereby, we wanted to preclude that possible deviations in the neuronal patterning upon manipulation of Vegf ligands were secondary effects of vessel defects.
For this purpose, we took advantage of the *cloche* mutant, which was described for the first time in 1995 as bearing a mutation in a gene at the top of the vascular and hematopoietic cell lineage specification cascade (Stainier et al. 1995). These mutants lack the axial vascular structure including the aorta and the posterior cardinal veins. As a consequence these mutants also lack intersegmental vessels and a DLAV, and there is no blood flow perfusion. At later stages, these mutants show slight compensation and some primitive endothelial cells can be detected in the more posterior parts of the embryo, and these cells are most likely the so-called" somatic derived endothelial cells" that have a different embryonic origin than the aortic and PCV endothelium. The group of Stainier, 21 years after first describing the phenotype of the cloche mutants, finally discovered which gene deficit accounts for the vascular phenotype: via tremendous sequencing and candidate validation of all 20 possible candidates using CRISPR/Cas9, they finally could show that the bHLH-PAS transcription factor *npas4l* (Reischauer et al. 2016) is functionally responsible.

We observed that in *cloche (npas4l*^{m378}) mutants in the absence of trunk vasculature CaP axons exited the neural tube in a regular and stereotyped manner, comparable to WT controls. Furthermore, the growing lateral line nerve (LLN) was positioned at the anatomically correct position and growing in the usual rostrocaudal direction through the complete trunk and tail (Figure 28t-v) – similar to what one observed in WT embryos. Also

the ventral CaP axon extension and distal bifurcation formation occurred normally in *npas4l*^{m378} homozygous mutants (Figure 28t-v), and the CaP axon length between exit of the NT and the bifurcation was not affected (Figure 28z).
These data suggest that the global or macro patterning of motoneurons was not affected by the loss of the blood vasculature.

We next focussed in more detail on the axonal micro-aborizations. In the mutants, we noted slightly fewer CaP axon side branches (Figure 28t).). However, it needs to be stated that the *cloche* mutants were very dysmorphogenic, i.e. they were curved and many organs including the developing musculature appeared disrupted. At present, we therefore cannot state that loss of blood vessels is the direct cause of the neuronal phenotype, or whether neuronal defects are due the dysmorphogenesis and the more widespread morphological problems because of lacking of oxygen and nutrient supply.

To substantiate our study we next focussed on analysing CaP growth in Vegf ligand LOF and GOF scenarios. Reducing Vegf inhibits ISV formation, whereas augmenting Vegf promotes ISV branching (Wild et al. 2017) – thus providing two scenarios to investigate changes in axonal patterning.
Insufficient Vegf levels are implied in motoneuron degeneration in amyotrophic lateral sclerosis (ALS) (Storkebaum et al. 2011), yet the impact of Vegf on axonal patterning and motoneuron development has not been analysed in depth so far. To obtain loss of *vegfaa*, we crossed *vegfaa* mutants (kind gift from A. Siekmann, MPI, Muenster) with neuronal and vascular reporter transgenics. For analysis we used the *vegfaa*$^{-/-}$ full mutants in the double transgenic line *Tg(kdrl:GFP)*^{s843};*Tg(Xla.Tubb:DsRed)*^{zf148} and compared them with WT embryos. *Vegfaa*$^{-/-}$ mutants lack intersegmental vessels; axial vessels are formed but show defects in expression of AV markers, and the embryos do not develop proper perfusion.
We found that the CaP axon exit from the NT into the periphery was not affected in *vegfaa* -/- mutants, and the trajectory of the LLN was normal (Figure 28w-y,z). Also the ventral trajectory of CaP axons as well as the formation of a distal bifurcation was intact. At the micro-level, quantification of the CaP axon length revealed that they were slightly shorter when compared with WT embryos. However, it needs to be emphasized that *vegfaa*$^{-/-}$ mutants are slightly dysmorphogenic due to lack of perfusion and ISVs, and care

should be taken in interpretation of small phenotype. We conclude that, similar to the observations in *cloche* mutants, the global patterning of motoneurons was unaffected in *vegfaa*$^{-/-}$ mutant embryos lacking an appropriate trunk vasculature. At the micro-level, Vegfaa may be involved in the regulation axon branching and length; however, given the apparent dysmorphogenesis associating with lack of blood vessels, at this point it is difficult to make a statement on whether they are primary or secondary effects in this setting.

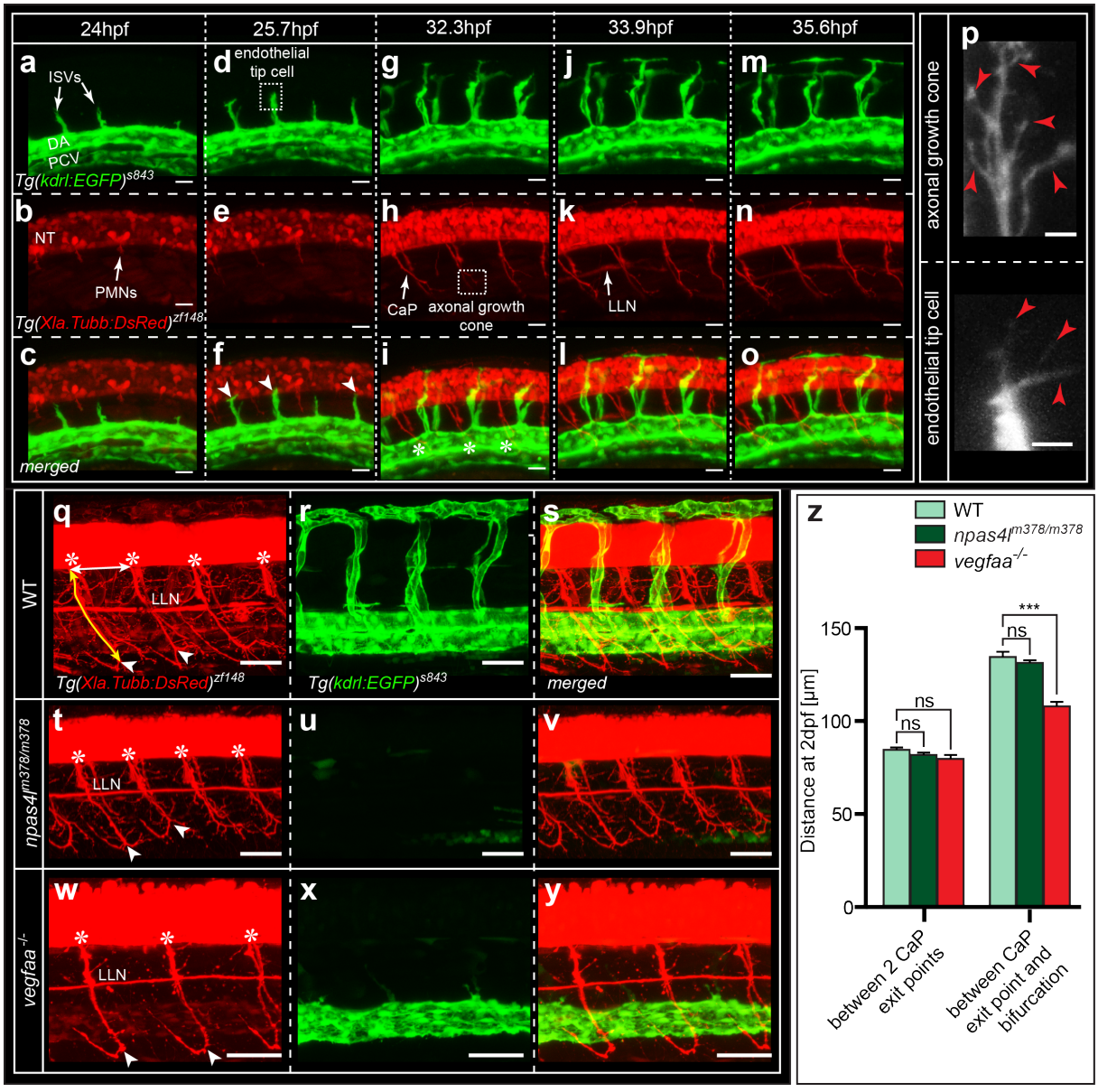

Figure 28| Development of the early neurovascular interface in the zebrafish embryo.

(**a-o**) Still images of a time lapse confocal movie of the emerging motoneuron axons and ISVs in the double transgenic line *Tg(kdrl:GFP)*^{s843};*Tg(Xla.Tubb:DsRed)*^{zf148}. (**d-f**) The first contact between the dorsally growing vessels and the NT occurs at 25.7hpf, indicated by white arrowheads. (**g-i**) At approximately 32hpf the ventrally growing CaP axons encounter the axial vessels, marked by white asterisks. (**j-o**) After 34hpf the ISVs form

anastomosis directly above the NT. Arrowheads in q,t,w, location of CaP bifurcation; asterisks in q,t,w, CaP exit points. (**p**) High-magnification images of the axonal growth cone and the endothelial tip cell as outlined by white dotted rectangles in h and d, respectively. Both consist of numerous filopodia extensions, as indicated by red arrowheads. (**t-v**) Development of CaP axon extensions in the absence of blood vessels. *Npas4l*$^{m378/m378}$ (also known as *clo*$^{m378/m378}$) mutants are lacking a functional vasculature, but CaP motoneurons can still extend normally into the ventral direction and make distal bifurcations. In green, somite-derived ECs. (**w-y**) *Vegfa*$^{-/-}$ mutants have no ISVs. Note that also in the absence of ISVs CaP axons can grow ventrally and bifurcate. (**z**) Quantification of the distance between two CaP exit points and length between CaP exit point and bifurcation, indicated by white and yellow lines in q, respectively. Note that outgrowth and length of the motoneuron axons is not affected per se by the absence of blood vessels in *npas4l*$^{m378/m378}$, but loss of *vegfaa* affects the CaP length. LLN, lateral line nerve; NT, neural tube; PMNs, primary motoneurons. Quantification in (z), mean ± s.e.m; t-test; n≥9 distances from ≥3 embryos per genotype and parameter. Scale bar, 50µm.

In a recent study we could show that that motoneurons expressed *vegfaa* as well *flt1. Flt1* is spliced in *mflt1* and *sflt1*, and in motoneurons we noted particularly high expression of *sflt1* when compared to *mflt1* (Wild et al. 2017). This leaves open the possibility that *flt1* expressed by neurons may provide a local scavenging receptor that binds Vegf, hence acting as a local Vegf reservoir – waiting to be unleashed for example after competition by other Flt1-specific ligands like Plgf or Vegfb. Indeed, Taqman data indicate that neurons expressed *plgf* and *vegfb*, and in motorneurons, *plgf* production occurs concomitantly with the guidance receptor and Vegf co-receptor *nrp1a*.

To determine the impact of such a putative motoneuronal Vegfaa reservoir, we aimed at analysing the consequences of a Vegfaa release from Flt1 on the motoneuronal system. To this end we overexpressed the Flt1-specific ligands *plgf* and *vegfb* and measured parameters including CaP exit point, bifurcation and length. In *plgf*^{cMC} embryos, the CaP exons projected into the periphery at normal positions at 28hpf (Figure 29b,h), bifurcated regularly at 32hpf (Figure 29d) and had a normal length at 28 and 32hpf (Figure 29i). Similarly, the LLN had a trajectory comparable to WT embryos (Figure 29c,d). Ubiquitous overexpression of *vegfb* (*vegfb*^{ubi}) by injecting *vegfb* mRNA revealed that also in this scenario of putative *vegfa*a GOF neither the position of the CaP exit points nor the CaP bifurcation and length were disturbed (Figure 29e,f,j,k).

Taken together, motoneuronal patterning was not affected by the absence of blood vessels, and neither loss of *vegfaa* nor gain of the Flt1-specific ligands *plgf* or *vegfb* altered the motor axonal pathfinding at the macro-level.

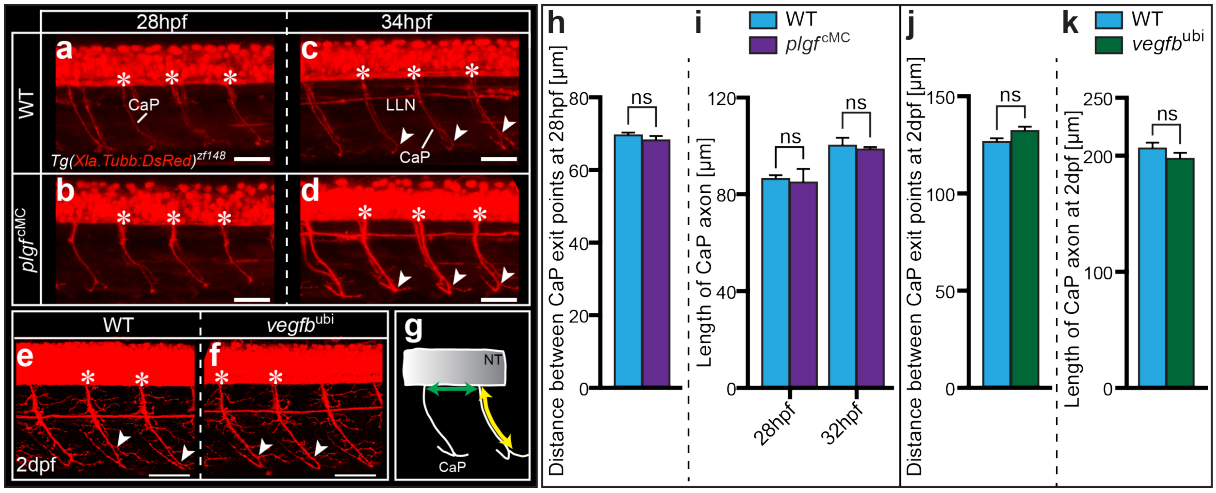

Figure 29| Neuronal development in *plgf* and *vegfb* GOF embryos.

(**a-f**) Representative confocal images of *plgf* and *vegfb* GOF embryos in the pan-neuronal reporter line *Tg(Xla.Tubb:DsRed)*^{zf148}. White asterisks, CaP exit points; white arrowheads, CaP bifurcation. (**a,b**) Primary CaPs develop normally in *plgf*^{cMC}. (**c,d**) Also the LLN and secondary CaP-like motoneurons (here also referred to as CaPs) display proper axonal patterning in *plgf*^{cMC}. (**e,f**) Ubiquitous *vegfb* GOF (*vegfb*^{ubi}) by injecting 100ng/µl *vegfb* mRNA does not affect the axonal patterning. (**g**) Illustration of CaP axon length measurement (yellow) and determination of the distance between two CaP exit points (green). (**h-k**) Quantification of the axonal growth parameters depicted in (g) of WT, *plgf* and *vegfb* GOF embryos at the indicated time points. Note that quantification reveals that *plgf* and *vegfb* GOF embryos do not have any axon growth defects. Quantification in (h-k), mean ± s.e.m; t-test; (h,i) n≥15 CaP exit point distances or CaP axon lengths, respectively, from 3 embryos per genotype and time point; (j) n=12 CaP exit point distances from 4 embryos per genotype;(k) n≥13 CaP axons from 4 embryos per genotype. LLN, lateral line nerve; MN, motoneuron; NT, neural tube. Scale bar 50µm.

As we had detected *plgf* expression in motoneurons (Figure 9,Figure 10), we decided to further analyse its potential endogenous role in motoneuronal patterning. Analysis of *plgf*$^{-/-}$ mutants in the pan-neuronal reporter line *Tg(Xla.Tubb:DsRed)*^{zf148} revealed no deviations with respect to CaP exit point, CaP axon length and bifurcation at 2dpf (Figure 30a,b,g,h). Also the extension of the neuronal network by CaP axon side branches at 3dpf occurred regularly in *plgf*$^{-/-}$ mutants (Figure 30c,d, yellow asterisks). Analysis of dorsal root ganglia,

which contain the sensory neuron somata, and Rohon-Beard neurons in the *Tg(-3.1ngn1:GFP)* line revealed that also sensory neuronal cells were unaffected by loss of *plgf* (Figure 30e,f).

Taken together, although being expressed in the nervous system, LOF and GOF of *plgf* did not affect motoneuron axonal patterning or growth of sensory nerves. These data suggest that – at least for motoneurons – Plgf is not acting as angioneurin.

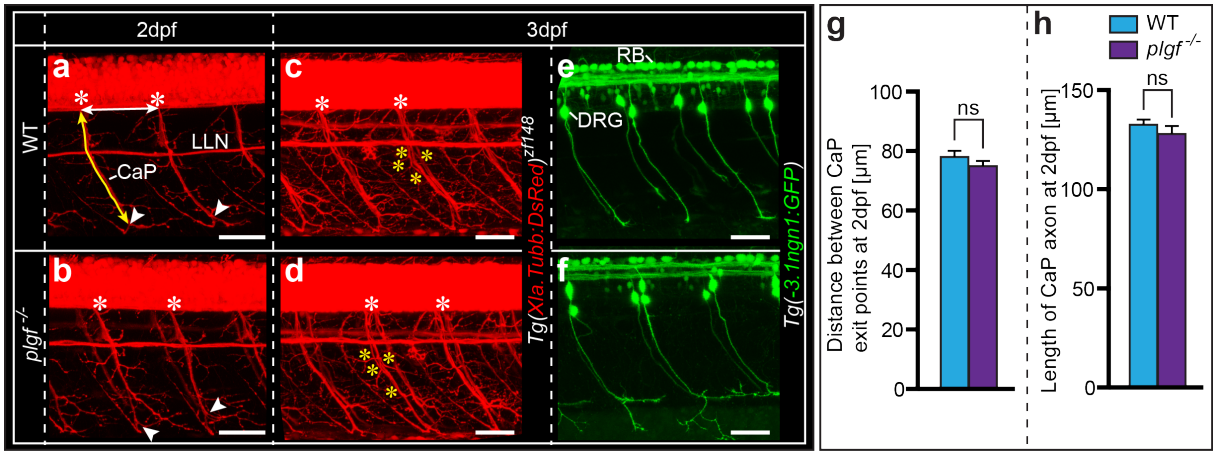

Figure 30| Early development of motoneurons and sensory neurons in *plgf*$^{-/-}$ embryos.

(**a-d**) Representative confocal images of the neuronal zebrafish trunk of WT and *plgf*$^{-/-}$ embryos in the pan-neuronal reporter line *Tg(Xla.Tubb:DsRed)*^{zf148}. White asterisks, CaP exit point; white arrowheads, CaP bifurcation. (**a,b**) The outgrowth of the CaP axons (yellow arrowheads), the CaP bifurcation (white arrowheads) and the LLN growth are normal in *plgf*$^{-/-}$ mutants. (**c,d**) At 3dpf proper motoneuronal network extension by axonal arborization (yellow asterisks) is taking place in *plgf*$^{-/-}$ embryos. (**e,f**) The RB sensory neurons as well as the DRG, which contain sensory neuron somata, develop normally in *plgf*$^{-/-}$ mutants as visualized by the *Tg(-3.1ngn1:GFP)* line. (**g,h**) Quantification of the distance between two CaP exit points and the CaP axon length as depicted with white and yellow line in a, respectively. Note that none of these parameters is different in *plgf*$^{-/-}$ mutants compared to WT embryos. DRG, dorsal root ganglion; LLN, lateral line nerve; RB, Rohon-Beard sensory neurons. Quantification in (g,h), mean ± s.e.m; t-test; n=10 CaP exit point distances distances or CaP axon lengths, respectively, from 5 embryos per genotype and time point. Scale bar, 50µm.

Some nerves and vessels are running directly in parallel. We determined whether this patterning was affected in *plgf*$^{-/-}$ mutants at 4dpf.

The parallel trajectories of the costal arteries (CAs) and the dorsal extensions of the CaP bifurcation were not disturbed in *plgf*$^{-/-}$ mutants (Figure 31a,b). Also the parachordal vessel (PAV) developed regularly in parallel to the LLN in the absence of *plgf* (Figure 31e,f). The

path of the motoneuron below the DA, which is guided by Vegfc – Flt4 signalling (Kwon et al. 2013), was not affected in *plgf*$^{-/-}$ mutants (Figure 31c,d). The interface of the ISVs with the neural tube was intact in these mutants (Figure 31g,h).

In summary, the neurovascular interface was not affected by loss of *plgf*.

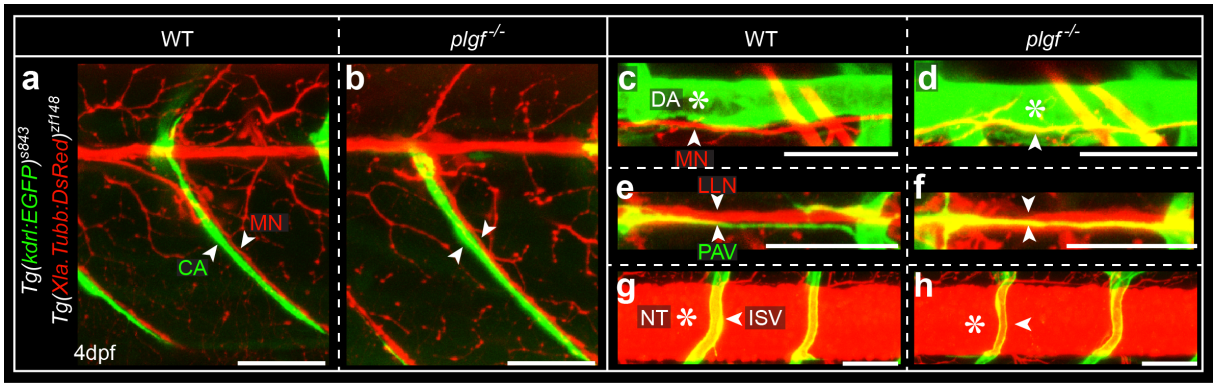

Figure 31| Neurovascular interface in *plgf*$^{-/-}$ mutants.

(**a-g**) Representative confocal images of the neurovascular interface at 4dpf in the double-transgenic reporter line *Tg(kdrl:GFP)*^{s843}*;Tg(Xla.Tubb:DsRed)*^{zf148}. (**a,b**) MN and CA are running in parallel in *plgf*$^{-/-}$ and WT. (**c,d**) MN (arrowhead) is ventrally aligned with the DA (asterisk) in both genotypes. (**e,f**) LLN and PAV have a parallel trajectory in *plgf*$^{-/-}$ and WT embryos. (**g,h**) ISVs are in close contact with the NT. Representative images of n>10 embryos per genotype and time point. CA, costal artery; DA, dorsal aorta; ISV, intersegmental vessel; LLN, lateral line nerve; MN, motoneuron axon; NT, neural tube; PAV, parachordal vessel. Scale bar, 50µm.

5 Discussion

5.1 Arterial Flt1 scavenges Vegfaa to control vessel diameter

Adaption of the arteriolar tree to changes in blood flow is essential for satisfying the metabolic demands of an organism. Such adaption can be achieved either by the formation of new blood vessels during angiogenesis or by the adjustment of the arterial diameter. The radial expansion or growth of arterioles is also called structural outward remodelling, as opposed to functional enlargement of arterioles involving active vasodilation by active relaxation of surrounding smooth muscle cells. In ischemic diseases, opening of pre-existing bypass collaterals involves flow-driven structural outward remodelling, and this process was originally referred to as “arteriogenesis” by Wolfgang Schaper, one of the pioneers in collateral vessel research (Schaper & Ito 1996). During subsequent years, it has been recognized that besides recruitment of native collaterals, additional collateral networks may also be derived from “upgrading” capillary network into small conductive arteriolar networks. This process, sometimes referred to as *de novo* arteriogenesis (Cristofaro et al. 2013) involves both outward remodelling and imprinting of artery identity in capillary endothelial cells. Arteriogenesis is considered an important therapeutic target for treating ischemic cardiovascular diseases, and several molecules have been suggested for this purpose including ThymosinB4 (Bongiovanni et al. 2015; Hinkel et al. 2014) and VEGF. VEGF is the key factor for vascular development in health and disease and it is implied in numerous aspects of creating functional vascular networks including structural aspects like vascular branching, vascular diameter, functional aspects like permeability but also molecular aspects including arterial identity (Lawson et al. 2002; Weis & Cheresh 2005; Swift & Weinstein 2009; Koch & Claesson-Welsh 2012). Given its potency, VEGF has been for a long time in the centre as cytokine of choice for therapeutic neovascularization (Grundmann et al. 2007). However, experimental and clinical studies showed that VEGF is indeed very potent but very difficult to deliver locally in the right dosage. Many trials showed adverse side effects including formation of hemangiomas, hypotension and aberrant vascular remodelling, in line with vessels being very sensitive to VEGF and high VEGF levels being harmful. The outstanding question in the field is how to use the “good” or “desirable” functions of VEGF while avoiding the detrimental ones.

Here, we show that arterial Flt1 may provide a means to unleash the potency of Vegfaa in promoting outward remodelling while limiting adverse side effects. We provide evidence for the following model (Figure 32): Flt1, both the soluble form *sflt1* and the membrane-bound *mflt1*, are selectively expressed in arteries and Flt1 protein is distributed in close proximity to the arterial system. As a consequence, Flt1 binds Vegfaa in close proximity to arteries. Arteries express Vegf receptors; hence, the Flt1 receptors are providing a Vegfaa reservoir close to the signalling receptors (Figure 32a). However, Vegfaa cannot participate in signalling since it is bound, and we found no evidence for Flt1:Kdrl heterodimers in signalling in the zebrafish embryo. Loss of *flt1* increases arterial diameter, suggesting that arterial Flt1 normally acts to restrict outward remodelling. To release Vegfaa from Flt1 we took advantage of the Flt1-specific ligand Plgf (Figure 32b). Overexpression of *plgf* in close proximity to the developing arterioles, for example in the surrounding skeletal musculature (of note: collaterals in the hindlimb of mouse and human are also surrounded by skeletal muscle), promote structural outward remodelling of arterioles – within 24 hours the arterioles double their size, hence, increased flow capacity by factor 16. In venules, there was only a 20% increase. Pharmacological and genetic interventions showed that this outward remodelling response was dependent on R2 signalling converging onto phospho-Akt. Similar observations were made with *vegfb*, suggesting that this response is conserved between Flt1-specifc ligands. However, while most of the evidence show that R2 is the main driver of the effect, R2 inhibitors did not completely rescue outward remodelling in response to Plgf, and a small contribution of other receptors like neuropilin-1 may be involved.

We propose that arterial Flt1 acts as a reservoir for Vegfaa in a local manner in close proximity to the Kdrl receptor. Releasing Vegf from the arterial Flt1 results in the local release of a small and therapeutically relevant dosage of Vegf that is necessary and sufficient to drive outward remodelling.

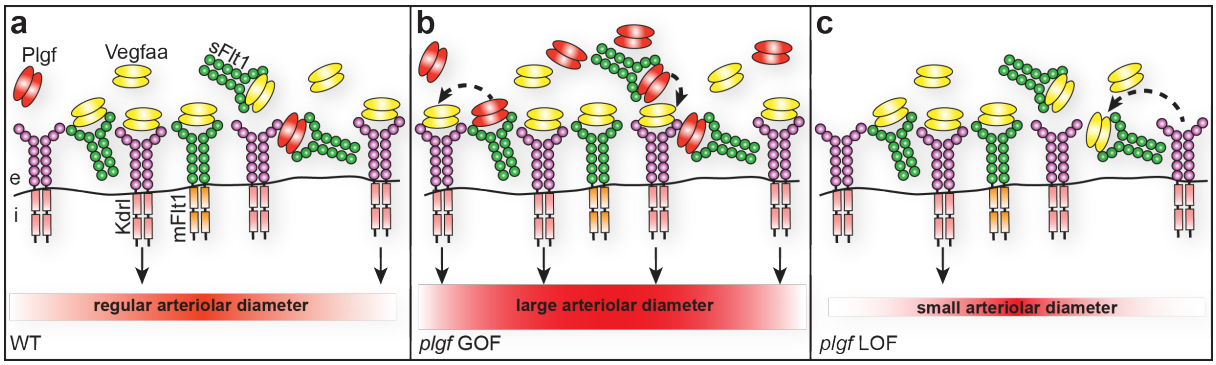

Figure 32| Arterial diameter regulation by Flt1-bound Vegfaa reservoir.

(**a-c**) Model of arteriolar Vegfaa bioavailability regulation by Flt1 and Plgf. (**a**) In the WT scenario, mFlt1- and sFlt1 bind Vegfaa in the close vicinity of the arteries and thereby restrict the Kdrl signalling-mediated outward remodelling. Flt1-specific ligand Plgf competes with Vegfaa for Flt1 binding and thus represents a second level of Vegfaa reservoir mediator. Note that Kdrl and mFlt1 are present on the same cell and that sFlt1 is very close to the cell surface. (**b**) In the *plgf* GOF scenario, Plgf outnumbers Vegfaa and thereby replaces Vegfaa bound to Flt1. The released Vegfaa binds to the directly adjacent Kdrl, and the increased Kdrl signalling leads to outward remodelling of the arteries. (**c**) In the absence of Plgf, more mFlt1 and sFlt1 become available for Vegfaa binding. As Vegfaa affinity to Flt1 is higher than to Kdrl, Vegfaa is released from Kdrl and binds to Flt1, and the decreased Kdrl signalling results in arteries with a smaller diameter.e, extracellular side; i, intracellular side.

Most of the biological actions of VEGF are signalled via KDR (VEGFR-2). Flt1 (VEGFR-1) has a 10-fold higher affinity for VEGF than KDR, and hence, Flt1 is considered to act as VEGF scavenging receptor, limiting VEGF bioavailability and signalling through KDR. Flt1 is spliced in two isoforms, the membrane-bound form containing an intracellular signalling domain and a soluble form, sFlt1. At present it is believed that Flt1, regardless of the isoform, is produced in the stalk cells of growing blood vessels. It is furthermore postulated that the sFlt1 protein diffuses over long distances and aids in guiding sprouting angiogenesis. We previously reported that vascular Flt1 is dispensable for sprouting angiogenesis in the zebrafish embryo (Wild et al. 2017). Instead, we found that neuronal Flt1 controls sprouting of intersegmental veins, a vascular domain that is actually expressing no or only limited levels of *flt1*. We show that *flt1* is predominantly expressed in arteries, and we have no evidence for production being restricted to stalk cells only – we observe *flt1* along the arterial sprouts and the aorta. We thus wondered why *flt1* was expressed in arteries if not for regulating branching. Therefore, we decided to re-examine *flt1* expression and protein distribution, unbiased by previous concepts. For this purpose, we first generated the knock-

in line *TgTm(flt1_E3_HAHA)*^{ka610}, allowing visualization of Flt1 protein by immunohistochemistry. We show that Flt1 protein is localized at the endothelial cell membrane or in very close proximity to the arterial vasculature. In addition, at the single cell level we find abundant Flt1 protein inside the cell and the cell nucleus, consistent with the nuclear localization signal (NLS) signal in the Flt1 protein. As such it seems that Flt1 is providing a "coating" around the arteries, presumably to protect against harmful Vegfaa dosages coming from the developing skeletal musculature surrounding the intersegmental vessels.

To test for the biological relevance of arterial Flt1, we analysed a series of Flt1 and Flt1 ligand loss- and gain-of-function models. We show that loss of *flt1* augments arterial diameter and therefore decided to investigate this in more detail. Although loss of *flt1* predicts Vegfaa gain-of-function, we show that overexpression of *vegfaa* – both constitutive and inducible – did not phenocopy loss of *flt1*. Instead, in these *vegfaa* GOF scenarios we observed aberrant vascular remodelling and non-functional vasculatures as also observed previously (Flamme et al. 1995). With such GOF approaches Vegfaa levels can rise very high, even up to the potentially toxic range. We thus argued that we needed more subtle elevations in local Vegfaa. Flt1 selectively binds Plgf and Vegfb, and these ligands may compete Vegfaa away from Flt1 (Figure 32,Figure 33). In addition, both Plgf and Vegfb are specific to Flt1 and do not bind to Kdrl, hence cannot activate Kdrl signalling (Rossi et al. 2016). While Flt1:Kdr heterodimers may exist, their signalling efficiency has been controversially discussed (DiSalvo et al. 1995; Cao et al. 1996). We furthermore have no evidence for a functional role of mFlt1 in early vascular morphogenesis (Wild, Klems et al. 2017) and the heterodimer scenario can thus be disregarded (Figure 33f).

We cloned zebrafish *plgf* and *vegfb* and mapped their expression using a combination of WISH and transgenic reporters. We find that they are expressed in developing nervous system, hypochord, skeletal muscle and developing gut and eye – domains that have not been reported before. We next generated CRISPR/Cas9 loss of function embryos and show that loss of *plgf* decreases arterial diameter by the factor 0.7 compared to WT diameter.

We show that overexpression of *plgf* under a constitutive muscle promoter (*503unc*) selectively promotes outward remodelling of arteries involving both a component related to endothelial cell proliferation and to cell migration. This response is sensitive to R2 signalling, as R2 inhibitor ki8751 annihilated the outward remodelling response. We furthermore find increased phospho-Akt upon *plgf* GOF, and wortmannin, an Akt signalling blocker, reduced outward remodelling, suggesting that outward remodelling is signalled through Kdrl and converges onto Akt.

In older studies addressing the role of Flt1 in vascular development, it is often mentioned that mFlt1 signalling in macrophages promotes invasion of macrophages into sites of active vascular remodelling. To test this we examined macrophage distribution in *flt1* and *plgf* LOF and GOF scenarios using both macrophage reporter lines and WISH with l-*plastin* as marker. We show that in our setting, the remodelling process does not associate with invasion of macrophages as no altered macrophage migration was observed in $plgf^{cMC}$ embryos (Figure 18f). In $flt1^{-/-}$ mutants, macrophage distribution was also not associated with vascular development. Thus, in contrast with other studies (Pipp et al. 2003) but in line with Odorisio et al (2002), in our hands arteriogenesis/outward remodelling does not associate with macrophage accumulation. In conclusion: Plgf-mediated, Flt1-dependent outward remodelling is endothelial cell-autonomous and not influenced by macrophages and nerves.

Interestingly, although arteries in *flt1* mutants did not show ectopic branches we do find evidence for hyperactivity including numerous filopodia extensions emanating from perfused vessels (Wild, Klems et al. 2017). Similar observations were made in Flt1 ligand GOF scenarios (Figure 17,Figure 21b). A recent *in vitro* study proposed the involvement of lateral filopodia formation in lumen formation by a VEGF-A – KDR-activated DOCK4-DOCK9-Cdc42 signalling pathway (Abraham et al. 2015). The contribution of this pathway and the necessity of filopodia in the remodelling process shown here remain to be analysed. Considering the unique *in vivo* imaging techniques available for zebrafish, future analysis of the remodelling process presented in this study will enable answering fundamental questions in vascular research: How do arterioles grow in diameter? How is a large increase in lumen formation accomplished with respect to cytoskeletal and junctional rearrangements?

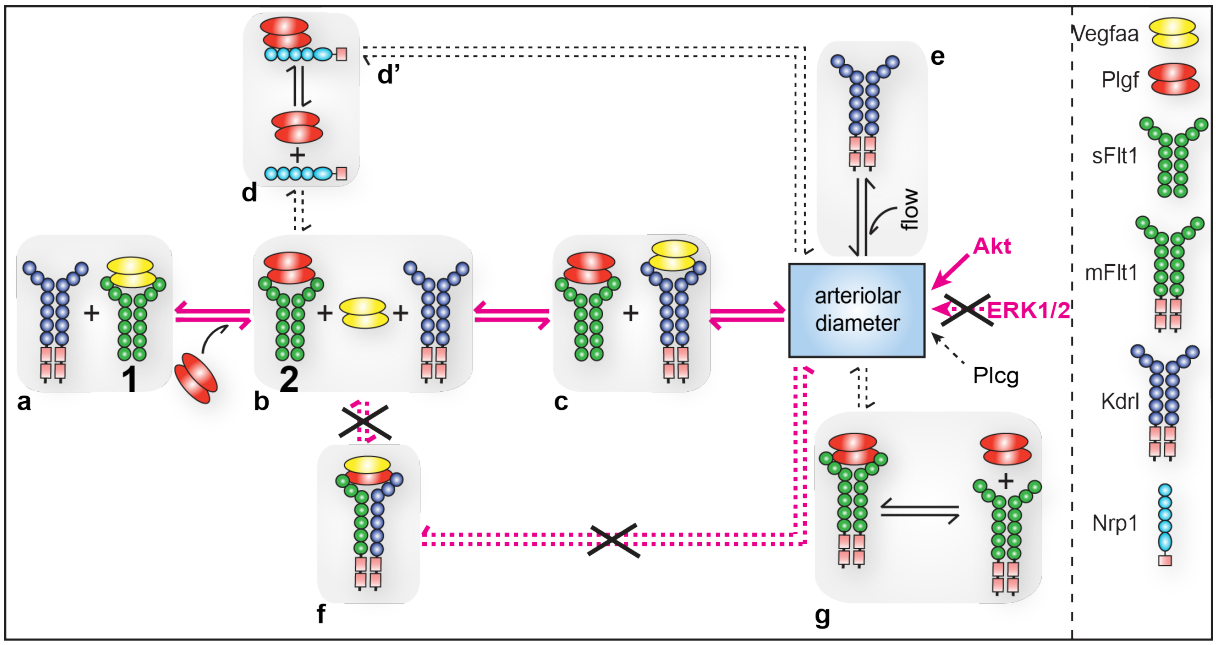

Figure 33| Arterial diameter is mediated by a balance of different factors.

Schematic depiction of the balance of Vegf receptor signalling contributing to arteriolar diameter control. (**a**) Flt1 (sFlt1 as depicted here, but also mFlt1) limits Kdrl signalling by scavenging Vegfaa. Vegfaa has a higher affinity to Flt1 than to Kdrl, thereby Flt1 is forming an arterial Vegfaa reservoir, the first level (1) of Vegfaa regulation. (**b**) Plgf competes with Vegfaa for Flt1 binding, thereby eventually releases Vegfaa. This is the second level (2) of Vegfaa regulation. Nrp1 binding, however, might regulate Plgf bioavailability as possible third level of Vegfaa reservoir regulation (**d**). (**c**) In turn, Vegfaa can bind to Kdrl and induce a signalling cascade involving Akt, but not ERK1/2, resulting in AOR. The contribution of Plcg remains to be established. (**d'**) Whether Plgf – Nrp1 signalling can contribute to outward remodelling remains to be determined. (**e**) Flow-induced, ligand-independent Kdrl signalling can mediate arterial diameter in a mechanosensory complex (Baeyens & Schwartz 2016). (**f**) There is no evidence for a contribution of Flt1:Kdrl heterodimers to arteriolar diameter control. (**g**) The implication of Plgf – mFlt1 signalling in this process remains to be established. Pink arrows, pathways discovered in this study to regulate arteriolar diameter; pink dotted arrows, pathways not involved in arteriolar diameter control; black arrow, known pathways involved in diameter vontrol; dotted pathways, pathways with unknown functions in arterial diameter regulation.

5.2 The impact of blood flow and shear stress on arterial remodelling

Haemodynamic factors, in particular shear stress, are major mediators of vascular adaption. Acute changes in blood flow are encountered with the production of vasodilative or -constrictive substances, while chronic deviations from a certain shear stress range induce vascular remodelling according to the shear stress set point theory. Low flow/shear stress results in inward remodelling, whereas high flow/shear stress induces outward remodelling

(Hoefer et al. 2013; Baeyens & Schwartz 2016). Poiseuille's law describes that the resistance of blood flow depends on the three parameters vessel length, viscosity and vessel radius. As viscosity is normally constant and vessel length does not vary much in a developed vasculature, blood vessel resistance and flow are mainly determined by the vessel radius.

In all three arteriolar outward remodelling scenarios presented in this study, i.e. *plgf*^{cMC}, *vegfb*^{cMC} and *flt1*$^{-/-}$, the vessel diameter normalized at around 3dpf. Applying the shear stress set point theory to the arterial outward and inward remodelling results in the model depicted in Figure 34 using the example of *plgf*^{cMC} embryos. The shear stress set point is assumed to be the WT shear stress level (Figure 34, dotted line). For simplicity, only R2 signalling is depicted, although possibly also other Plgf signalling might contribute to the outward remodelling. In addition, flow is assumed here to be proportional to heart rate, as flow rate determination in the zebrafish embryo is intricate.
With the R2-mediated doubling of arterial diameter and concomitant constancy of the heart rate at approximately 1.5dpf, the shear stress is reduced by the factor 8 (Figure 34a,e). When the heart rate in *plgf*^{cMC} increases at 2dpf, the shear stress is slightly raised (Figure 34b,e). However, the radius (r^{-3}) has a much bigger impact on shear stress than the flow rate (Q); therefore, inward remodelling occurs until the shear stress set point is reached (Figure 34c,d).

Another factor contributing to the inward remodelling is probably that AV remodelling occurs around 2dpf, an event generating circulating and stable perfusion. Hence it is likely that at this developmental stage hemodynamics starts to occupy a key role in vascular architecture and superimposes the R2 outward remodelling signalling. How shear stress set point sensing works is not completely understood so far. One model is the shear stress junctional mechanosensory complex in which VEGFR2 or -3 are associated with VE-cadherin's transmembrane domain; mechanical forces on platelet endothelial cell adhesion molecule (PECAM-1) activates a Src family kinase, which in turn induces VEGFR phosphorylation and downstream signalling (Coon et al. 2015; Baeyens et al. 2015; Baeyens & Schwartz 2016).

It also has to be taken into account that for an increase in diameter, the blood volume has to adapt accordingly to prevent underfilling or shock. Murray stated in 1926 that for keeping the energy needed for appropriate blood supply to a minimum, the cost of blood production should equal the cost of pumping the blood through the vessels. With respect to the outward remodelling presented in this study it is likely that although the energy to pump blood through these large arteries is very low, the cost of blood production is too high, as the blood volume had to be significantly raised in case of *plgf* GOF. From an energetic point, it is thus probably favourable for the growing embryo to normalize the diameter instead of producing large blood volumes.

In summary, we show that Vegfaa – Kdrl signalling has the capacity to induce outward remodelling, but as there is no hemodynamic need for arterioles with a doubled diameter in the developing embryo, mechanosensory inward remodelling of arteries is induced.
Thus, it will be worthwhile to analyse whether Vegfaa – Kdrl-mediated outward remodelling can persist in models with arterial occlusions where there is an increased shear stress in neighbouring collaterals and thus a hemodynamic need for outward remodelling.

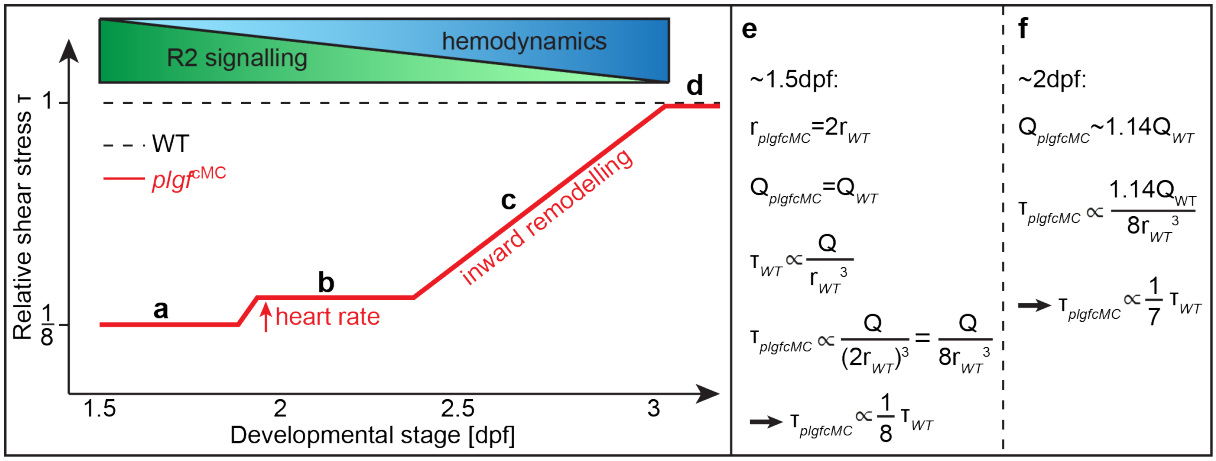

Figure 34| Schematic depiction of the shear stress in aISVs of *plgf*^{cMC} embryos.

Shear stress (τ) is proportional to blood flow (Q) and inversely proportional to the radius to the power of three (r^3). In this model, WT aISV shear stress represents the shear stress set point (dotted line). (**a**) In the early aISVs, Vegfaa – Kdrl (R2) signalling induces aISV outward remodelling, leading to a large shear stress difference between WT and *plgf*^{cMC} (calculation in e). (**b**) The heart rate of *plgf*^{cMC} embryos is increased at 2dpf compared to WT by the factor 1.14. Assuming that heart rate is proportional to blood flow, shear stress is thereby slightly increased (calculation in f), but remains remarkably smaller than the WT set point. (**c**) As the radius is the determining force for shear stress, inward remodelling occurs in order to adjust *plgf*^{cMC} embryo shear stress to

WT set point levels (**d**). Note that upon AV remodelling around 2dpf hemodynamics become superimposed to R2 signalling in this model.

5.3 Clinical implications

To improve the disease outcome in patients with arteriolar occlusions it is important to reduce the blood flow resistance at the level of the occluded site for an optimal flow recovery. The most important vessel parameter herein is the vessel lumen radius. In several clinical trials, intracoronary or intravenous VEGF gene transfer or protein delivery was tested as pro-arteriogenic stimulus in patients suffering from coronary or peripheral artery disease, but VEGF mostly failed to reach the primary trial end points (Grundmann et al. 2007). In other experimental settings, VEGF induced uncontrolled vascularization, suggesting that VEGF dosage is a major issue in therapeutic approaches. Here, we show that dosage limitations might be overcome by taking advantage of the endogenous arteriolar Flt1-bound Vegfaa reservoir. By competitive binding with Plgf, Vegfaa can be released locally in the close vicinity of Kdrl, thereby doubling the arteriolar diameter. Vegfaa does not have to diffuse far, so that this approach does probably not depend on the ECM composition.

Importantly, one would expect that increased Vegfaa levels cause increased permeability (Dor et al. 2002) and thus vessel shrinkage, but the opposite happens in the Vegfaa GOF scenarios shown in this study. In addition, no oedema formation could be observed. Therefore, we suggest that Vegfaa release from the endogenous reservoir negotiates the obstacle of proper dosage for stimulating arteriogenesis.
Plgf overexpression as Vegfaa replacement strategy was furthermore well tolerated with respect to the neuronal system, particularly axon guidance, and it did not attract macrophages for remodelling, thus the risk of inflammations and atherogenesis, which was described as major drawback of previous arteriogenic studies (Grundmann et al. 2007), will presumably be manageable.

However, for efficient and persistent perfusion capacity it is essential that blood vessels undergo maturation by pericytes recruitment. Thus, the stimulation of arteriogenesis is only beneficial when a pro-angiogenic stimulus is combined with a maturation factor (Hinkel et al. 2014). A highly interesting pathway is the Thymosin β 4 (T β 4)/ Myocardin-related

transcription factor (MRTF)-4/ serum response factor (SRF) axis, which induces both angiogenesis via CCN1 as well as pericyte recruitment via CCN2. T β 4 –MRTF-4 can thereby improved collateral blood flow in different animal models of coronary and peripheral ischemia (Hinkel et al. 2014). As the zebrafish ISVs are only very poorly covered by pericytes during early embryonic stages (Wild, Klems et al. 2017), the effect of arteriolar outward remodelling by Plgf will have to be further assessed in vessels that are covered with pericytes. In addition, it will be important to determine which co-administration is suitable to stabilize the vessel by pericytes in order to ensure optimal perfusion and durability of the vessels.

Taken together, we show in this study that vascular mFlt1 and sFlt1 mediate arterial diameter by forming an arteriolar Vegfaa reservoir, and release of this reservoir by Plgf leads to a doubling of the arteriolar diameter. Thus, Plgf represents an alternative to conventional Vegf administration in pro-arteriogenic therapeutic approaches.

6 Material and methods

6.1 Material

All chemicals were purchased from Sigma-Aldrich if not stated otherwise.

Table 1| Transgenic lines

Transgenic line	Marked cells/ Tissues	Publication
Tg(-3.1ngn1:GFP)	Sensory neurons, RB neurons	
Tg(fli1a:nGFP)^{y7}	ECs, NCCs; nucleus	(Roman et al. 2002)
Tg(flt1^{enh}*:tdTomato)*	Arteries; cytosol	(Bussmann et al. 2010)
Tg(flt4:mCitrine)^{hu7135}	Mainly in the PCV, also in vISVs; cytosol	(van Impel et al. 2014)
Tg(kdrl:GFP)^{s843}	Blood vessels; cytosol	(Jin et al. 2005)
Tg(kdrl:hsa.HRAS-mcherry)^{s916}	Blood vessels; membranes	(Hogan et al. 2009)
Tg(mpeg1:GAL4-VP16)^{gl24}*;Tg(UAS-E1b:Kaede)*^{s1999t}	Macrophages	(Ellett et al. 2011)
Tg(Xla.Tubb:DsRed)^{zf148}	Mature neurons	(Peri & Nüsslein-Volhard 2008)
TgBAC(flt1:YFP)^{hu4624}	*flt1*-expressing cells	(Krueger et al. 2011)

Table 2| Primers

Primer name	Sequence (5'→3')
plgf_HA1_control_fw	GGAAGACGCAATTTGGACAT
plgf_HA2_control_rev	CTCGGAGTGTGTGCAGGTAA
plgf_HA1_mCit_fw	GGGCGGACTACTGTTTGGATTTTCCTTCAATTAAACTTGTCTTGGCGTTCACCATGGTGA GCAAGGGCGAGGAG
plgf_HA2_kanR_rev	AGGCTCAACTGCACCGCGGCAAATATTCGTAACAGTGACGTCAAATAACTTCAGAAGAA CTCGTCAAGAAGGCG
pTarBAC_HA1_iTol2_fw	GCGTAAGCGGGGCACATTTCATTACCTCTTTCTCCGCACCCGACATAGATCCCTGCTCGA GCC GGGCCCAAGTG
pTarBAC_HA2_iTol2_rev	GCGGGGCATGACTATTGGCGCGCCGGATCGATCCTTAATTAAGTCTACTAATTATGATCC TCT AGATCAGATC
pTarBAC_HA1_control_fw	CTGTCAAACATGAGAATTGGTC
amp_HA1_control_rev	ACATTTCCCCGAAAAGTGG
amp_HA2_control_fw	CTGAGATAGGTGCCTCACTG
pTarBAC_HA2_control_rev	GAGAGCCTTCAACCCAGTC
Citrine _HA1_control_rev	GGACACGCTGAACTTGTGG
kanR_HA2_control_fw	TCCTCGTGCTTTACGGTATC
sFlt1_2HA_ODN_1	CTTATTCTTTATAGCGGCCCGGCGCGGCTGGCCTACCCATACGACGTCCCAGACTACGCT TACCCATACGACGTCCCAGACTACGCTTGAGGTGGAGGAGGCCCAGGGAGAGTGGAGT TGTGG
Flt1_XhoI_fw	GAAGTCTCGAGACCATGGGTTTCGATATATTATTTG
sFlt1_HAHA_Xba	AGGTCTCTAGATTAAGCGTAGTCTGGGACGTCGTATGGGTAAGCGTAGTCTGGGACGTC GTATGGGTATGCGAGTCTAGCCGGGCC
SDM_Flt1delta7_fw	ATGAAGGAGGGAGAGCCCTT

SDM_Flt1delta7_rev	CGACTGCACCTTCACAAAAGG
HA_rev	TGGGACGTCGTATGGGTAAGCG
sflt1_fw	ACTATCCTTACTGGGATCCAGC
plgf_E3_gDNA_fw	TGTGTGTTCATGTGTGTGTTTCTCTCTC
plgf_E3_gDNA_rev	CCGGCTCATGACAGACTTAAATAGGGC
Flt1_E3_gDNA_fw	CAGCTCAACACACACAGTATTGTTTTA
Flt1_E3_gDNA_rev	ACACCTGAAGCATCTTACCTGTGA
plgfE3_sgRNA_O1	TAGGTTCAGGAGTACCCAGGGG
plgfE3_sgRNA_O2	AAACCCCCTGGGTACTCCTGAA
Vegfb_ISH1_rev	TCGGCCTCTTCTTGTTGTCT
Vegfb_ISH2_fw	CAACAAGAAGAGGCCGAAAG
Vegfb_ISH3_fw	ACAAGGACTGGACGTTGGAC
Vegfb_ISH3_rev	CAAAGTTGGATCGGTGGATT
SmaI_Plgf_CDS_fw	ATCCCCGGGAGTTATTTGACGTCACTGTTACG
XhoI_Plgf_CDS_rev	ATCCTCGAGTTACCTGCGGGGAGGCTGACACCGG
SmaI_Vegfb_CDS_fw	ATC CCC GGG GGGATCAAGCTGAGGGTTA
XhoI_Vegfb_CDS_rev	AGT CTC GAG CTATTCACTTTGGGTTTCACATC
XhoI_Vegfb_fw	ATC CTCGAG ATGGGGATCAAGCTGAGG
XbaI_Vegfb_rev	AGT TCTAGA CTATTCACTTTGGGTT
HindIII_Plgf_CDS_fw	ATC AAG CTT ATG AGT TAT TTG ACG TCA CTG TT
XhoI_Plgf_CDS_nostop_rev	AGT CTC GAG CCT GCG GGG AGG CTG ACA
Flt1_XhoI_fw	GAAGTCTCGAGACCATGGGTTTCGATATATTATTTG
sFlt1_HAHA_Xba	AGGTCTCTAGATTAAGCGTAGTCTGGGACGTCGTATGGGTAAGCGTAGTCTGGGACGTC GTATGGGTATGCGAGTCTAGCCGGGCC

Table 3| Plasmids generated elsewhere

Plasmid	Publication	Purpose
pCR8GW-itol2-amp	(Bussmann & Schulte-Merker 2011)	BAC recombineering
pCS2+_mCitrine_kanR		
pRedET		
pCS2FA	(Kwan et al. 2007)	tol2 transposase mRNA
DR274	(Hwang et al. 2013)	sgRNA cloning
l-plastin probe	(Herbomel et al. 1999)	WISH
pME_eGFP- p2A_SmaI	(Wild et al. 2017)	pME cloning

Table 4| Online tools

Online tool	Description	Website
NCBI	Genome browser	http://www.ncbi.nlm.nih.gov
UCSC	Genome browser	https://genome.ucsc.edu
Ensembl	Genome browser	http://www.ensembl.org
Primer3	Primer design	http://primer3.ut.ee
ZiFit	sgRNA oligonucleotide cloning	http://zifit.partners.org/ZiFiT/
CHOPCHOP	sgRNA finder	http://chopchop.cbu.uib.no

6.2 Methods

6.2.1 Zebrafish methods

6.2.1.1 Zebrafish maintenance – ethics statement

Zebrafish maintenance and experiments were performed according with the German animal protection standards and were approved by the Government of Baden-Württemberg, Regierungspräsidium Karlsruhe, Germany (Akz.: 35-9185.81/G-93/15).

6.2.1.2 Maintenance of embryos and prevention of melanization

In cases where pigmentation was undesirable for further experiments, the embryos were transferred at 24hpf into 1x E3 medium (60x E3 medium: 34.8g NaCl; 1.6g KCl; 5.8g $CaCl_2 \cdot 2 H_2O$; 9.78g $MgCl_2 \cdot 6 H_2O$; in 2l H_2O) supplemented with 0.2mM PTU, a tyrosinase inhibitor, to prevent melanisation.

The embryonic chorions were removed either manually by forceps or enzymatically by incubating the embryos in a pronase solution (1mg/ml in egg water).

Embryos were fixed in 4% (w/v) PFA for 2h at RT or over night (o/n) at 4°C and washed three times for 5min with PBT (1xPBS, 0.1% (v/v) Tween-20).

6.2.1.3 Microinjections

Zebrafish embryos at the one-cell stage were placed into an injection ramp, which had been prepared by placing a mould in 2% (w/v) liquid agarose in egg-water in a 90mm petri dish. Microinjection needles had been generated by pulling 1mm capillary tubes with filaments (World Precision Instruments) in a needle puller (Sutter Instrument Co.). Embryos were injected into the cytoplasm at the one-cell stage by moving the needle with a micromanipulator (World Precision Instruments) and by applying pressure to release 1-2nl with the FemtoJet Microinjector (Eppendorf).

The injection solutions for transgenesis contained 25ng/µl *tol2 transposase* mRNA and 25ng/µl plasmid DNA. For BAC transgenesis 40 ng/µl *tol2 transposase* mRNA and 200 ng/µl BAC DNA were co-injected. Generation of zebrafish *plgf*$^{-/-}$ mutants via CRISPR/Cas9 was accomplished by injecting 25ng/µl *sgRNA*$^{plgf\ Exon\ 3}$ with 300ng/µl *Cas9* mRNA.

6.2.1.4 Inhibitor treatments

Inhibitor stock solutions were prepared in DMSO. To block VEGFR2 signalling embryos were treated with 0.125µM ki8751 (Sigma). PI3K/AKT signalling was inhibited with 1.25µM wortmannin (Sigma). Control embryos were treated with an equal volume of DMSO. For inducible GOF with the Gal4-ERT2 system endoxifen (Sigma) was dissolved in DMSO and 0.5µM were added to the embryos, which were subsequently incubated in the dark.

6.2.2 Staining methods

6.2.2.1 WISH

Tissue permeabilization of fixed embryos was achieved by a gradual transfer in 100% Methanol (25, 50, 75% (v/v) in 1xPBT), followed by a descending Methanol series back to PBT. Additional permeabilization was achieved using proteinase K at a concentration of 10µg/ml in PBT with the following incubation times: embryos at 24hpf for 3min, at 30hpf for 4min and at 48hpf for 8min. Subsequently, embryos were fixed in 4% PFA for 20min. In order to minimize unspecific background, embryos were prehybridized in hybridization mix for 1h at 65°C (50% (v/v) formamide; 5×SSC; 0.1% (v/v) Tween-20; 50µg ml^{-1} of heparin; 500µg ml^{-1} of RNase-free tRNA).

Embryos were then incubated with the RNA probe (Table 8) in hybridization mix o/n at 65°C. Next, the removal of the formamid was obtained by a decreasing series of hybridization mix in 2xSSC at 65°C and a final washing step in 0.2xSSC at room temperature (RT).

Non-hybridized RNA was removed using RNase A (Thermo Fisher Scietific) in RNase buffer (HEPES 0.1 M pH 7.5; NaCl 0.15 M; 0.1% Tween-20) for 45 min at RT followed by a washing step in 1xMAB-T (1x maleic acid buffer; 0.1% (v/v) Tween-20). 1l of 5x maleic acid buffer was prepared by adding 58g maleic acid, 43.5g NaCl and approximately 37.5g NaOH up to pH 7.5. Subsequently, non-specific antibody binding sites were blocked by incubation in 2% (w/v) Blocking Reagent in 1xMAB-T. The alkaline phosphatase-conjugated antibody anti-digoxigenin-AP, Fab fragments (Roche) was diluted 1:4000, added to the mbryos and blocked o/n at 4°C. Next, the embryos were washed 4 times in 1xMAB-T for 30min, washed twice for 15min in NTMT (0.1M Tris-HCl pH 9.5; 0.1M NaCl; 1% Tween-20; 50mM $MgCl_2$), followed by colour development in the dark with BM-Purple (Roche), a colorimetric alkaline phosphatase substrate.

6.2.2.2 Immunohistochemistry

For permeabilizing fixed embryos a descending followed by an ascending methanol series was performed as described above (6.2.2.1). The embryos' heads were chopped off and the bodies were incubated for 2h in a blocking buffer (1% (v/v) Triton X-100, 3% (w/v) BSA in 1xPBS). The primary antibody was diluted in 0.5% (v/v) Triton X-100, 1% (w/v) BSA in 1xPBS and samples were incubated o/n at 4°C. Embryos were washed 5 times for 10min with PBT before the secondary antibody was added for 2h at RT. Before imaging, samples were washed 5 times for 20min in PBT.

Table 5| Antibodies for IHC

1° Antibody	Manufacturer	Dilution	2° Antibody	Manufacturer	Dilution
anti-GFP (ab5450)	Abcam	1:500	donkey anti-goat IgG (H+L) Alexa Fluor 568	Invitrogen (A-11057)	1:1000
anti-HA (HA.11, MMS-101P)	Covance	1:1000	goat anti-mouse IgG (H+L) Alexa Fluor 488	Invitrogen (A-11029	1:1000

6.2.3 Molecular biological methods

6.2.3.1 DNA preparations

For plasmid minipreparations or midipreparations 3ml or 100ml LB medium (20g LB medium ad 1l H_2O), respectively, supplemented with the appropriate antibiotic were inoculated by picking single clones grown on a plate. Following incubation for 14h-16h at 37°C, 300rpm, 2ml or 95ml of the bacteria culture were harvested for plasmid extraction with the Qiagen Plasmid Mini Kit or Qiagen Plasmid Midi Kit.

In cases where no single bands could be obtained from a single PCR reaction, the desired bands had to be cut out of an agarose gel. Single bands were cut with a sterilized scalpel under a transilluminator. DNA was extracted from the gel using the GeneJET Gel Extraction Kit (Thermo Fisher Scientific) according to the manufacturer's manual.

6.2.3.2 PCR

Polymerase chain reactions (PCRs) for cloning were performed with the high fidelity Phusion Hot Start II DNA polymerase in the Mastercycler GX2/GX2e (Eppendorf); for genotyping

purposes the DreamTaq DNA polymerase (Thermo Fisher Scientific) was used. A total reaction volume of 20µl contained 0.4U Phusion or 1U DreamTaq DNA Polymerase and the respective buffer, 0.2µM of each primer and 200µM dNTPs (dNTP Mix, 10 mM each, Thermo Fisher Scientific).

In order to maximize the specificity and efficiency of a PCR, the optimal primer annealing temperature for any new combination of template-primer pair was determined via a temperature gradient PCR, usually in a range between 56°C-68°C. Apart from this, standard PCR programs were used.

6.2.3.3 Agarose gel electrophoresis

Nucleic acids were analysed with agarose gel electrophoresis. Samples were mixed with loading buffer (5x loading buffer: 0.5% (w/v) orange G; 50% (v/v) glycerol; 25mM EDTA; pH 8.0), loaded on the gel and run in 0.5x TAE buffer (20mM Tris-base; 10mM acetic acid; 0.5mM EDTA; pH 8.0).

For standard applications 1% (w/v) agarose gels were run at 120V, whereas the separation of fragments with size differences between 10-30bp was accomplished in 3% agarose gels at 100V. The intercalating dye RedSafe Nucleic Acid Staining Solution (iNtRON) allowed visualization of DNA upon UV light exposure.

6.2.3.4 Bacterial transformation

Chemically competent *E. coli* strains were transformed with plasmids according to the manufacturer's descriptions, plated on LB agar plates (20g LB medium ad 1l H_2O; 1.5% (w/v) agar-agar) supplemented with the appropriate antibiotic and incubated o/n at 37°C.

DH5-α cells were used for re-transformations. Subcloning, blue/white screening and Gateway clonings were performed in One Shot TOP10 Chemically Competent *E. coli* (Thermo Fisher Scientific). Cloning of plasmids encoding sgRNAs was accomplished in XL10-Gold Ultracompetent Cells (Agilent).

6.2.3.5 Restriction enzyme digestion

5-10 fold over digestion of DNA with restriction enzymes (all from NEB) was performed for 1-2h at the enzyme-specific incubation temperature and in the buffer recommended by the manufacturer.

6.2.3.6 Cloning

If not stated otherwise, PCR reactions for subsequent cloning reactions were done with cDNA as template. After restriction enzyme digest plasmids were dephosphorylated using calf intestinal alkaline phosphatase (NEB). Ligation was done with T4 DNA ligase (NEB). ISH probes were cloned into the pGEM-T Easy vector (Promega) according to the manufacturer's instructions; as PCR products from Phusion PCRs were blunt-ended, 3' A-overhangs were added with Taq PCR (purified PCR product; 0.2mM dATP; 1x PCR buffer; 1U DreamTaq DNA polymerase (Thermo Fisher Scientific); ad 20µl H_2O; 72°C, 20min). During cloning procedures DNA was purified with the Monarch PCR & DNA Cleanup Kit (NEB).

Table 6| Cloned plasmids

Cloned plasmid	Forward Primer	Backbone	Reverse Primer	Restriction enzymes
pME_GFP-p2A-plgf	SmaI_Plgf_CDS_fw	pME_eGFP-p2A_SmaI	XhoI_Plgf_CDS_rev	SmaI, XhoI
pME_GFP-p2A-vegfb	SmaI_Vegfb_CDS_fw	pME_eGFP-p2A_SmaI	XhoI_Vegfb_CDS_rev	SmaI, XhoI
pCS2+_vegfb	XhoI_Vegfb_fw	pCS2+	XhoI_Vegfb_rev	XhoI, XbaI
pCMV6-entry_plgf	HindIII_Plgf_CDS_fw	pCMV6-entry	XhoI_Plgf_CDS_nostop_rev	HindIII, XhoI
pCDNA3.1_sflt1-HAHA	Flt1_XhoI_fw	pCDNA3.1	sFlt1_HAHA_Xba	XhoI, XbaI
pME_sflt1-HAHA	Flt1_XhoI_fw	pME_MCS	sFlt1_HAHA_Xba	XhoI, XbaI
vegfb ISH probe 1	Vegfb_ISH3_fw	pGEM-T Easy	Vegfb_ISH1_rev	-
vegfb ISH probe 2	Vegfb_ISH2_fw	pGEM-T Easy	Vegfb_ISH3_rev	-
vegfb ISH probe 3	Vegfb_ISH3_fw	pGEM-T Easy	Vegfb_ISH3_rev	-

6.2.3.7 Generation of gateway expression vectors

For gateway recombination to generate expression vectors (Table 7), the LR Clonase II plus (Thermo Fisher Scientific) was used according to the manufacturer's protocol.

Table 7| Gateway expression vector cloning

p5E	pME	p3E	pDest	Resulting expression clone
p5E_503unc (Berger & Currie 2013)	pME_GFP-p2A-plgf	p3E_polyA (Kwan et al. 2007)	pDestTol2CG2 (Kwan et al. 2007)	503unc_GFP-p2A-plgf
p5E_503unc	pME_gal4-ERT2 (Wild et al.)	p3E_polyA	pDestTol2CG2	503unc_gal4-ERT2
p5E_503unc	pME_GFP-p2A_vegfb	p3E_polyA	pDestTol2CG2	503unc_GFP-p2A-vegfb
p5E_503unc	pME_GFP-p2A-vegfaa165 (Wild et al.)	p3E_polyA	pDestTol2CG2	503unc_GFP-p2A-vegfaa165
p5E_ $flt1^{enh}$	pME_ $flt1^{enh}$_sflt1-HAHA	p3E_polyA	pDestTol2CG2	$flt1^{enh}$_sflt1-HAHA
p5E_UAS (Kwan et al. 2007)	pME_GFP-p2A-vegfaa165	p3E_polyA	p3E_polyA	UAS_GFP-p2A-vegfaa165
p5E_Xla.Tubb-3.8	pME_GFP-p2A-plgf	p3E_polyA	p3E_polyA	Xla.Tubb_GFP-p2A-plgf

6.2.3.8 BAC recombineering

For the analysis of the endogenous expression of *plgf*, BAC transgenesis was performed according to Bussmann & Schulte-Merker (2011), involving a recombineering procedure. All transformations were carried out via electroporation with standard conditions for *E.coli*.

Using the UCSC genome browser, two suitable BACs were identified (CH73-297E11 and CH211-27O11, both with pTarBAC2.1 backbone) and ordered from BacPAC Resources Center. Bacteria were tested for bearing the correct BAC with the primers plgf_HA1_control_fw and plgf_HA2_control_rev in a colony PCR. Next, the bacteria carrying the BAC were transformed with the pRedET vector containing genes of the homology-directed repair machinery that was essential for the subsequent recombineering steps.

In order to enable transgenic insertion of the BAC via the *tol2* transposon system, in the first recombineering step *tol2* sites were inserted in the BAC backbone by recombination with the PCR product derived with pTarBAC_HA1_iTol2_fw and pTarBAC_HA2_iTol2_rev from the plasmid pCR8GW-itol2-amp (kindly provided by S. Schulte-Merker). Insertion of left *tol2* site was confirmed by PCR with pTarBAC_HA1_control_fw and amp_HA1_control_rev, of right *tol2* site with amp_HA2_control_fw and pTarBAC_HA2_control_rev.

In the second recombineering step, mCitrine was inserted behind the ATG of *plgf*.

The PCR product therefore was generated from template pCS2+_mCitrine_kanR (kind gift from S. Schulte-Merker) with primers plgf_HA1_mCit_fw and plgf_HA2_kanR_rev. Insertion of mCitrine behind the *plgf* ATG was confirmed first with plgf_HA1_control_fw and Citrine _HA1_control_rev, and second with kanR_HA2_control_fw and plgf_HA2_control_rev.

BAC DNA was prepared with the PureLink HiPure Plasmid Midiprep Kit (Invitrogen) according to the manual by Bussmann & Schulte-Merker (2011).

6.2.3.9 *In vitro* transcription

In vitro transcription (IVT) of *Cas9-nls* mRNA was done with the mMessage MACHINE T7 ULTRA Transcription Kit, of *tol2 transposase* (pCS2FA, Kwan et al. 2007) with the mMessage MACHINE SP6 ULTRA Transcription Kit, and sgRNAs were transcribed with the MAXIscript T7 Transcription Kit according to the manufacturer's instructions (all from Thermo Fisher Scientific).

For ISH RNA probe generation, 2µl 100mM DTT (Sigma-Aldrich), 2µl DIG RNA Labeling Mix (Roche), 1µl RNasin Ribonuclease Inibitor (Promega) and RNA polymerase with respective buffer were added to the DNA in a total volume of 20µl.

Cas9 and *tol2 transposase* RNA were purified with the RNeasy Mini Kit, DNA was digested with the RNase-Free DNase Set (both from Qiagen).

sgRNAs were purified using the NucleoSpin miRNA kit (Machery-Nagel) as described in the manual's section "Fractionation of pre-purified RNA in small RNA and large RNA", with the small RNA fraction containing the sgRNA.

Table 8| *In vitro* transcription

mRNA	RNA polymerase	Restriction enzyme for linearization
Cas9-nls	T7	SnaBI
tol2 transposase (*pCS2FA*)	SP6	BstBI
sgRNA in DR274	T7	DraI
vegfb	SP6	NotI
plgf ISH probe (AS)	T7	SpeI
plgf ISH probe (S)	SP6	ApaI, SacII
vegfb ISH probe 1 (AS)	SP6	NcoI
vegfb ISH probe 2 (AS)	T7	SpeI
vegfb ISH probe 3 (AS)	SP6	NcoI
vegfb ISH probe 3 (S)	T7	SpeI

l-plastin ISH probe (AS)	T7	SpeI

6.2.3.10 sgRNA identification and cloning for CRISPR/Cas9

Using the online-tool CHOPCHOP, short guide RNAs (sgRNAs) with the constraint NGG as PAM sequence were identified. Any sequences in the genome with up to three mismatches in the protospacer, the 20bp stretch complementary to the genomic sequence, were considered as off-targets and therefore discarded as appropriate sgRNAs. Oligonucleotides with appropriate overhangs for cloning the sgRNA sequence into BsaI-digested DR274 were designed using the online ZiFiT targeter. For annealing, each oligonucleotide was added in a final concentration of 4pmol/µl to 50µl 1x annealing buffer (10mM Tris, pH 7.5-8.0; 50mM NaCl; 1mM EDTA); this annealing solution was heated for 5min at 95°C in a heating block, subsequently let cool down to 30°C and the annealed oligonucleotides were diluted 1:10 in H_2O. For the o/n ligation at 16°C with the T4 DNA Ligase (NEB) a ratio of 1:9 of diluted annealed oligos:digested vector was used.

For later transcription of the *sgRNA*$^{plgf\ Exon3}$, the plgfE3_sgRNA_O1 and plgfE3_sgRNA_O2 were cloned into the DR274.

6.2.4 Generation of mutants and transgenics

sgRNA and *Cas9* mRNA were transcribed as listed in Table 8, and 300ng/µl *Cas9* mRNA and 25ng/µl *sgRNA* were injected in one-cell stage embryos.

Plgf mutants were generated with the *sgRNA*$^{plgf\ Exon3}$. F0 founder were crossed with different reporter lines, and F1 zebrafish with a 10bp deletion, leading to a frameshift, were identified by sequencing (Table 9). These fish were again incrossed to obtain a homozygous *plgf*$^{-/-}$ (*plgf*$^{ka609/ka609}$) mutant line.

The knock-in line *TgTm(flt1_E3_HAHA)*^{ka610} was generated by Raphael Wild by injecting 300ng/µl *Cas9* mRNA, 25ng/µl *sgRNA*^{flt1Exon3} (Wild et al. 2017) and 12.5pg/µl oligonucleotide sFlt1_2HA_ODN_1. The oligonucleotide was encoding two hemagglutinin (HA) tags followed by a stop codon, flanked by two homology arms with a length of 33nt each. Founders were identified by the presence of an additional, 60bp larger PCR product (Table 9), and in-frame integration of the HAHA tag was verified by DNA sequencing of the PCR product.

For generation of the transgenic line *Tg(flt^{enh}: sflt1-Δ7-HAHA)^{ka611}* by Raphael Wild, the base pairs coding for seven amino acids important for Vegfaa binding to sFlt1 were deleted from pDestCG2_flt1^{enh}_sflt1-HAHA by site-directed mutagenesis (SDM) with the primers SDM_Flt1delta7_fw and SDM_Flt1delta7_rev. For SDM the PCR product was phosphorylated with T4 polynucleotide kinase (NEB), followed by blunt end ligation with T4 DNA ligase. Remaining template plasmid was digested with DpnI. The resulting pDestCG2_flt1^{enh}_sflt1-Δ7-HAHA was injected with *tol2 transposase* mRNA, fish were raised and founders were identified by PCR (Table 9).

6.2.4.1 Genotyping

Genomic DNA was isolated from fin clips of adult zebrafish or from whole embryos via the HotSHOT (Hot Sodium Hydroxide Tris) method (Truett et al. 2000). In brief, the tissue was boiled in 30- 100µl alkaline solution (pH 12) for 20min at 95°C, centrifuged, and 1-5µl supernatant were used as PCR template. Mutants with insertion-deletion mutations (InDels) <10bp were sequenced, InDels ≥10bp were analysed on a 3% agarose gel (Table 9).

Vegfaa$^{-/+}$ and *npasl$^{r/+}$* heterozygous adult mutants were identified by pairwise incross and phenotypic analysis of the vasculature of the offspring (no ISVs or no functional vasculature, respectively, in 25% of the embryos).

Table 9| Genotypings

Mutant line	Official designation	Mutation	Forward Primer	Reverse Primer	Analysis
plgf$^{-/-}$	*plgf^{ka609}*	-10bp in exon 3	plgf_E3_gDNA_fw	plgf_E3_gDNA_rev	Gel
flt1$^{-/-}$	*flt1$^{ka601/601}$*	-1nt in exon 3	Flt1_E3_gDNA_fw	Flt1_E3_gDNA_rev	Seq.
flt1$^{-/-}$; plgf$^{-/-}$	*flt1$^{ka601/602}$; plgf$^{ka609/ka609}$*	ka601: -1nt ka602: -5nt ka609: -10nt	Flt1_E3_gDNA_fw plgf_E3_gDNA_fw	Flt1_E3_gDNA_rev plgf_E3_gDNA_fw	Seq. Seq. Gel
TgTm(flt1_E3_HAHA)	*TgTm(flt1_E3_HAHA)^{ka610}*	HAHA knockin in exon 3	Flt1_E3_gDNA_fw	Flt1_E3_gDNA_fw	Gel
Tg(flt1^{enh}: sflt1_Δ7HAHA)	*Tg(flt1^{enh}: sflt1_Δ7HAHA)^{ka611}*	*sflt1_Δ7HAHA*	HA_rev	sflt1_fw	Gel

6.2.5 Biochemical methods

6.2.5.1 Protein extraction from zebrafish

For protein extraction 100 embryos per sample were dechorionated,and their yolk sac was removed by passaging them eight times through a 200µl pipette tip in ice-cold PBS. Embryos were passaged six times through a narrow-gauge needle (Sterican G27, B Braun) in lysis buffer (50mM HEPES pH 7.4; 15mM NaCl; 1mM MgCl2; 10% (v/v) glycerol; 1% (v/v) Triton X-100), supplemented with 1x Protease Inhibitor Cocktail (Cell Signaling Technology) and 1x phosphatase inhibitor PhosSTOP (Roche). Lysed embryos were centrifuged for 10min at 13.000rpm at 4°C. 60µl supernatant was cooked at 95°C for 5min with 15µl 5x Western blot loading buffer (250mM Tris pH6.8; 5% (w/v) SDS; 50% (v/v) glycerol; 500mM β-mercaptoethanol; 0.5% (w/v) bromophenol blue). 5 embryos were loaded per lane in a SDS-PAGE.

6.2.5.2 SDS-PAGE and Western blot

For sodium dodecyl sulfate polyacrylamide gel electrophoresis (SDS-PAGE), a 12% resolving gel was used for Co-IP, for AKT and ERK1/2 blots a 10% resolving gel (Table 10). For both a 5% stacking gel was used (Table 10). The gel was run first run for approximately 20min at 80V to allow proteins to line up in the stacking gel; protein separation was accomplished at 150V for about 1h. The running buffer consisted of 0.1% (w/v) SDS, 25mM Tris and 125mM glycine. The semi-dry blot was done with blotting buffer composed of 25mM Tris, 192mM glycine, 0.1% (w/v) and a nitrocellulose membrane. For background reduction, the blot was incubated for 30min in 5% (w/v) nonfat dry milk in TBS-T (50mM Tris-HCl pH 7.4; 150mM NaCl; 0.05% (v/v) Tween-20). The membrane was washed three times in TBS-T, and the 1° antibody, diluted in TBS-T, was incubated o/n at 4°C. Afterwards, the membrane was washed again with TBS-T, before the 2° antibody, again diluted in TBS-T, was added for 2h at RT. The membrane was washed with TBS-T and incubated for 5min with alkaline phosphatase (AP) buffer (100mM Tris-HCl pH 9.5; 100mM NaCl). The blot was developed in the dark with 10ml AP buffer and 200µl NBT/BCIP (Roche).

Table 10| Composition of resolving and stacking gels for SDS-PAGE

Reagent	Amount for 10% resolving gel (ml)	Amount for 12% resolving gel (ml)	Amount for 5% stacking gel (ml)
H_2O	1.9	1.6	0.68
30% acryl-bisacrylamide mix	1.7	2.0	0.17
1.5M Tris (pH 8.8)	1.3	1.3	-
5M Tris (pH 6.8)	-	-	0.13
10% SCS	0.05	0.05	0.01
10% ammonium persulfate	0.05	0.05	0.01
TEMED	0.002	0.002	0.001

Table 11| Antibodies for pAKT/AKT and pERK/ERK blots

1° Antibody	Manufacturer	Dilution	2° Antibody	Manufacturer	Dilution
p42/44 MAPK (ERK1/2) (137F5), rabbit (#4695)	Cell Signaling Technology	1:1000	Alkaline Phosphatase AffiniPure Goat Anti-Rabbit IgG (H+L) (111-005-003)	Jackson Immuno-research	1:2000
Akt antibody, rabbit (#9272)					
Phospho-Akt (Ser473) (D9E), rabbit (#4060)					
Phospho-p44/42 MAPK (Erk1/2) (Thr202/Tyr204) (197G2), rabbit (#4377)					

6.2.5.3 Co-IP

For Co-IP, HeLa cells were grown in 25cm^2 cell culture flasks to a confluency of 60-70%. Cells were subsequently co-transfected with 2.5µg pCMV6-entry_plgf and 2.5µg pCDNA3.1_sflt1-HAHA using TurboFect Transfection Reagent (Thermo Fisher Scientific) according to the manufacturer's manual.

The cells of 2 flasks were pooled, pelleted and resolved in 350µl RIPA buffer (50mM Tris-HCl pH 7.5; 150mM NaCl; 2mM $CaCl_2$; 1% (v/v) Triton X-100; 1% (w/v) NaDOC; 0.1% (w/v) SDS), supplemented with 1x Protease Inhibitor Cocktail (Cell Signaling Technology) and 1x phosphatase inhibitor PhosSTOP (Roche). For cell lysis, cells were passaged six times through a narrow-gauge needle (Sterican G27, B Braun). The lysed cells were centrifuged for 10min at 13000rpm, 4°C. 50µl supernatant were supplemented with 3µg anti-HA antibody (HA.11, MMS-101P; Covance), and this suspension was incubated for 45min at 4°C to allow antibody binding. Protein G Sepharose, Fast Flow beads (Sigma-Aldrich) were washed three times with RIPA buffer, added to the protein-antibody solution and incubated for further 45min at 4°C to allow antibody binding to the beads. The beads were washed again three times with

RIPA buffer before 50µl H_2O and 10µl 5x Western blot loading buffer were added to the beads, this solution was cooked for 5min at 95°C and the supernatant was used for SDS-PAGE.

6.2.6 Microscopy

For *in vivo* confocal imaging, embryos were first anaesthetized with 0.7x Tricaine (Sigma-Aldrich) in E3 and subsequently embedded in microscopy dishes (MatTek) in 0.7x (w/v) low-melting NuSieve GTG Agarose (Lonza) in E3 medium. The hardened agarose was then covered with 0.7x Tricaine in E3 to keep the embryos anaesthetized during the imaging. Imaging was done with the Leica TCS SP8 Confocal inverted microscope using 20x or 40x objectives. Time lapse images were performed at 28.5°C.

In order to image WISH staining, embryos were gradually transferred into 80% glycerol (v/v, in PBS). Imaging of WISH stainings and brightfield imaging was done with a Leica MZFLIII microscope and a QICAM 12-Bit colour camera (QImaging).

6.2.7 Computational methods

6.2.7.1 Genome browsers, *in silico* analyses, computational analyses

Primers were designed *in silico* with the online tool Primer3. For *in silico* cloning purposes as restriction enzyme cloning, Gateway cloning and T/A cloning the SnapGene software was used. The genome browsers NCBI, UCSC and Ensembl were used for genomic computational analyses, including their tools like BLAST, BLAT and Conserved Domain Search.

6.2.7.2 Image processing

Image processing was performed using Fiji, i.e. maximum intensity z projections, merging or separating channels in multicolour images.

For determining the ratios of pERK/ERK and pAKT/AKT, in a first step the blot images of the blot stained with AKT and ERK and the one with pAKT and pERK staining were merged into a single TIF file; this TIF file was converted to 8-Bit and the pAKT/AKT and pERK/ERK ratios were determined for every sample using the Gel analysis tool of Fiji.

6.2.8 Statistical analysis

Statistical analysis was done with GraphPad Prism 6. Results are presented as mean ± standard error of the mean (s.e.m.). In order to determine whether two data sets were significantly different from each other, the two-tailed Student's t-test was used. The following asterisk rating was used to summarize p-values: ns (not significant), $p>0.05$; *, $p\leq0.05$; **, $p\leq0.01$; ***, $p\leq0.001$; ****, $p\leq0.0001$.

7 Bibliography

Abraham, S. et al., 2015. A Rac/Cdc42 exchange factor complex promotes formation of lateral filopodia and blood vessel lumen morphogenesis. *Nature communications*, 6, p.7286.

Anisimov, A. et al., 2013. The Basis for the Distinct Biological Activities of Vascular Endothelial Growth Factor Receptor–1 Ligands. *Science Signaling*, 6(282), p.52.

Autiero, M. et al., 2003. Role of PlGF in the intra- and intermolecular cross talk between the VEGF receptors Flt1 and Flk1. *Nature medicine*, 9(7), pp.936–943.

Baeyens, N. et al., 2015. Vascular remodeling is governed by a vegfr3-dependent fluid shear stress set point. *eLife*, 4, pp.1–35.

Baeyens, N. & Schwartz, M.A., 2016. Biomechanics of vascular mechanosensation and remodeling. *Molecular Biology of the Cell*, 27(1), pp.7–11.

Beis, D. et al., 2005. Genetic and cellular analyses of zebrafish atrioventricular cushion and valve development. *Development*, 132(18), pp.4193–4204.

Berger, J. & Currie, P.D., 2013. 503Unc, a Small and Muscle-Specific Zebrafish Promoter. *Genesis*, 51(6), pp.443–447.

Betz, C. et al., 2016. Cell behaviors and dynamics during angiogenesis. *Development*, 143(13), pp.2249–2260.

Blanco, R. & Gerhardt, H., 2013. VEGF and Notch in tip and stalk cell selection. *Cold Spring Harbor Perspectives in Medicine*, 3(1), pp.1–20.

Blum, Y. et al., 2008. Complex cell rearrangements during intersegmental vessel sprouting and vessel fusion in the zebrafish embryo. *Developmental Biology*, 316(2), pp.312–322.

Bongiovanni, D. et al., 2015. Thymosin β4 attenuates microcirculatory and hemodynamic destabilization in sepsis. *Expert Opinion on Biological Therapy*, 15, pp.203–210.

Burnstock, G. & Ralevic, V., 1994. New insights into the local regulation of blood flow by perivascular nerves and endothelium. *British Journal of Plastic Surgery*, 47(8), pp.527–543.

Bussmann, J. et al., 2010. Arteries provide essential guidance cues for lymphatic endothelial cells in the zebrafish trunk. *Development*, 137(16), pp.2653–7.

Bussmann, J. et al., 2008. Zebrafish VEGF receptors: A guideline to nomenclature. *PLoS Genetics*, 4(5), pp.4–5.

Bussmann, J., Bakkers, J. & Schulte-Merker, S., 2007. Early endocardial morphogenesis requires Scl/Tal1. *PLoS Genetics*, 3(8), pp.1425–1437.

Bussmann, J. & Schulte-Merker, S., 2011. Rapid BAC selection for tol2-mediated transgenesis in zebrafish. *Development*, 138(19), pp.4327–4332.

Bussmann, J., Wolfe, S. a & Siekmann, A.F., 2011. Arterial-venous network formation during brain vascularization involves hemodynamic regulation of chemokine signaling. *Development*, 138(9), pp.1717–1726.

Cao, Y.H. et al., 1996. Heterodimers of placenta growth factor vascular endothelial growth factor - Endothelial activity, tumor cell expression, and high affinity binding to Flk-1/KDR. *The Journal of Biological Chemistry*, 271(6), pp.3154–3162.

Carmeliet, P. et al., 1996. Abnormal blood vessel development and lethality in embryos lacking a single VEGF allele. *Nature*, 380(6573), pp.435–439.

Carmeliet, P., 2003. Angiogenesis in health and disease. *Nature Medicine*, 9(6), pp.225–226.

Carmeliet, P., 2000. Mechanisms of angiogenesis and arteriogenesis. *Nature medicine*, 6(3), pp.389–395.

Carmeliet, P. et al., 2001. Synergism between vascular endothelial growth factor and placental growth factor contributes to angiogenesis and plasma extravasation in pathological conditions. *Nature medicine*, 7(5), pp.575–83.

Carmeliet, P. & Collen, D., 2000. Transgenic mouse models in angiogenesis and cardiovascular disease. *J Pathol*, 190(3), pp.387–405.

Carmeliet, P. & Tessier-Lavigne, M., 2005. Common mechanisms of nerve and blood vessel wiring. *Nature*, 436(7048), pp.193–200.

Chappell, J.C. et al., 2009. Local Guidance of Emerging Vessel Sprouts Requires Soluble Flt-1. *Developmental Cell*, 17(3), pp.377–386.

Charkoudian, N. & Rabbitts, J.A., 2009. Sympathetic Neural Mechanisms in Human Cardiovascular Health and Disease. *Mayo Clinic Proceeings*, 84(9), pp.822–830.

Clauss, M. et al., 1996. The vascular endothelial growth factor receptor Flt-1 mediates biological activities Implications for a functional role of placenta growth factor in monocyte activation and. *Journal of Biological Chemistry*, 271(30), pp.17629–17634.

Coon, B.G. et al., 2015. Intramembrane binding of VE-cadherin to VEGFR2 and VEGFR3 assembles the endothelial mechanosensory complex. *Journal of Cell Biology*, 208(7), pp.975–986.

Corada, M., Morini, M.F. & Dejana, E., 2014. Signaling pathways in the specification of arteries and veins. *Arteriosclerosis, Thrombosis, and Vascular Biology*, 34(11), pp.2372–2377.

Covassin, L.D. et al., 2009. A genetic screen for vascular mutants in zebrafish reveals dynamic roles for Vegf/Plcg1 signaling during artery development. *Developmental Biology*, 329(2), pp.212–226.

Cristofaro, B. et al., 2013. Dll4-Notch signaling determines the formation of native arterial collateral networks and arterial function in mouse ischemia models. *Development*, 140(8), pp.1720–1729.

Davies, P.F. et al., 2013. The atherosusceptible endothelium: Endothelial phenotypes in complex haemodynamic shear stress regions in vivo. *Cardiovascular Research*, 99(2), pp.315–327.

Dewerchin, M. & Carmeliet, P., 2012. PlGF: A multitasking cytokine with disease-restricted activity. *Cold Spring Harbor Perspectives in Medicine*, 2(8), p.a011056.

DiSalvo, J. et al., 1995. Purification and characterization of a naturally occurring vascular endothelial growth factor.placenta growth factor heterodimer. *Journal of Biological Chemistry*, 270(13), pp.7717–7723.

Dor, Y. et al., 2002. Conditional switching of VEGF provides new insights into adult neovascularization and pro-angiogenic therapy. *EMBO Journal*, 21(8), pp.1939–1947.

Du, H. et al., 2010. Vascular endothelial growth factor signaling implicated in neuroprotective effects of placental growth factor in an in vitro ischemic model. *Brain Research*, 1357, pp.1–8.

Eichmann, A. et al., 2005. Guidance of vascular and neural network formation. *Current Opinion in Neurobiology*, 15(1), pp.108–115.

Eilken, H.M. & Adams, R.H., 2010. Dynamics of endothelial cell behavior in sprouting angiogenesis. *Current Opinion in Cell Biology*, 22(5), pp.617–625.

Ellett, F. et al., 2011. Mpeg1 Promoter Transgenes Direct Macrophage-Lineage Expression in Zebrafish. *Blood*, 117(4), pp.e49–e56.

Faber, J.E. et al., 2014. A brief etymology of the collateral circulation. *Arteriosclerosis, Thrombosis, and Vascular Biology*, 34(9), pp.1854–1859.

Faber, J.E. et al., 2011. Aging causes collateral rarefaction and increased severity of ischemic

injury in multiple tissues. *Arteriosclerosis, Thrombosis, and Vascular Biology*, 31(8), pp.1748–1756.

Fan, X. et al., 2014. Endometrial VEGF induces placental sFLT1 and leads to pregnancy complications. *Journal of Clinical Investigation*, 124(11), pp.4941–4952.

Fantin, A. et al., 2010. Tissue macrophages act as cellular chaperones for vascular anastomosis downstream of VEGF-mediated endothelial tip cell induction. *Blood*, 116(5), pp.829–840.

Ferrara, N. et al., 1996. Heterozygous embryonic lethality induced by targeted inactivation of the VEGF gene. *Nature*, 380(6573), pp.439–442.

Ferrara, N., Gerber, H.P. & LeCouter, J., 2003. The biology of VEGF and its receptors. *Nat Med*, 9(6), pp.669–676.

Flamme, I. et al., 1995. Overexpression of Vascular Endothelial Growth Factor in the Avian Embryo Induces Hypervascularization and Increased Vascular Permeability without Alterations of Embryonic Pattern Formation. *Developmental Biology*, 171(2), pp.399–414.

Folkman, J. et al., 1971. Isolation of a tumor factor responsible for angiogenesis. *The Journal of experimental medicine*, 133(2), pp.275–88.

Fong, G.-H.H. et al., 1995. Role of the Flt-1 receptor tyrosine kinase in regulating the assembly of vascular endothelium. *Nature*, 376(6535), pp.66–70.

Gebala, V. et al., 2016. Blood flow drives lumen formation by inverse membrane blebbing during angiogenesis in vivo. *Nature Cell Biology*, advance on(4), pp.443–450.

Gerety, S.S. et al., 2013. An inducible transgene expression system for zebrafish and chick. *Development*, 140(10), pp.2235–43.

Gerhardt, H. et al., 2003. VEGF guides angiogenic sprouting utilizing endothelial tip cell filopodia. *Journal of Cell Biology*, 161(6), pp.1163–1177.

Gore, A. V. et al., 2012. Vascular Development in the Zebrafish. *Cold Spring Harbor Perspectives in Medicine*, 2(5), pp.a006684–a006684.

Grundmann, S. et al., 2007. Arteriogenesis: Basic mechanisms and therapeutic stimulation. *European Journal of Clinical Investigation*, 37(10), pp.755–766.

Helisch, A. & Schaper, W., 2003. The Development and Growth of Collateral Arteries. *Microcirculation*, 10, pp.83–97.

Herbert, S.P. & Stainier, D.Y.R., 2011. Molecular control of endothelial cell behaviour during blood vessel morphogenesis. *Nature reviews. Molecular cell biology*, 12(9), pp.551–64.

Herbomel, P., Thisse, B. & Thisse, C., 1999. Ontogeny and behaviour of early macrophages in the zebrafish embryo. *Development*, 126(17), pp.3735–45.

Hinkel, R. et al., 2014. MRTF-A controls vessel growth and maturation by increasing the expression of CCN1 and CCN2. *Nature communications*, 5, p.3970.

Hiratsuka, S. et al., 1998. Flt-1 lacking the tyrosine kinase domain is sufficient for normal development and angiogenesis in mice. *Proceedings of the National Academy of Sciences of the United States of America*, 95(16), pp.9349–54.

Ho, V.C. et al., 2012. Elevated vascular endothelial growth factor receptor-2 abundance contributes to increased angiogenesis in vascular endothelial growth factor receptor-1-deficient mice. *Circulation*, 126(6), pp.741–752.

Hod, T., Cerdeira, A.S. & Karumanchi, S.A., 2015. Molecular mechanisms of Preeclampsia. *Cold Spring Harbor Perspectives in Medicine*, 5, p.a023473.

Hoefer, I.E., Den Adel, B. & Daemen, M.J.A.P., 2013. Biomechanical factors as triggers of vascular growth. *Cardiovascular Research*, 99(2), pp.276–283.

Hogan, B. et al., 2009. ccbe1 is required for embryonic lymphangiogenesis and venous

sprouting. *Nature Genetics*, 41(4), pp.396–398.
Hoier, B. & Hellsten, Y., 2014. Exercise-induced capillary growth in human skeletal muscle and the dynamics of VEGF. *Microcirculation*, 21(4), pp.301–314.
Hong, C.C. et al., 2006. Artery/Vein Specification Is Governed by Opposing Phosphatidylinositol-3 Kinase and MAP Kinase/ERK Signaling. *Current Biology*, 16(13), pp.1366–1372.
Hwang, W.Y. et al., 2013. Efficient genome editing in zebrafish using a CRISPR-Cas system. *Nature Biotechnology*, 31(3), pp.227–229.
van Impel, A. et al., 2014. Divergence of zebrafish and mouse lymphatic cell fate specification pathways. *Development*, 141(6), pp.1228–38.
Isogai, S. et al., 2003. Angiogenic network formation in the developing vertebrate trunk. *Development*, 130(21), pp.5281–5290.
Iwama, H. et al., 2006. Cardiac Expression of Placental Growth Factor Predicts the Improvement of Chronic Phase Left Ventricular Function in Patients With Acute Myocardial Infarction. *Journal of the American College of Cardiology*, 47(8), pp.1559–1567.
Jakobsson, L. et al., 2010. Endothelial cells dynamically compete for the tip cell position during angiogenic sprouting. *Nature Cell Biology*, 12(10), pp.943–953.
Jensen, L.D. et al., 2015. VEGF-B-Neuropilin-1 signaling is spatiotemporally indispensable for vascular and neuronal development in zebrafish. *Proceedings of the National Academy of Sciences of the United States of America*, 112(44), pp.E5944-53.
Jin, S.-W. et al., 2005. Cellular and molecular analyses of vascular tube and lumen formation in zebrafish. *Development*, 132(23), pp.5199–209.
Kaipainen, A. et al., 1995. Expression of the fms-like tyrosine kinase 4 gene becomes restricted to lymphatic endothelium during development. *Proceedings of the National Academy of Sciences of the United States of America*, 92(8), pp.3566–70.
Kamei, M. et al., 2006. Endothelial tubes assemble from intracellular vacuoles in vivo. *Nature*, 442(7101), pp.453–456.
Kappas, N.C. et al., 2008. The VEGF receptor Flt-1 spatially modulates Flk-1 signaling and blood vessel branching. *Journal of Cell Biology*, 181(5), pp.847–858.
Koch, S. & Claesson-Welsh, L., 2012. Signal transduction by vascular endothelial growth factor receptors. *Cold Spring Harbor Perspectives in Medicine*, 2(7), pp.1–21.
Korn, C. & Augustin, H.G., 2015. Mechanisms of Vessel Pruning and Regression. *Developmental Cell*, 34(1), pp.5–17.
Krueger, J. et al., 2011. Flt1 acts as a negative regulator of tip cell formation and branching morphogenesis in the zebrafish embryo. *Development*, 138(10), pp.2111–20.
Kwan, K.M. et al., 2007. The Tol2kit: A multisite gateway-based construction Kit for Tol2 transposon transgenesis constructs. *Developmental Dynamics*, 236(11), pp.3088–3099.
Kwon, H.-B.H.-B. et al., 2013. The parallel growth of motoneuron axons with the dorsal aorta depends on Vegfc/Vegfr3 signaling in zebrafish. *Development*, 140(19), pp.4081–4090.
Lanahan, A.A. et al., 2014. PTP1b is a physiologic regulator of vascular endothelial growth factor signaling in endothelial cells. *Circulation*, 130(11), pp.902–909.
Lange, C. et al., 2016. Vascular endothelial growth factor: a neurovascular target in neurological diseases. *Nature Reviews Neurology*, 12(8), pp.439–454.
Lawson, N.D., Vogel, A.M. & Weinstein, B.M., 2002. Sonic hedgehog and vascular endothelial growth factor act upstream of the Notch pathway during arterial endothelial differentiation. *Developmental Cell*, 3(1), pp.127–136.
Lemmon, M.A. & Schlessinger, J., 2010. Cell signaling by receptor tyrosine kinases. *Cell*,

141(7), pp.1117–1134.
Limbourg, A. et al., 2007. Notch ligand delta-like 1 is essential for postnatal arteriogenesis. *Circulation Research*, 100(3), pp.363–371.
Liu, H. et al., 2006. Neuroprotection by PlGF gene-modified human mesenchymal stem cells after cerebral ischaemia. *Brain*, 129(10), pp.2734–2745.
Lowery, L.A. & Van Vactor, D., 2009. The trip of the tip: understanding the growth cone machinery. *Nature Reviews Molecular Cell Biology*, 10(5), pp.332–43.
Maes, C. et al., 2002. Impaired angiogenesis and endochondral bone formation in mice lacking the vascular endothelial growth factor isoforms VEGF164 and VEGF188. *Mechanisms of Development*, 111(1–2), pp.61–73.
Maglione, D. et al., 1991. Isolation of a human placenta cDNA coding for a protein related to the vascular permeability factor. *Proceedings of the National Academy of Sciences of the United States of America*, 88(20), pp.9267–9271.
Martyn, U. & Schulte-Merker, S., 2004. Zebrafish neuropilins are differentially expressed and interact with vascular endothelial growth factor during embryonic vascular development. *Developmental Dynamics*, 231(1), pp.33–42.
Mattila, E. et al., 2008. The protein tyrosine phosphatase TCPTP controls VEGFR2 signalling. *Journal of Cell Science*, 121(Pt 21), pp.3570–3580.
Mazzag, B.M., Tamaresis, J.S. & Barakat, A.I., 2003. A Model for Shear Stress Sensing and Transmission in Vascular Endothelial Cells. *Biophysical Journal*, 84(6), pp.4087–4101.
Mukouyama, Y.S. et al., 2002. Sensory nerves determine the pattern of arterial differentiation and blood vessel branching in the skin. *Cell*, 109(6), pp.693–705.
Murakami, M. et al., 2006. Signaling of vascular endothelial growth factor receptor-1 tyrosine kinase promotes rheumatoid arthritis through activation of monocytes / macrophages. *Inflammation*, 108(6), pp.1849–1856.
Murray, C.D., 1926. The Physiological Principle of Minimum Work. The Vascular System and the Cost of Blood Volume. *Proceedings of the National Academy of Sciences of the United States of America*, 12(3), pp.207–214.
Painter, P.R., Edén, P. & Bengtsson, H.-U., 2006. Pulsatile blood flow, shear force, energy dissipation and Murray's Law. *Theoretical Biology & Medical Modelling*, 3, p.31.
Pardanaud, L. et al., 2016. Sympathetic Innervation Promotes Arterial Fate by Enhancing Endothelial ERK Activity. *Circulation Research*, 119(5), pp.607–620.
Park, J.E. et al., 1994. Placenta growth factor: Potentiation of vascular endothelial growth factor bioactivity, in vitro and in vivo, and high affinity binding to Flt-1 but not to Flk-1/KDR. *Journal of Biological Chemistry*, 269(41), pp.25646–25654.
Dela Paz, N.G. & D'Amore, P.A., 2009. Arterial versus venous endothelial cells. *Cell and Tissue Research*, 335(1), pp.5–16.
Peri, F. & Nüsslein-Volhard, C., 2008. Live imaging of neuronal degradation by microglia reveals a role for v0-ATPase a1 in phagosomal fusion in vivo. *Cell*, 133(5), pp.916–27.
Phng, L.-K., Stanchi, F. & Gerhardt, H., 2013. Filopodia are dispensable for endothelial tip cell guidance. *Development*, 140(19), pp.4031–4040.
Pipp, F. et al., 2003. VEGFR-1-selective VEGF homologue PlGF is arteriogenic: Evidence for a monocyte-mediated mechanism. *Circulation Research*, 92(4), pp.378–385.
Pittman, R.N., Golub, A.S. & Schleicher, W.F., 2005. Rate of decrease of PO2 from an arteriole with arrested flow. *Advances in Experimental Medicine and Biology*, 566, pp.257–262.
Poesen, K. et al., 2008. Novel role for vascular endothelial growth factor (VEGF) receptor-1 and its ligand VEGF-B in motor neuron degeneration. *The Journal of Neuroscience*,

28(42), pp.10451–10459.
Pugh, C.W. & Ratcliffe, P.J., 2003. The von Hippel-Lindau tumor suppressor, hypoxia-inducible factor-1 (HIF-1) degradation, and cancer pathogenesis. *Seminars in Cancer Biology*, 13(1), pp.83–89.
Reischauer, S. et al., 2016. Cloche is a bHLH-PAS transcription factor that drives haemato-vascular specification. *Nature*, 535(7611), pp.294–298.
Rensen, S.S.M., Doevendans, P.A.F.M. & van Eys, G.J.J.M., 2007. Regulation and characteristics of vascular smooth muscle cell phenotypic diversity. *Netherlands Heart Journal*, 15(3), pp.100–8.
Roman, B.L. et al., 2002. Disruption of acvrl1 increases endothelial cell number in zebrafish cranial vessels. *Development*, 129(12), pp.3009–3019.
Rossi, A. et al., 2016. Regulation of Vegf signaling by natural and synthetic ligands. *Blood*, 128(19), pp.2359–2367.
van Royen, N. et al., 2009. A Critical Review of Clinical Arteriogenesis Research. *Journal of the American College of Cardiology*, 55(1), pp.17–25.
Ruhrberg, C. et al., 2002. Spatially restricted patterning cues provided by heparin-binding VEGF-A control blood vessel branching morphogenesis. *Genes and Development*, 16(20), pp.2684–2698.
Sandoo, A. et al., 2010. The endothelium and its role in regulating vascular tone. *The Open Cardiovascular Medicine Journal*, 4, pp.302–12.
Satchell, S.C. & Braet, F., 2009. Glomerular endothelial cell fenestrations: an integral component of the glomerular filtration barrier. *American Journal of physiology. Renal Physiology*, 296(5), pp.F947-56.
Sawano, A. et al., 2001. Flt-1, vascular endothelial growth factor receptor 1, is a novel cell surface marker for the lineage of monocyte-macrophages in humans. *Blood*, 97(3), pp.785–791.
Schaper, W., 2009. Collateral circulation. Past and present. *Basic Research in Cardiology*, 104(1), pp.5–21.
Schaper, W. & Ito, W.D., 1996. Molecular Mechanisms of Coronary Collateral Vessel Growth. *Circulation Research*, 79(5), p.911 LP-919.
Sealock, R. et al., 2014. Congenic fine-mapping identifies a major causal locus for variation in the native collateral circulation and ischemic injury in brain and lower extremity. *Circulation Research*, 114(4), pp.660–671.
Selvaraj, D. et al., 2015. A Functional Role for VEGFR1 Expressed in Peripheral Sensory Neurons in Cancer Pain. *Cancer Cell*, 27(6), pp.780–796.
Shibuya, M., 2006. Vascular endothelial growth factor receptor-1 (VEGFR-1/Flt-1): a dual regulator for angiogenesis. *Angiogenesis*, 9(4), pp.225–230.
Silverthorn, D.U. et al., 2016. *Human physiology : an integrated approach*,
Simons, M. & Eichmann, A., 2015. Molecular controls of arterial morphogenesis. *Circulation Research*, 116(10), pp.1712–1724.
Simons, M., Gordon, E. & Claesson-Welsh, L., 2016. Mechanisms and regulation of endothelial VEGF receptor signalling. *Nature Reviews Molecular Cell Biology*, 10, pp.611–25.
Snuderl, M. et al., 2013. Targeting placental growth factor/neuropilin 1 pathway inhibits growth and spread of medulloblastoma. *Cell*, 152(5), pp.1065–1076.
Stainier, D.Y. et al., 1995. Cloche, an early acting zebrafish gene, is required by both the endothelial and hematopoietic lineages. *Development*, 121(10), pp.3141–3150.
Storkebaum, E. et al., 2011. Cerebrovascular disorders: molecular insights and therapeutic

opportunities. *Nature Neuroscience*, 14(11), pp.1390–1397.
Swift, M.R. & Weinstein, B.M., 2009. Arterial-venous specification during development. *Circulation Research*, 104(5), pp.576–588.
Takeda, Y. et al., 2009. Treatment With Recombinant Placental Growth Factor (PlGF) Enhances Both Angiogenesis and Arteriogenesis and Improves Survival After Myocardial Infarction. *Circulation Journal*, 73(9), pp.1674–1682.
Tam, S.J. & Watts, R.J., 2010. Connecting Vascular and Nervous System Development: Angiogenesis and the Blood-Brain Barrier. *Annual Review of Neuroscience*, 33(1), pp.379–408.
Tintu, A. et al., 2009. Hypoxia induces dilated cardiomyopathy in the chick embryo: Mechanism, intervention, and long-term consequences. *PLoS ONE*, 4(4), pp.1–11.
Truett, G.E. et al., 2000. Preparation of PCR-quality mouse genomic dna with hot sodium hydroxide and tris (HotSHOT). *BioTechniques*, 29(1), pp.52–54.
Ulrich, F. et al., 2011. Neurovascular development in the embryonic zebrafish hindbrain. *Developmental Biology*, 357(1), pp.134–151.
Vieira, J.M., Ruhrberg, C. & Schwarz, Q., 2010. VEGF receptor signaling in vertebrate development. *Organogenesis*, 6(2), pp.97–106.
Weis, S.M. & Cheresh, D.A., 2005. Pathophysiological consequences of VEGF-induced vascular permeability. *Nature*, 437(7058), pp.497–504.
Westerhof, N., Lankhaar, J.W. & Westerhof, B.E., 2009. The arterial windkessel. *Medical and Biological Engineering and Computing*, 47(2), pp.131–141.
Wild, R. et al., 2017. Neuronal sFlt1 and Vegfaa determine venous sprouting and spinal cord vascularization. *Nature Communications*.

8 Abbreviations

aISV	arterial intersegmental vessel
AV	arteriovenous
BAC	bacterial artificial chromosome
bp	base pair
BSA	bovine serum albumin
CA	costal artery
CaP	caudal primary motoneuron
Cas9	CRISPR associated protein 9
cDNA	complementary DNA
cMC	constitutive muscle cell-specific GOF
cNC	constitutive neuronal cell specific-GOF
CNS	central nervous system
Co-IP	Co-immunoprecipitation
CRISPR	Clustered Regularly Interspaced Short Palindromic Repeats
CtA	central artery
CV	cardinal vein
DA	dorsal aorta
DIG	digoxigenin
DLAV	dorsal longitudinal anastomotic vessel
Dll1-4	delta-like 1-4
DNA	deoxyribonucleic acid
DNase	deoxyribonuclease
dNTP	deoxynucleotide triphosphate
DOCK4/9	dedicator of cytokinesis 4/9
dpf	days post fertilization
DTT	dithiothreitol
EC	endothelial cell
ECM	extracellular matrix
EDTA	ethylenediamine tetraacetic acid
eGFP	enhanced green fluorescent protein
eNOS	endothelial nitric oxide synthase
ERK1/2	extracellular-signal-regulated kinase 1/2
F-actin	filamentous actin
FACS	fluorescence-activated cell sorting
FGF	fibroblast growth factor
Fli1a	Fli1 proto-oncogene
Flt1	Fms-like tyrosine kinase1/VEGFR-1
Flt4	Fms-like tyrosine kinase 4/VEGFR-3
GFP	green fluorescent protein
GOF	gain of function

HC	hypochord
HMS	horizontal myoseptum
hpf	hours post fertilization
Ig	immunoglobulin
IHC	immunohistochemistry
iMC	inducible muscle cell-specific GOF
ISV	intersegmental vessel
IVT	*in vitro* transcription
kDa	kilo Dalton
KDR	kinase insert domain receptor/VEGFR-2
kdrl	kinase insert domain receptor-like
LLN	lateral line nerve
LOF	loss of function
MAPK	mitogen-activated protein kinase
mFlt1	membrane-bound Flt1
MMP	matrix metalloproteases
MN	motoneuron
mRNA	messenger RNA
NC	notochord
NICD	Notch intercellular domain
NICD	Notch intracellular domain
NLS	nuclear localization signal
NO	nitric oxide
NRP1/2	neuropilin-1/2
NT	neural tube
o/n	over night
PAGE	polyacrylamide gel electrophoresis
PAV	parachordal vessel
PBS	phospate buffered saline
PBS-T	phospate buffered saline-Tween 20
PCR	polymerase chain reaction
PCV	posterior cardinal vein
PFA	paraformaldehyde
PI3K	phosphoinisitide-3 kinase
PLCy	Phospholipase C gamma 1
PlGF	placental growth factor
PMN	primary motoneuron
PTU	1-phenyl-2-thiourea
R2	VEGFR-2
RI	remodelling index
RNA	ribonucleic acid
RNase	ribonuclease

rpm	revolutions per minute
RTK	receptor tyrosine kinase
s.e.m.	standard error of the mean
SDS	sodium dodecylsulfate
sFlt1	solube Fms-like tyrosine kinase1/sVEGFR-1
sgRNA	short guide RNA
SMC	smooth muscle cell
Taq	*Thermus aquaticus*
TEMED	N, N, N', N'-tetramethylethylendiamin
Tg	transgenic
Tris	tris(hydroxymethyl)-aminomethane
VE-cadherin	vascular endothelial cadherin (cdh5)
VEGF	vascular endothelial growth factor/ VEGF-A
VEGFR	vascular endothelial growth factor receptor
vISV	venous intersegmental vessel
WISH	whole-mount *in situ* hybridization
WT	wild type
YFP	yellow fluorescent protein

9 List of figures

Figure 1| Schematic illustration of blood vessel development. 13
Figure 2| Blood vessel development in the zebrafish. 15
Figure 3| Proposed mechanisms of lumen formation. 18
Figure 4| Collateral circulation. 21
Figure 5| The VEGF family. 23
Figure 6| Poiseuille's law. 30
Figure 8| *Flt1* expression and protein localization. 38
Figure 9| WISH of *plgf* in the zebrafish embryo. 40
Figure 10| Analysis of *plgf* expression via BAC transgenesis. 42
Figure 11| WISH of *vegfb* in the zebrafish embryo. 44
Figure 12| Dynamic analysis of ISV diameter in *flt1*$^{-/-}$ embryos. 45
Figure 13| Analysis of the vascular phenotype of muscle-specific *vegfaa* GOF. 48
Figure 14| Analysis of the ISV diameter in *plgf*^{cMC}. 50
Figure 15| Analysis of downstream signalling involved in the outward remodelling. 53
Figure 16| Western blot analysis of pAkt and pERK1/2 in *plgf*^{cMC} embryos. 55
Figure 17| Analysis of filopodia in *plgf*^{cMC}. 56
Figure 18| Analysis of EC number in *plgf*^{cMC} embryos. 57
Figure 19| Analysis of ectopic sprouts in *plgf* GOF embryos at later stages. 58
Figure 20| Analysis of the AV distribution, heart rate and morphological development of *plgf*^{cMC} embryos. 60
Figure 21| Analysis of ISV diameter in *vegfb*^{cMC} embryos. 61
Figure 22| Generation of *plgf* mutants using CRISPR/ Cas9. 63
Figure 23| Analysis of early trunk vasculature in *plgf*$^{-/-}$ embryos. 64
Figure 24| Artery-vein distribution and morphological development of *plgf*$^{-/-}$ mutant embryos. 65
Figure 25| Cerebral vascular development in *plgf*$^{-/-}$ mutant embryos. 66
Figure 26| Expression of *plgf* in *flt1*$^{-/-}$ mutant embryos and analysis of vasculature of *plgf*$^{-/-}$;*flt1*$^{-/-}$ double mutants. 67
Figure 27| Functional conservation of zebrafish Plgf and Flt1. 69
Figure 28| Development of the early neurovascular interface in the zebrafish embryo. 73
Figure 29| Neuronal development in *plgf* and *vegfb* GOF embryos. 75
Figure 30| Early development of motoneurons and sensory neurons in *plgf*$^{-/-}$ embryos. 76
Figure 31| Neurovascular interface in *plgf*$^{-/-}$ mutants. 77
Figure 32| Arterial diameter regulation by Flt1-bound Vegfaa reservoir. 80
Figure 33| Arterial diameter is mediated by a balance of different factors. 83
Figure 34| Schematic depiction of the shear stress in aISVs of *plgf*^{cMC} embryos. 85

10 List of tables

Table 1| Transgenic lines 88
Table 2| Primers 88
Table 3| Plasmids generated elsewhere 89
Table 4| Online tools 89
Table 5| Antibodies for IHC 92
Table 6| Cloned plasmids 94
Table 7| Gateway expression vector cloning 95
Table 8| *In vitro* transcription 96
Table 9| Genotypings 98
Table 10| Composition of resolving and stacking gels for SDS-PAGE 100
Table 11| Antibodies for pAKT/AKT and pERK/ERK blots 100

11 List of publications

Wild, R., **Klems, A.**, Takamiya, M., Hayashi, Y., Strähle, U., Ando, K., Mochizuki, N., van Impel, A., Schulte-Merker, S., Krueger, J., Preau, L., le Noble, F, 2017. Neuronal sFlt1 and Vegfaa determine venous sprouting and spinal cord vascularization. **Nature Communications**. DOI: 10.1038/NCOMMS13991.